CRANFIELD UNIVERSITY

SHUIB HUSIN

AN EXPERIMENTAL INVESTIGATION INTO THE CORRELATION BETWEEN ACOUSTIC EMISSION (AE) AND BUBBLE DYNAMICS

SCHOOL OF ENGINEERING

PhD THESIS

Academic Year: 2010 - 2011

Supervisor: Professor David Mba
Co-supervisor: Dr Abdulmajid Addali

August 2011

CRANFIELD UNIVERSITY

SCHOOL OF ENGINEERING

PhD THESIS

Academic Year 2010 - 2011

SHUIB HUSIN

An Experimental Investigation into the Correlation between Acoustic Emission (AE) and Bubble Dynamics

Supervisor: Professor David Mba
Co-supervisor: Dr Abdulmajid Addali

August 2011

This thesis is submitted in partial fulfilment of the requirements for the degree of Doctor of Philosophy

ABSTRACT

Bubble and cavitation effects phenomena can be encountered in two-phase gas-liquid systems in industry. In certain industries, particularly high-risk systems such as a nuclear reactor/plant, the detection of bubble dynamics, and the monitoring and measurement of their characteristics are necessary in controlling temperature. While in the petro-chemical engineering industry, such as oil transportation pipelines, the detection and monitoring of bubbles/cavitation phenomena are necessary to minimise surface erosion in fluid carrying components or downstream facilities. The high sensitivity of Acoustic Emission (AE) technology is feasible for the detection and monitoring of bubble phenomena in a two phase gas-liquid system and is practical for application within the industry.

Underwater measurement of bubble oscillations has been widely studied using hydrophones and employing acoustic techniques in the audible range. However, the application of Acoustic Emission (AE) technology to monitor bubble size has hitherto not been attempted. This thesis presents an experimental investigation aimed at exploring AEs from gas bubble formation, motion and destruction. AE in this particular investigation covers the frequency range of between 100 kHz to 1000 kHz.

The AE waveform analysis showed that the AE parameter from single bubble inception and burst events, i.e. AE amplitude, AE duration and AE energy, increased with the increase of bubble size and liquid viscosity. This finding significantly extends the potential use of AE technology for detecting the presence of bubbles in two-phase flow.

It is concluded that bubble activity can be detected and monitored by AE technology both intrusively and non-intrusively. Furthermore, the bubble size can be determined by measurement of the AE and this forms the significant contribution of this thesis.

Keywords:
Acoustic Emission, bubble dynamics, two-phase flow

PAPERS AND PRESENTATIONS FROM THIS RESEARCH

Several papers presenting the findings of this research and reviewing the application of AE in engineering have been published in international journals and presented at conferences;

Journals:

1. Husin, S., Addali, A. and Mba, D (2011) "Observation of Acoustic Emission from gas bubble inception and burst". Journal of Mechanical Process Engineering, Part E, IMechE.

2. Husin, S., Addali, A. and Mba, D. "Feasibility of using Acoustic Emission technology for on-line monitoring of flow patterns in two phase flow". Elsevier, Journal Flow Measurement and Instrumentation. (Submitted for publication on 19th July 2011).

3. Husin, S., Addali, A. and Mba, D. "Sensitivity of Acoustic Emission (AE) Technology in Monitoring Oxide Formation on an Aluminium Surface". INSIGHT-BINDT. (Accepted for publication on 17th Sept 2011).

Conferences:

1. Husin, S., Mba, D., Idris A. and Raja Hamzah, R.I. (2009). "Acoustic Emission Technology and Its Application in Industries; Machine Tools, Rotating Machinery, Rail-Track, Piping- Transportation of Two-phase Gas-Liquid". 2nd Int. Conf. on Engineering Technology, Kuala Lumpur, Malaysia, 8-10 December 2009, Penerbit Universiti, Universiti Kuala Lumpur, ISBN: 978-983-43833-1-2.

2. Husin, S., Mba, D. and Raja Hamzah, R.I. (2010). “Viability of the Application of Acoustic Emission Technology for the Process and Management of Maintenance in Industries: Defect Detection, On-Line Condition Monitoring, Diagnostic and Prognostic Tools”. International Multi Conference of Engineers and Computer Scientists, Hong Kong, 17-19 March 2010, International Association of Engineers, ISBN: 978-988-18210-5-8, ISSN: 2078-0958, pp. 1698-1706.

3. Husin, S. and Raja Hamzah, R.I. (2010). “Acoustic Emission technology as a complementary tool for providing early warnings of serious equipment problem in industrial rotating machinery: Defect detection, on-line condition monitoring, diagnostic and prognostic”. The Seventh International Conference on Condition Monitoring and Machinery Failure Prevention Technology, The British Institute of Non-Destructive Testing, 22-24 July 2010, Stratford-upon-Avon, England. ISBN 978-1-901892-33-8.

4. Husin, S. and Mba, D. (2010). “Acoustic Emission of Single Bubble Activities”. International Multi Conference of Engineers and Computer Scientists London, 30 Jun-2 July 2010, International Association of Engineers, ISBN: 978-988-18210-7-2, ISSN: 2078-0958, pp. 1466-471.

5. Husin, S. and Raja Hamzah, R.I. (2010). “Benefits and Capabilities of AE Technology: Defect Detection, On-Line and Condition Monitoring, Diagnostic and Prognostic tools for the Process and Management of Maintenance in Industries”. 23rd International Congress on Condition Monitoring and Diagnostic Engineering Management (COMADEM 2010), Nara, Japan, 28 June – 2 July, 2010. ISBN: 978-4-88325-419-4, pp. 365-372.

6. Husin, S., Addali, A. and Mba, D. (2010). “Acoustic Emission for monitoring two-phase flow”. 29th European Conference on Acoustic Emission Testing, Vienna, Austria, 8-10 September, 2010. ISBN 978-3-200-01956-0.

7. Husin, S., Folashade, A., Addali, A. and Mba, D. (2011). “Observation of slug flow using acoustic emission”. 24th International Congress on Condition Monitoring and Diagnostics Engineering Management (COMADEM 2011), Stavanger, Norway, 30 May-1 June 2011.

8. Husin, S., Addali, A. and Mba, D. (2010). “Study of the application of acoustic emission (AE) technology for on-line monitoring of bubble phenomena and flow patterns in two phase gas-liquid flow”. Sixth International Conference on Computational and Experimental Methods in Multiphase and Complex Flow, Kos, Greece, 15-17 June, 2011.

9. Husin, S., Addali, A. and Mba, D. (2010). “Acoustic frequency for bubble size correlation using AE”. Sixth International Conference on Computational and Experimental Methods in Multiphase and Complex Flow, Kos, Greece, 15-17 June, 2011.

10. Husin, S., Addali, A. and Mba, D. (2011). “An Experimental Monitoring of Aluminium Surface Degradation Using AE Technology”. Eighth International Conference on Condition Monitoring and Machinery Failure Prevention Technologies, The British Institute of Non-Destructive Testing, 21-23 June 2011, Cardiff, Wales, UK.

ACKNOWLEDGEMENTS

I would like to express my deep and sincere gratitude to my supervisor Professor David Mba, for his guidance and support throughout this research programme. His wide knowledge, experience, helpful suggestions and comments have all contributed significantly to the success of this research work.

I would like to thank the Malaysian government generally, and specifically Majlis Amanah Rakyat (MARA) and my employer, the Universiti Kuala Lumpur-Malaysian Spanish Institute for sponsorship during this Doctorate study.

Sincere thanks to my father, Hj Husin Musa who motivated me to be involved in academia and to aim as high as possible in this career, and to my mother, Hjh Samsiah Lebai Itam, my lovely wife, Rafidah Mohd Hidir and my wonderful children, Nur Aliah, Muhammad Amir, Muhammad Ali, Nur Asma and Nur Aqilah for their prayers and support.

TABLE OF CONTENTS

LIST OF FIGURES

LIST OF TABLES

LIST OF EQUATIONS

NOMENCLATURE

Symbol	Denotes
A	Smallest chord length
AE	Acoustic Emission
B	Largest chord length
cP	Centipoise(s)
d	Bubble diameter
d_{eq}	Equivalent diameter
E_b	Bubble energy
f_0	Frequency of bubble oscillation
FT	Fourier transform
FFT	Fast Fourier transform
g	Gas
GVF	Gas Void Fraction
P_g	Gas pressure
Po	Atmospheric pressure
R	Radius of bubble
R_{max}	Maximum radius

S	Scale parameters (dilation)
SNR	Signal noise ratio
STFT	Short time Fourier transform
T	Translation (time shift variable)
t	Time
U	Electrical energy
U_B	Potential bubble energy
U_{mf}	Incipient fluidization rate
V	Voltage
VSG	Superficial gas velocity
VSL	Superficial liquid velocity
WT	Wavelet transform
α	Upper limit of integral
σ	Surface tension
ρ	Fluid density
γ	Polytrophic gas index
ω_i	Image frequency
ω_p	Pump frequency
π	Pi (Value=3.14)

ψ	Basic function
ψ^*	Complex conjugate
$\psi(t)$	Wavelet

1 INTRODUCTION AND THESIS STRUCTURE

1.1 Introduction

This chapter starts with a broad definition of bubble dynamics specifically in the context of this research. A brief of problem statement that led to the selection of the research topic is discussed. It is followed by presenting a general view of bubble and cavitation phenomena and the relevant acoustic techniques for either detection or measurement of bubble size. This is then followed by the identification of the research topic based on available published work, and finally the aims and objectives identified for the purpose of the research programme are detailed.

1.2 Definition of bubble and bubble dynamics

A bubble, as defined by The Concise Oxford Dictionary, is an air-filled cavity in a liquid. Physically the appearance of a bubble means the existence of a closed surface which divides the regions of liquid and air. This dividing closed surface is usually called the bubble wall (Hsieh, 1965). Bubble dynamics are defined as studies of the behaviour of bubbles and their interactions with the surrounding liquid (Hsieh 1965). Bubble dynamics also refer to the way bubbles grow and collapse though they can also be used to refer to any motion of the bubble such as oscillation (Hsieh, 1965; Plesset and Prospretti, 1977; Hirt, 1991; Sathyam et al, 1995; Farhat et al, 2006). In this investigation programme, the words ‘bubble dynamics’ refer to bubble formation at the nozzle and burst at the free surface. These two events are associated with the acoustic emission (AE) at high frequency range (100 kHz – 1 MHz) are measured using AE transducers.

1.3 Problem statement

The cavitation/bubble phenomenon consists of the formation, coalescence and collapse of vapour or gas bubbles in a liquid due to pressure gradients under either static or dynamic conditions (Szkodo, 2006). The most obvious consequences of cavitation are high levels of noise and vibration, and loss of efficiency of the system. The cavitation process often involves large fluctuating forces and if the frequency content of these fluctuations matches one of the natural frequencies of part of the machine or equipment, severe vibration with premature ageing and possible breakage may result. Eventually, cavitation will damage the internal surfaces of fluid-carrying components, such as a pump's blade or a ship's propeller, by removing material from the surface, as well as premature failure of seals and bearing damage (Neill et al., 1997; Szkodo, 2006). Cavitation damages all types of solids, brittle or ductile, hard and soft, chemically active or chemically inert (Brennen, 1995; Leighton, 1994a; Plesset, 1966; Hammit, 1966).

Investigation of the cavitation phenomenon using a single gas bubble produced under laboratory conditions provides a means to understand the physics of bubble activities: formation, coalescence and collapse/burst. The bubble formation at the nozzle, coalescence in the liquid and burst at a free surface are the potential sources for acoustic emission (AE) and this will be proved during this investigation. These events generate transient pressure pulses that are broadband in nature which it is expected can be detected by an AE piezoelectric sensor. The stress or pressure change in a material/medium (solid or liquid) excited by external force or any process which can strained the structure or resulted surface wave (shock wave) to the material/medium, can be detected by an AE piezoelectric transducer/sensor and convert this AE activity into an electrical signal/output.

The energy of bubble collapse is a function of bubble properties and liquid properties (Divoux et al., 2008); this is because bubble activities such as inception, coalescence and burst, definitely occur in a liquid and are dependent

on the bubble's properties such as size and shape including cusp length immediately before burst. Thus it is possible to measure the bubble radius using the measured sound emitted by a collapsing bubble using appropriate sensors such as AE sensors and hydrophone (Brennen, 2011; Divoux et al., 2008). This may suggest that if bubble collapse is associated with a transient pressure pulse, then it may imply that measurement of the AE at bubble collapse will allow an estimate of bubble size.

The techniques of photography (such as high speed camera, x-ray) and ultrasonic (such as ultrasound probe; where the attenuation of ultrasound transmitted, Doppler technique; where the waves reflected back from the bubble surface) have been used to determine bubble size but have a number of disadvantages, such as limitations with very small bubbles and being limited only to the local size measurement. In addition, analysis of photographs is expensive (needs a high speed camera), tedious, impractical in many cases (e.g. in opaque conditions such as crude oil, and in steel pipes or containers), and is of arguable accuracy (Pandit et al., 1992).

Two-phase gas-liquid flow plays an important role in many industrial applications particularly in the oil and gas industries. This type of flow is complex with such key parameters as slug flow and gas void fraction (GVF); and thus requires a robust technique for their measurement (Kuwahara and Yamaguchi, 2007). The application of AE technology as a monitoring tool in two-phase gas-liquid flow is in its infancy; however, it is now gaining attention, given the advantages of AE technology over other measuring techniques, such as the ability to be fitted non-intrusively to pipes or containers. There are, therefore, strong reasons why a robust, non-invasive and effective detection and measurement technique for the monitoring of two-phase flow should be developed to provide a better understanding of gas-liquid flows.

1.4 General overview

The scientific study of the dynamics of small bubbles may be considered to have begun in 1917 with the work of Lord Rayleigh (1917) who derived the potential bubble energy (U_B) associated with bubble radius, (De-Bosset et al., 2007; Xu et al., 2004; Shangguan et al., 1997; Plesset, 1966; Gaitan, 1990).

In certain industrial processes, on-line or in-process monitoring of bubble activities such as formation, coalescence and collapse/burst is necessary and control of these parameters is important and could benefit from the development of new, more sensitive, yet robust acoustic techniques.

Recently, the application of acoustic techniques to fluid flow in pipelines has gained attention as a research technique for investigating liquid flow parameters and cavitation (Evans et al., 2004; Al-Lababidi et al., 2009). The application of AE technology has been extended to liquid-transportation pipelines where GVF is a parameter of great interest and has been successfully correlated with absolute AE energy and slug velocities (Al-Lababidi et al., 2009, Addali, 2010). Whilst it is known that the process of bubble collapse in pumps (cavitation) can be observed with AE, no attempt to date has specifically related AE to determining the size and the mechanics of bubble formation, propagation and collapse of a single bubble.

It is interesting that the application of acoustic techniques can be used to characterise liquid (surface tension and density) from the measurements of bubble activities (Sinha, 2003, 2006). Sinha (2003 and 2006) demonstrated the inter-correlation between bubble resonance frequency, terminal velocity and shape oscillation frequency to the surface tension and density of the host liquid. Liquid viscosity possibly can be determined using measurable bubble data (e.g. AE bubble activity). Acoustic techniques are capable of extracting information from bubble activities and currently hydrophones (frequency range up to 200 kHz for typical audio work) are widely used in detecting sound underwater and for bubble sizing (Leighton, 1994a). However, hydrophones are an intrusive

method. An alternative acoustic technique is to use an ultrasonic system consisting of a transmitter and receiver. However, such an active method where a transmitter is needed, tends to be relatively more complicated to set up and more expensive than passive AE technology.

Use of AE technology as a tool for in-process monitoring, condition monitoring and non-destructive tests is well recognised and established for machine structures, bearings and gear systems (Miller and McIntire, 1987; Al-Ghamdi and Mba, 2006; Toutountzakis et al., 2005; Al-Dossary et al., 2008, 2009; Al-Ghamdi et al., 2004; Elforjani and Mba, 2009; Tan and Mba, 2005; Tan et al., 2005; Raja Hamzah and Mba, 2007, 2009; Bruzelius and Mba, 2004). Interestingly, some initial investigative work carried out at Cranfield University has shown that AE technology can be used as an on-line monitoring and measurement tool for bubble phenomena in liquid flow or two-phase gas-liquid flow systems (Al-Maskari, 1985; Al-Fayez, 2004; Al-Fayez and Mba, 2005; Al-Lababidi et al., 2009; Addali, 2010; Husin and Mba, 2010).

A summary of other acoustic techniques used in relation to cavitation/bubble phenomena are shown in Table 1-1 (page 6). In this study programme, a simple, non-invasive technique for detection, measuring and monitoring of gas bubbles was developed specifically for two-phase gas-liquid flow systems and process equipment where it could provide a new reference for single gas bubble or cavitation bubble studies employing AE technology.

Table 1-1: Summary of bubble investigation techniques used

Acoustic Technique	Published Work	Parameter investigated
Hydrophone	Leighton and Walton, 1987; Leighton et al., 1991a, 1991b; Pandit et al., 1992; Leighton et al., 1993, 1996; Boyd and Varley, 2004; Kolaini, 1999; Holler et al., 2003; Tien et al.,2007; Manasseh et al., 2007, 2008	Bubble oscillation, bubble formation, coalescence and collapse/burst
Microphone	Divoux et al., 2008	Bubble burst
Ultrasonic	Al-Lababidi and Sanderson, 2004	Gas void fraction
Acoustic Emission (AE)	Al-Maskari, 1985; Al-Fayez, 2004; Al-Fayez and Mba, 2005; Neill et al., 1997; Al-Lababidi et al., 2009; Addali, 2010; Husin and Mba, 2010	Incipient cavitation, Developed cavitation, correlation AE with Gas Void Fraction, Bubble inception and burst

1.5 Identification of research topic

Boyd and Varley (2004), and Sinha (2006) have described how the radius of a bubble in a liquid can be determined by acoustic techniques, and that an enormous advantage of the technique is that it can be used in opaque conditions. Boyd and Varley (2004) used a Bruel and Kjaer 8103 hydrophone which has a frequency range between 0.1 and 100 kHz, whilst Sinha (2003, 2006) used a hollow cylindrical piezoelectric transducer (2.55 cm long, 2.30 cm inner diameter, 1.20 mm thick, Boston Piezo-Optics, Mass) with frequency ranges up to 5 kHz. The application of acoustic techniques to measure a bubble radius began in 1933 when Minnaert (1933) generated air bubbles from a nozzle underwater and showed that bubble oscillation frequency was associated with the volume pulsation of the bubble. He compared the frequencies of the sounds emitted by bubbles with the frequency of sounds from

tuning forks (acoustic resonator in the form of a two-pronged fork formed from a U-shaped bar of steel) and established “Minnaert’s natural frequency bubble oscillation formula”, see Eq 2-6 (page 30). Strasberg (1956) showed an oscillogram of the sound pulse from an individual gas bubble released from a nozzle synchronised with a high-speed camera, see Figure 2-6 (page 23) which shows linear sound pressure from a monopole source. This demonstrated that the sound starts just as the bubble closes (pinches off) and separates from the nozzle.

To date, much research has used hydrophones to measure sound underwater or sound emitted from bubble oscillations in water (Leighton and Walton, 1987; Leighton et al., 1991a, 1991b; Pandit et al., 1992; Leighton et al., 1993, 1996; Boyd and Varley, 2004; Kolaini, 1999; Holler et al., 2003; Tien et al., 2007; Manasseh et al., 2007, 2008). A more recent acoustic technique to detect cavitation or bubble in a liquid is to use high frequency Acoustic Emission (AE) technology. For example, Al-Maskari (1985) employed AE technology to detect cavitation in a centrifugal pump where he was successful at detecting developed cavitation. Neill et al. (1997) demonstrated that AE was capable of detecting incipient cavitation and this was confirmed by Al-Fayez and Mba (2005). In 2002, Yen and Lu demonstrated that an AE detection system combined with an artificial neural network could successfully recognise four major flow patterns: bubbly, slug, churn and annular, in a vertical air-water flow column. Recently, Al-Lababidi et al. (2009) and Addali (2010) successfully correlated AE with GVF in two-phase gas-liquid flow in a horizontal pipeline.

Successful studies have used high frequency AE technology for cavitation detection but no real attempt has been made to use AE for measuring bubble size. It is the goal of this work to investigate the use of AE in this regard. The strategy proposed was focused on measuring AE from bubble activities and to establish correlations between AE and bubble size. The strategy proposed was (see Figure 1-1);

1) Strategy 1 (1st trial): to detect frequency of bubble oscillation, f_0, with AE sensor during its initial stages as it rises through the liquid, to determine bubble radius using Minneart's natural frequency bubble oscillation formula, see Equation 2-6 (page 30) [Minneart, 1933; Leighton, 1994]:

2) If the first line of investigation on detection of bubble oscillation was not successful, an attempt then would be made focused on measuring AE from the other bubble activities during its evolution (e.g. formation at a nozzle and burst at free surface). Strategy 2 and 3 (2nd and 3rd trials): to establish correlations with bubble size.

The research strategy adopted is shown in detail in Figure 1-1.

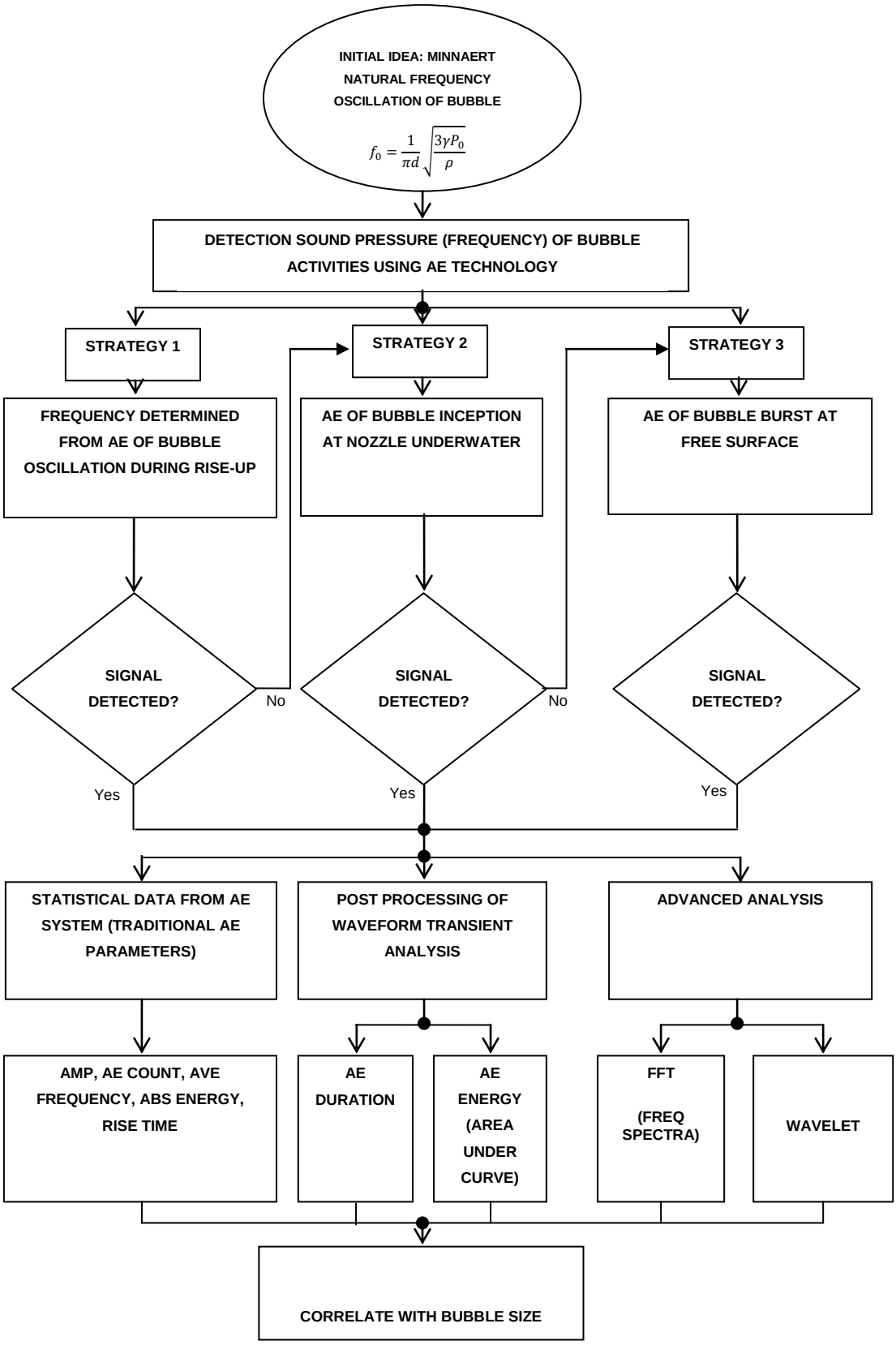

Figure 1-1: Research Strategy

1.6 Main contributions of the present work

- First known attempt at applying AE technology to single bubble detection and sizing.
- Establish a correlation between AE energy and bubble size for a defined liquid viscosity.
- The findings formed the basis for assessing the applicability of AE to monitoring gas content in multi-phase flow.
- Provide a new reference of the application of AE technology for a single bubble sizing.

1.7 Research aim and objectives

The aim of this research programme is to develop an AE technique able to monitor bubble size and detect and quantify the dynamics of a single bubble in a vertical liquid-filled column.

In support of the aims of this study the following objectives are proposed:

1) Carry out a literature review of previous work in this area,
2) Design and build an experimental rig to allow the study of artificially created bubbles,
3) Establish a measurement/test procedure,
4) Ascertain if AE can detect the bubble inception and burst,
5) Analyse AE parameters generated from various bubble sizes,
6) Measure AE energy released from a single bubble during its inception and burst at the liquid free surface,
7) Investigate the influences of liquid viscosity on the AE energy during bubble formation and burst,
8) Identify the critical/key AE parameters for indicating bubble activities, and

9) Establish correlations between AE energy emitted by a single bubble burst with other parameters tested.

It is believed that the outcomes of this research will make a significant contribution towards the advancement of AE technology as a measuring tool for bubble sizing and void fraction, detection of cavitation phenomena and monitoring flow in a two-phase system.

1.8 Thesis Structure

Chapter 2 gives overview of the bubble: the definition of a bubble, bubble pressure model and its association with ‘cavity’. This chapter also presents a classical oscillogram of the sound pulse from a gas bubble leaving a nozzle detected by using a hydrophone, which is justification to explore the application of AE technology to single bubble activity. Lastly, a brief introduction is given to bubble activity, inception and burst, followed by shockwave mechanism which is useful for pressure pulse detection in a liquid.

Chapter 3 deals with AE: it commences with the definition of AE and includes AE history and technology. A brief discussion of AE signal and source types is provided before detailed definitions of AE parameters are given. This chapter also presents a brief overview of the applications of AE technology. A discussion of signal processing methods for AE waveform analysis is also presented which includes fast Fourier transforms (FFT) and Wavelet transform (WT). The limitations and advantages of each method over the others are discussed. The advantages and disadvantages of AE technology are listed at the end of this chapter.

The experimental rig used in this work is described in **Chapter 4**. The components and devices used in the bubble test rig such as nozzle sizes, liquids used and gas injection methods in creating bubble, are described. The

data acquisition system, procedure set up of sensors and the calibration process are also covered in this chapter. The procedures involved in test rig design, set-up and measurements are discussed in **Chapter 5**.

Chapter 6 presents the main results and observations. Detailed discussion on the investigated parameters is presented in this chapter, including the best and most reliable indicators from the AE system for bubble detection. Results from post-processing such as average AE duration and average AE energy are also presented. Trend comparisons of plots from the waveform analysis and post-processing methods are discussed and conclusions drawn from the effect of nozzle sizes used in the experiments and correlation to the AE burst event.

A brief description of the main findings of the project is given in **Chapter 7**. Recommendations for future work are made in **chapter 8**.

2 BUBBLE CHARACTERISTICS AND ACOUSTIC MEASUREMENT

This chapter provides a background of bubble characteristics and activity, particularly bubble inception at a nozzle and burst at free surface. Previous work measuring bubble size using audible acoustic techniques will also be discussed in this chapter.

2.1 Background

When a bubble experiences a relatively small change in volume, it undergoes non-inertial cavitation and emits a linear acoustic pressure wave (Leighton, 1996). Examples of the generation of such passive emissions are when a bubble is injected into a liquid, or a bubble fragments or when a bubble is excited by an external acoustic field (however, this latter case is more complicated and will include scattering which may be linear or even non-linear, in which case the scattered acoustic signal will include harmonics and combination frequencies) (Leighton, 1994a and 1994b; Leighton et al, 1993). All such emissions can be used to not only detect the presence of a bubble but also to determine its size since they are related to the natural resonant frequency of the bubble.

Bubble formation and cavitation are common phenomena in many industrial processes that involve gas-liquid systems or liquid flow, such as industrial processes which utilise gas or water jets blowing into a liquid to provide stirring processes, and gas-liquid flow is especially common in chemical processing plants. However, while cavitation may not affect the surface integrity of a liquid, the collapse of cavitation bubbles near the wall or other surfaces can cause rapid surface erosion, known as ‘cavitation damage’. In liquid-mass transportation industries, cavitation is a major contributor to failure and inefficiency in industrial pumps (Neill et al., 1997). While in fluid power systems

such as in gas-lift pumps, cavitation will cause vibration, noise, reduced efficiency and erosion at the valve surface (Rydberg, 2001).

One particular item of interest in this programme was the investigation of AE energy radiated from the bubble burst. A cavitation/gas bubble has potential energy which depends on the pressure within it and its volume. Weninger et al. (1999) stated that bubble-collapse generates some magnitude of energy in the form of a shockwave and its pressure pulse can be measured by transducers. It is possible to correlate pressure pulse from bubble activity with bubble size; in other words, by measuring the size of the bubble using an acoustic technique. Some bubble activities are believed to be potential sources of AE and the acoustic energy radiated from the bubble (or bubble resonant frequency) can be used to determine certain properties of the surrounding liquid (Sinha, 2006). In this programme, an attempt was made to use high frequency AE technology over the frequency range 100 kHz to 1 MHz to detect bubble activities and correlate them with bubble size.

Gas bubbles and cavitation bubbles are physically different in terms of their inception and gas pressure inside the bubble. A gas bubble has a given mass of gas inside it and its internal pressure will vary according to gas polytropic law ($PV^n=C$); where P is the pressure, V is volume, n is the polytropic index which has a value of unity in an isothermal process and a value of γ in a reversible adiabatic process, and C is a constant (Leighton and Walton, 1987). This equation is used to characterise process of certain systems, e.g. the compression and expansion of a gas (Eastop and McConkey, 1993). If the dynamics of a bubble are under constant volume conditions such as bubble oscillation, the process is said to be isentropic where γ is called the ratio of the specific heats of the gas enclosed in the bubble ($\gamma = c_p / c_v$), the ratio of specific heat at constant pressure (c_p) to the specific heat at constant volume (c_v) (Devin, 1959).

Cavitation bubbles or vapour bubbles contain no permanent mass of gas to determine the internal pressure. Neppiras (1980) differentiated cavitation into

four simple models: (1) *gas-stable cavity*, (2) *gas-transient cavity*, (3) *vapour-filled stable cavity* and (4) *vapour-filled transient cavity*. He noted stable cavities are bubbles that oscillate non-linearly around some equilibrium size, are relatively permanent and may continue oscillating for many cycles of the acoustic pressure. Transient cavities generally exist for less than one cycle, and then they collapse violently. Gas content within a bubble provides substantial damping during the collapse and so the speed of the liquid generated during the bubble collapse is considerably reduced with much less impingement force on solid surfaces (Leighton, 1994a; Brennen, 1995).

Vokurka (1990) and Rydberg (2001) noted that *cavitation* comes from *bubble* formation due to pressure drop induced by the fluid flow. While Baker et al. (2001) claimed that the term cavitation can be used to describe any *bubble phenomena*, and further simplified the term cavitation to mean the formation and life of *bubbles* in liquids. Neppiras (1980) also noted that some would say that *cavitation* occurs whenever a new surface is created in the body of a liquid. While Lauterborn and Ohl (1997, p.65), defined *cavitation* as "*the name given to the phenomenon of rupture of liquid and the effects connected with the motion of the cavities thus generated*." A rupture is the formation of a macroscopic or *visible bubble* (Ross, 1976).

According to Gaitan (1990), cavitation was first predicted by Leonhard Euler in 1754 when he suggested that negative pressures could be generated if the local velocity in a liquid was high enough and might 'break' the liquid. This 'breaking' phenomenon was given the name *cavitation* in 1895 by Froude to describe the appearance of voids and clouds of bubbles around propellers. Since then, the term *cavitation* has been used to describe the bubble phenomenon that appears when liquids are sufficiently stressed (e.g. in pumps, hydraulic systems, and propellers).

2.2 Bubble pressure model

The pressure inside a bubble and pressure in the surrounding liquid are related by the size of the bubble and bubble's surface energy (surface tension). Following the argument used by Leighton (1994), consider Figure 2.1 where the bubble is divided into two halves.

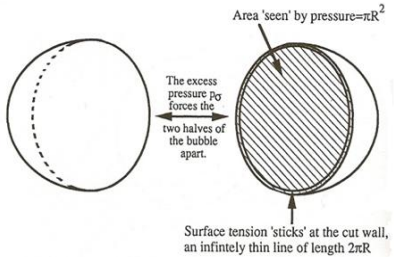

Figure 2-1: A bubble 'cut' in half, illustrating the effect and pressure due to surface tension (Leighton, 1994)

The cross-sectional area of the bubble is πR^2, where R is the radius of the bubble. The excess pressure in the bubble (internal pressure – pressure in the surrounding fluid) is P_{σ}. Assuming static conditions, the force acting over the cross-sectional area of the bubble will be $\pi R^2 P_{\sigma}$. This force acts to push the two halves of the bubble away from one another. The force which balances the excess pressure and keeps the bubble stable in size is called the surface tension.

Leighton, (1994, p.68) gives the tradition definition of surface tension, σ, as "*numerically equal to the force per unit length acting perpendicular to one side of a straight line in a liquid surface*." Here, of course the bubble has only one surface so the surface tension force acting over the line of the imaginary cut is $2\pi R\sigma$.

Thus:

$2\pi R\sigma = \pi R^2 P_\sigma$ **(2-1)**

Which gives

$$P_\sigma = \frac{2\sigma}{R} \quad \textbf{(2-2)}$$

The excess pressure inside a bubble which results from surface tension is also known as the *Laplace Pressure*. Eq. 2-2 shows that the smaller the local radii of curvature, the stronger the Laplace pressure, thus in the early stages of formation the internal pressure in cavitation bubbles can be very high.

Investigation on a single vapour or gas-bubble provides a means to understand bubble physically and theoretically (e.g. cavitation dynamics, energy of cavity when collapsing, cavitation noise and effect of liquid properties such as viscosity and surface tension on cavitation dynamics). It is useful here to review some basic formula that relate the pressure within and surrounding a bubble. A comprehensive theoretical analysis of bubble physics and dynamics can be found in Lautherborn (1976), Plesset and Prosperetti (1977), and Leighton (1994).

The Laplace pressure is dependence on the size of bubble. The resultant force due to the surface tension acts radially inwards to balance the force due to the internal excess pressure and has a role in ‘confining’ the gas (Leighton, 1994). Lautherborn, (1976) and Leighton (1994) have provides some relevant analysis (pressure model) for bubbles which contain both gas and vapour, See Figure 2-2 (page 18).

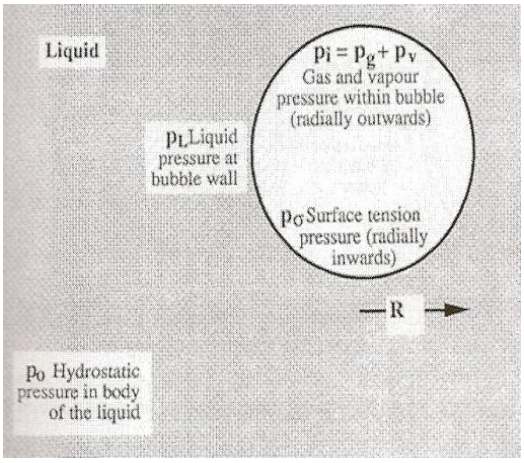

Figure 2-2: Bubble model (Leighton, 1994; Lautherborn, 1976)

If the internal pressure due to the gas has subscript $_g$ and internal pressure due to vapour has subscript $_v$ then from Dalton's law of partial pressures it follows at once that the total internal pressure P_i must be:

$$P_i = P_g + P_v \tag{2-3}$$

The total internal pressure must be the sum of local pressure in the liquid, which is assumed to be uniform over the surface of the bubble, and the excess pressure within the bubble:

$$P_i = P_L + P_\sigma \tag{2-4}$$

Because of the action of surface tension, the pressure inside the bubble is higher than that outside. However, the pressure immediately outside the bubble can be reduced below atmospheric (by e.g. local turbulence in the fluid), and if the difference in pressure between the inside and outside of the bubble exceeds the surface-tension effects, then the pressure inside (p_i) the bubble will be low enough for rapid vaporization to take place and rupture will occur. The pressure drop across a stationary free surface due to surface tension is, of course, given by Eq. (2-2) (page 17) (Leighton, 1994):

Rayleigh's theory takes the pressure just outside the bubble wall as equal to that inside the empty cavity. This is true for a vapour bubble/cavity in a relatively cold liquid (Rayleigh, 1917) where the pressure inside a static vapour bubble is given by:

$$P_i = P_v + p_g = P(R) + \frac{2\sigma}{R} \quad \textbf{(2-5)}$$

2.3 Bubble Formation Mechanisms

Figure 2-3 (page 20) shows the techniques for creating a single bubble in a water column; Minnaert (1933) used a steady flow of air; Leighton and Walton (1987) used a micrometer to achieve the gradual depression of a syringe; and, Longuet-Higgins et al. (1991) used an air bleeding technique via a syringe connected to a three-way valve. A constant-volume formation for a bubble and repeatability of bubble size produced can be achieved by gradually pressing the syringe's plunger as illustrated in Figure 2-3 (ii) (Leighton, 1994a).

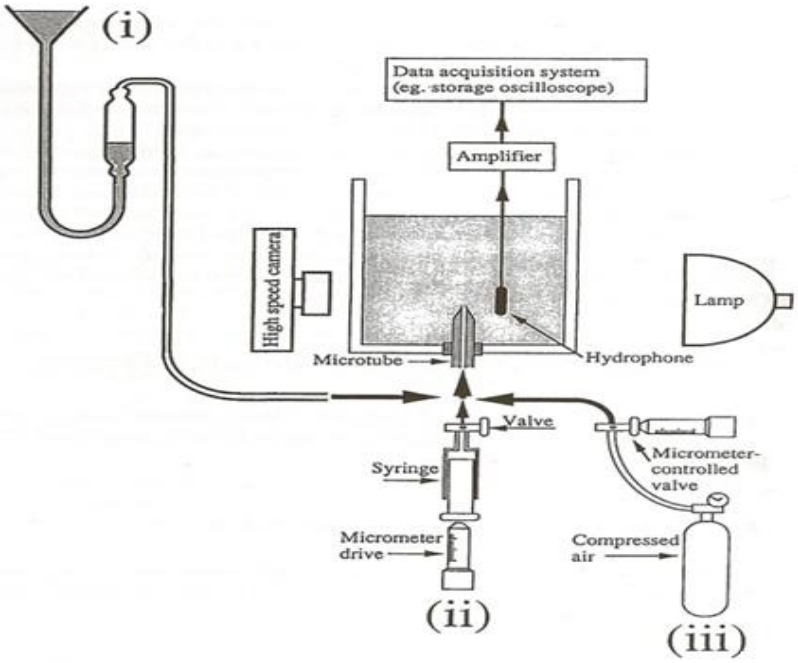

Figure 2-3: Three gas flow techniques for a single bubble formation (Leighton, 1994a); (i) Minnaert (1933) (ii) Leighton and Walton (1987) (iii) Longuet-Higgins et al. (1991)

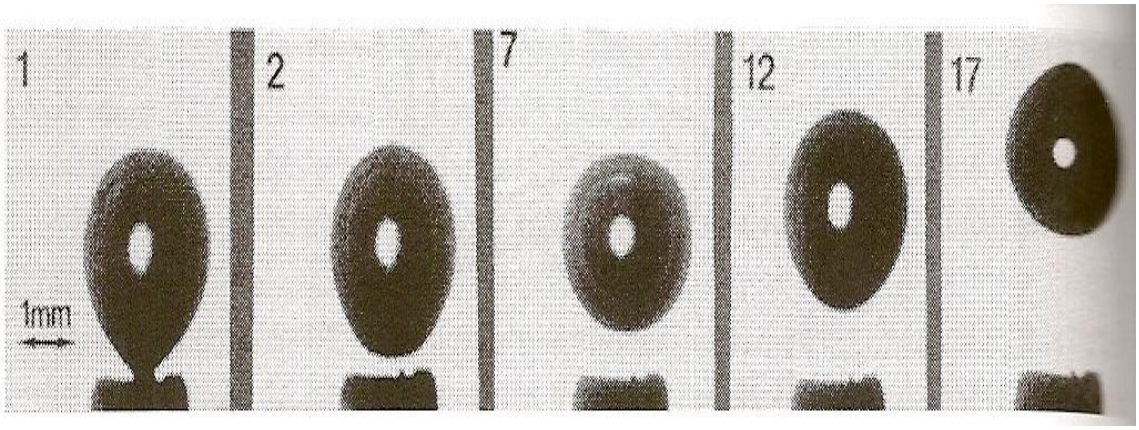

Figure 2-4: Photograph with inter-frame 0.71 m/s (Leighton et al., 1991a)

Gradual depression of syringe plunger connected to a nozzle produces a single gas bubble as shown in Figure 2-4. As the bubble grows, the pressure within it tends to drop owing to the increase in its radius and decrease in Laplace

pressure (see Equation 2-2, page 17). In addition, of course, there will be hydrostatic effects due to the upward displacement of the bubble's centroid (Longuet-Higgins et al.,1991). The bubble will grow larger which then causes the velocity through the gas-solids interface to decrease to the value of *Incipient fluidization rate (U_{mf})* and thereafter if the void were to grow larger its surface would no longer be stable (Davidson and Harrison, 1971). *Incipient fluidization rate (U_{mf})* is defined as the minimum flow rate for initial bubble formation: "*any flow in excess of U_{mf} will traverse up through the bed in the form of what one would unhesitatingly describe as bubbles*" (Davidson and Harrison, 1971, p.12). Once the void at the grid hole has reached its upper limit of size, the void wall is pressured from all sides by the surrounding fluid. The 'neck' of the void becomes the weakest region of the interface and eventually collapses due to the effect of the force of the liquid pressure at the 'neck' causing bubble pinch-off at the nozzle (Longuet-Higgins et al., 1991; Davidson and Harrison, 1971). Longuet-Higgins et al. (1991) illustrated the development of a bubble through a nozzle underwater as shown in Figure 2-5 (page 22). This is an illustration of the sequence of bubble shapes released underwater. It shows two stages of volume change over the radius of curvature; the first is a steady volume increase as radius R decreases (from R1.0 to 0.5, R is the radius of curvature of the upper surface). The second is a sharp increase in volume with little accompanying change in R. The volume continues to increase until (R0.65) the tangent at the neck becomes vertical. The volume will reach a maximum and if further air is forced in (at R0.652) the bubble must break off/pinch-off.

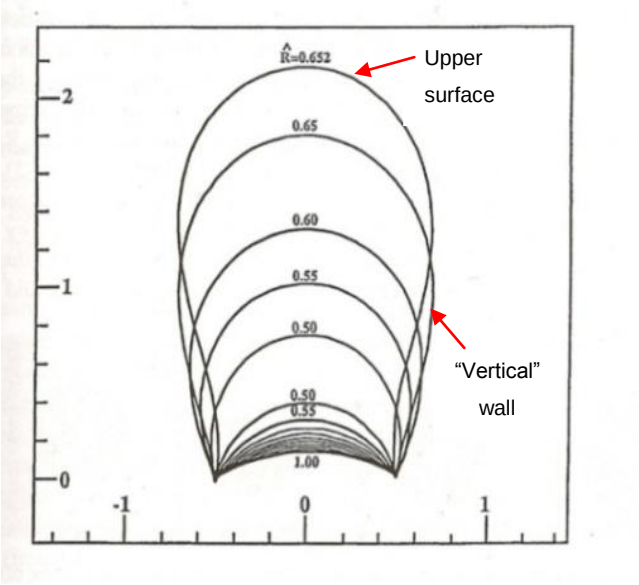

Figure 2-5: Successive bubble profiles emerging from a nozzle of diameter D=1.0 (dimensionless units) (Longuet-Higgins, 1991)

Clearly, once the bubble breaks away and begins to rise up through the water it can be seen that the bubble deviates from the spherical. This shape change during rising up is one of bubble oscillation, which can be referred to as "shape oscillation during rise-up". The shape of the bubble rising up keeps on changing due to the drag forces exerted on the top of the bubble's wall. However, the bubble volume does not change. The mode shape during bubble rise up is similar to mode 2, see Figure 2-11(page 30).

Strasberg (1956) recorded simultaneously high speed photographs of the inception of a gas bubble at an underwater nozzle and the oscillograph of the accompanying sound. His recorded work is shown in Figure 2-6 (page 23). The oscillograph shows that highest sound pressure occurs at the moment of gas bubble pinch-off and detachment from the nozzle. Later studies by Manasseh et al. (2001), and Deane and Czerski (2008) have shown the same observation supported by a series of photographs and corresponding acoustic signal, as shown in Figure 2-7 (page 24). Manasseh et al. (2001) and Deane and Czerski

(2008) have investigated AE signals from bubble inceptions and synchronised them with a high speed camera. Deane and Czerski (2008) also recorded bubble detachment from a nozzle tip with its concurrent pressure amplitude signal, see Figure 2-7 (page 24). The first image of the still picture shows the bubble shape immediately prior to pinch-off at the neck and there is very little acoustic pressure as indicated by the signal. The second image, which was taken 160 µs after pinch-off, implies a rapid collapse of the bubble neck resulting from the first pressure minimum. While the third image, taken 320 µs after detachment, shows a small re-entrant jet of water forming within the collapsing neck and it is this which gives the highest acoustic pressure amplitude.

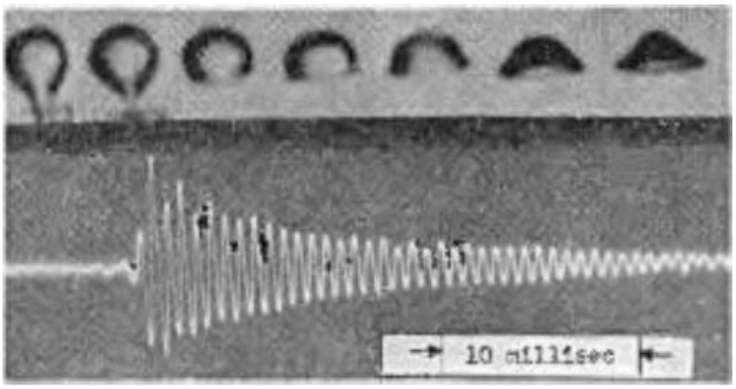

Figure 2-6: Oscillogram of sound pulses from an individual gas bubble leaving a nozzle (Strasberg, 1956)

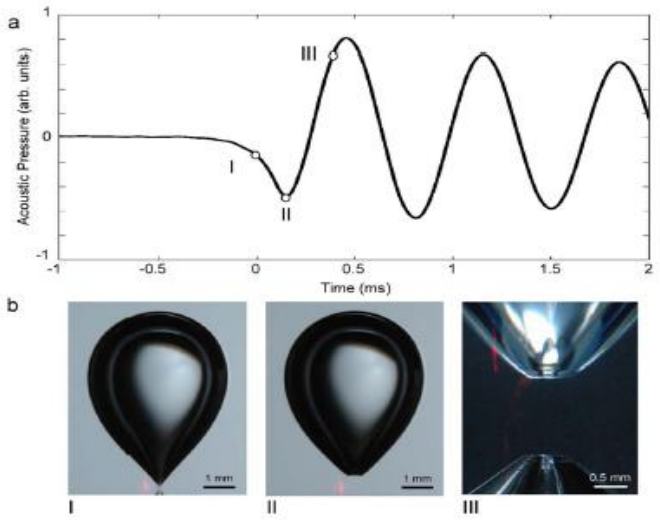

Figure 2-7: Acoustic emission and bubble release at a nozzle underwater (Deane and Czerski, 2008).

Both Figures 2-6 and 2-7 show the sound pressure of a bubble pinched off and detached from the nozzle with non-dimensionalised in the chart; the unit of acoustic pressure for the amplitude of the output plot commonly are dB, Volt and Pascal according to the device used.

The highest AE is always noticed as the bubble detaches and this corresponds to the retraction of the broken tip of the neck (Manasseh et al., 2001). This phenomenon and the dynamics of bubble inception are very different from free surface bubble burst dynamics, which might appear violent but the energy transmitted back to the liquid is less than at bubble inception at the nozzle.

Neill et al. (1997) postulated that the energy density associated with bubble inception is rather high and involves an associated shock which can be detected by a non-intrusive AE sensor. The energy released from bubble inception at pinch-off and detachment from the nozzle's end causing pressure/shock waves in the surrounding liquid (Kloeppel, 2002). This bubble formation event at the instance of bubble pinch-off is the origin of AE which can be detected due to liquid stress/pressure changes (Strasberg, 1956; Manasseh et al., 2001; Dean and Czerski, 2008).

2.4 Bubble Burst at Free Surface

Bubble burst at the free surface is the last evolution of bubble life in two-phase gas-liquid systems. This phenomenon is apparent in almost any industrial reactor or tank which deals with a two-phase gas-liquid system. Energy released by bubbles bursting might be related to bubble size and liquid properties, and could be interesting areas to be explored.

A collapsing bubble at a flat, free surface generates two jets in antipodal directions: the first jet across the bubble inwards to the liquid and a counter jet out of the free surface. Observations have shown that the counter jet out of the free surface is more violent and, according to Neill et al. (1997), its velocity can be as high as 110 m/s. The first jet moves the bubble wall inwardly towards the opposite wall in the liquid where the compression eventually forces the generation of a violent jet to the open space above the free surface.

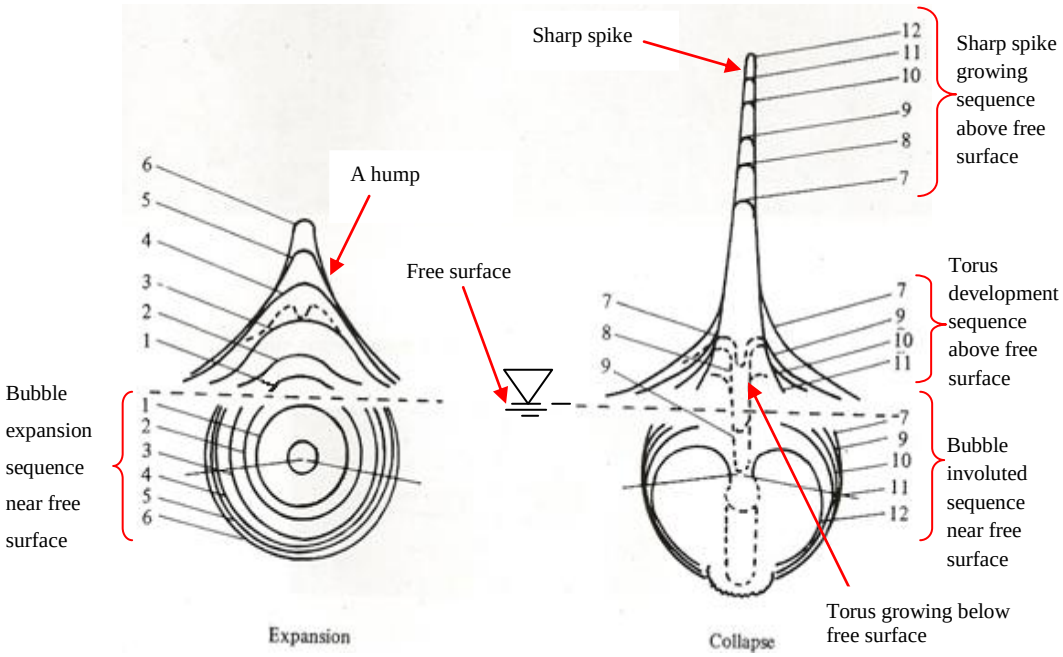

Figure 2-8: Collapse near a free surface showing antipodal directions of jets; micro jet crosses the bubble down along axis of symmetry and counter jet out of free surface (Blake and Gibson, 1981)

The dynamic of bubble collapse near a free surface was well elucidated by Blake and Gibson (1981), see Figure 2-8 (page 25). During the expansion, the bubble elongated along the axis of symmetry and caused surface distortion where a hump at the free surface can be observed. This hump evolves into a sharp spike that continues to grow along the axis of symmetry in the resulting bubble collapse. The development of this spike is concurrent with the torus formed by involution of the bubble until the bubble reached its minimum size. The numbering in Figure 2-8 is the sequence of bubble expansion and collapse near a free surface. The bubble becomes involuted from above as indicated by sequence No. 7. More concisely, the dynamic of bubble collapse involves bubble expansion where it develops a hump at the free surface which then grows to form a sharp spike and then the base involutes by the formation of a very slender jet that moves with great speed down the axis of symmetry in the opposite direction to the growing free surface spike. The dotted line represents the torus formed by involution of the bubble until it reaches the lower side of the bubble before the collapse is complete.

Rayleigh (1917) noted that the interest of researchers in sound generated by cavitation was due to the engineering problems caused by cavitation, for example, in screw-propellers and their effects on rigid boundaries. Ross (1976) and Kloeppel (2002) noted that the pressure wave from a bubble collapse in a liquid could cause shock waves in the surrounding liquid.

De-Bosset et al. (2007) observed that at the moment of cavity collapse, the emission of a high pressure front radiates from the collapse centre. They used a pressure sensor to record pressure changes due to bubble activities and their results confirmed the association of pressure peaks with the shockwaves emitted at cavity collapse. Bubble coalescing, i.e. a short pulse of sound, is also generated (Tse et al., 1998; Manasseh et al., 2008, 2007; Strasberg, 1956).

An ideal cavitation bubble collapsing in an ideal liquid contracts in size, then springs back, only to contract again, oscillating through a series of growths and collapses until it finally disappears (Farhat et al., 2006). A real cavitation bubble,

however, undergoes only a single cycle because the bubble breaks up into many smaller bubbles; the shock waves generated at the bubble collapse are spatially confined, which leads to the formation of a number of micro bubbles (Ross, 1976; Farhat et al., 2006). The presence of permanent gas content in the bubble will play a major role in bubble collapse because it provides a cushion for final collapse, storing some of the kinetic energy of the rapidly collapsing bubble (Ross, 1976). Thus, bubbles do not collapse completely to zero radius but instead to a minimum radius that may be from 2% to 10% of their maximum radius. The temporal progress of a bubble with respect to its radius is shown in Figure 2-9, where the plot depicts the rebound of micro-bubbles with some gas content. The plot for growth and collapse of an empty bubble (cavitation bubble) is shown in Figure 2-10 (page 28).

Gas bubble and cavitation bubble (vapour bubble) are two different types of bubble. The only difference is the vapour or gas content inside the bubble; with vapour the bubble grows and collapses much more readily and rapidly and so the bubble dynamics are different. While, gas content provides a damping during bubble burst and it effects such as pitting and surface erosion to a metal surface are less compared with cavitation/vapour bubble.

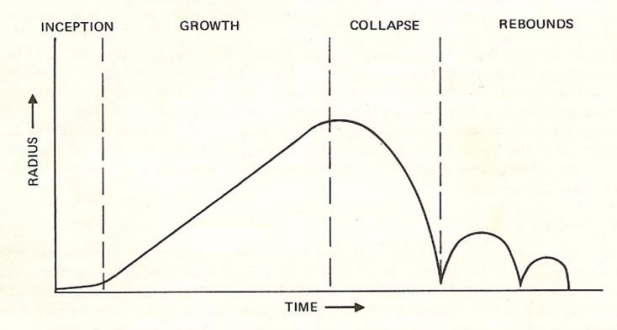

Figure 2-9: Growth and collapse of a gas bubble having finite gas content (Ross, 1976)

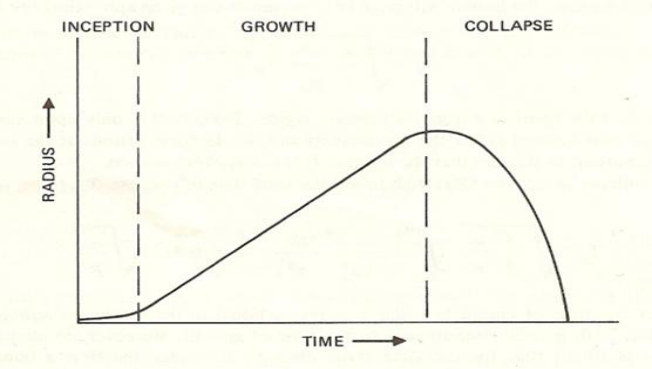

Figure 2-10: Growth and collapse of cavitation bubble in an ideal incompressible liquid, according to classical theory (Ross, 1976)

The shock wave generated is estimated to be about 10 to 15% of the bubble energy contributed to the generation of pressure impulses (Shangguan et al., 1997). Plesset (1966) noted that the duration of the stress pulse from a single bubble collapse was of the order of 1 μs. High pressures arises from such bubble activities causing compression of the liquid and transmission of a pressure pulse which radiates out from the bubble's collapse centre and may take the form of a shockwave (Benjamin and Ellis, 1966). The shockwave then propagates as a direct function of the pressure at any given point: the higher the pressure, the greater the velocity of the sound (Isseline et al., 1998). This shock wave propagation can be detected by underwater pressure sensors such as hydrophone, microphone and AE transducer. The release of energy from bubble activities propagates as a pressure wave which is then detected by the active element of a transducer. This might be an optical deflection or the voltage output of a piezoelectric element (Matthews and Hay, 1983).

2.5 Previous Works on Measuring Bubble Activity Acoustically

The hydrophone has been used to detect and monitor the acoustic effects caused by pressure fluctuations due to bubble oscillation (Leighton et al., 1991a; 1991b; Holler et al., 2003; Leighton and Walton, 1987; Pandit et al.,

1992). However, the major disadvantages of hydrophones are their limited frequency range and intrusive method. In measuring resonance frequency due to volume pulsations of bubble, a hydrophone device would have to be placed inside the tank.

Since Minnaert (1933), it has been known that that every single bubble at pinch-off (detachment from the nozzle) releases a sound. Based on his experiments, Minnaert showed that the sound was associated with the volume pulsations of the bubble with simple damping in the oscillating system and hypothesised that some of the sound of running water might be due to spherical gas bubbles undergoing periodic expansion and contraction (Strasberg, 1956). Since then, studies of the formation, growth, coalescence and bursting of bubbles have all received substantial attention from scientists and researchers. Leighton et al. (1991a) noted that the sound emission from an oscillating bubble is dominated by pulsations of the spherical zero order mode, see Figure 2-11 (page 30) (Pandit et al., 1992; Strasberg, 1956), while the shape oscillations of higher order contribute only a little additional sound pressure (Leighton et al.,1991a). A brief discussion of the shape oscillation modes can be found in Strasberg (1956) and Leighton (1994a). The photographed bubble oscillations of simple translational and volume oscillation as well as shape oscillation were presented by Tho et al. (2007) using streak photographs and micro-PIV velocity field measurements. Pandit et al. (1992) commented that gas bubbles entrained in water or liquid can generate large sound pressure when excited by external pressure fluctuation. Furthermore, they suggested that volume pulsations of the bubble give pressure pulses due to the oscillatory motion of the bubble wall.

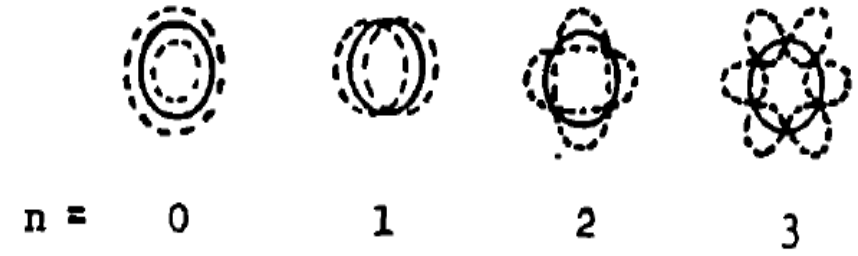

Figure 2-11: Shape oscillations mode (n = 0; Zero mode is simple coherent radial movement of the bubble surface: n = 1; translational mode, bubble oscillates left to right in this figure as a simple rigid body) (Strasberg, 1956)

Minnaert (1933) provided a formula, see Equation 2-6 (called Minnaert's natural frequency of oscillation of a bubble) that gives the natural (or resonant) frequency of the bubble in terms of the equilibrium bubble diameter radius (*d*); the polytrophic index of the gas inside the bubble (*γ*); the local liquid density (*ρ*) and the local hydrostatic pressure (P_o).

Gas content in the bubble will undergo polytropic process (expansion and contraction of gas) where it is a thermodynamic process that obey the relationship $PV^n=C$ where *P* is pressure, *V* is volume and n is called polytropic index or exponent which has range between 1 and 1.4; for isentropic or adiabatic process $\gamma = n = C_p/C_v$ is the ratio of specific heat at constant pressure (c_p) to the specific heat at constant volume (c_v).

$$f_o = \frac{1}{\pi d}\sqrt{\frac{3\gamma P_0}{\rho}} \qquad \textbf{(2-6)}$$

Thus if f_o is measured, the equilibrium radius can be readily determined (Boyd and Varley, 2004; Leighton et al., 1996; 1991a; Strasberg,1956); Pandit et al., 1992; Leighton, 1994a; Leighton and Walton, 1987; Sinha, 2006).

Sinha (2006) developed a technique for measuring the properties of bubbles from which certain physical properties of the liquid surrounding the bubbles can be determined; specifically density and surface tension. His apparatus uses a cylindrical transducer and Doppler probe as the invasive method, see Figure 2-12. The cylindrical transducer he used was operated at a frequency range up to 5 kHz. A vertical syringe was placed at the bottom of the container and used to inject air into the bulk of the liquid.

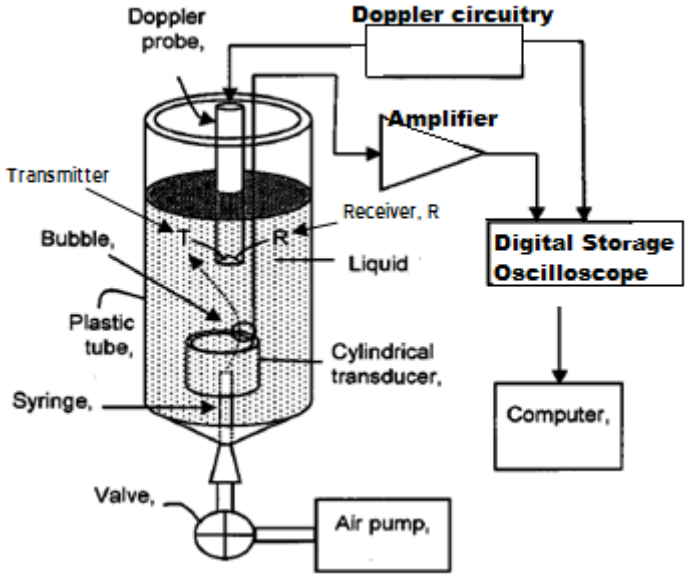

Figure 2-12: Invasive method (Sinha, 2006)

Most previous researchers used a tank or a column as the liquid container, and most used a hydrophone (maximum frequency up to 200 kHz) to monitor the acoustic emissions generated from a single bubble released from a nozzle underwater. A constant rate of air was usually supplied using a syringe as the best way for the air injection rate to be controlled, i.e. to be slow, gradual and accurate.

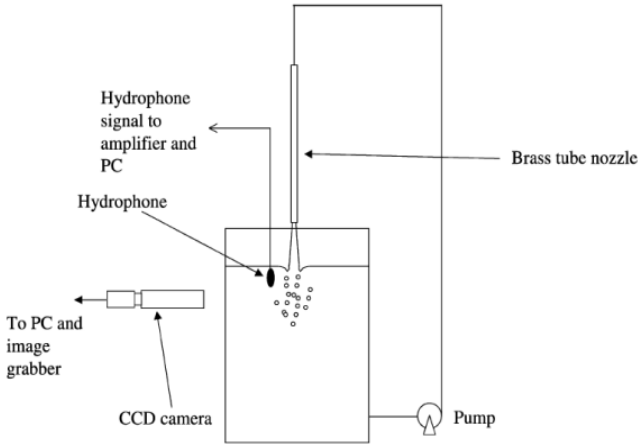

Figure 2-13: Apparatus of Boyd and Varley (2004)

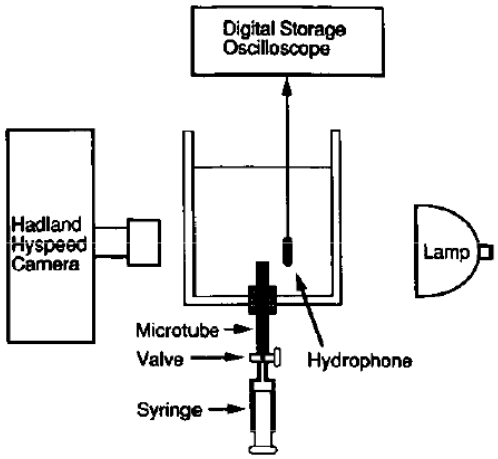

Figure 2-14: Apparatus of Leighton et al. (1991a)

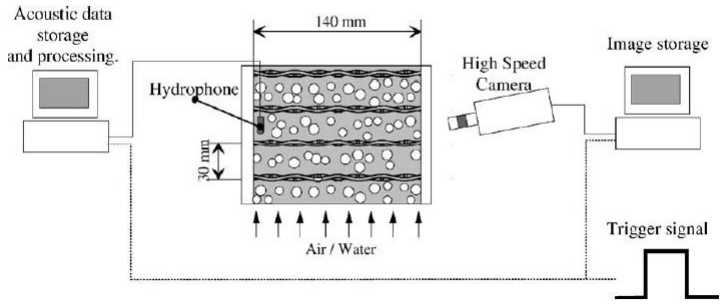

Figure 2-15: Apparatus of Holler et al. (2003)

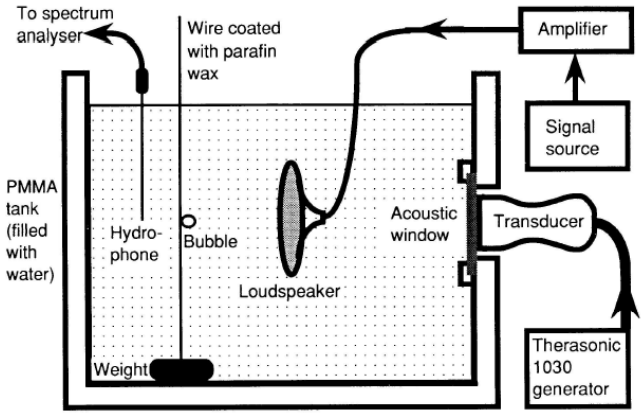

Figure 2-16: Apparatus of Leighton et al. (1991b) (subharmonic technique)

Generally, the apparatus developed by Boyd and Varley (2004), Leighton et al. (1991a), and Holler et al. (2003) are similar in that all three use a hydrophone, high speed photography and light for illumination, see Figures 2-13 to 2-16 (page 32 – 33). The major difference is the way the bubble was introduced into the tank: Boyd and Varley (2004) used a water jet aimed vertically downwards into the water surface; Holler et al. (2003) used a 0.7mm diameter multi-hole nozzle; Leighton et al. (1991a) used a syringe for introducing a single bubble at a time into the bulk liquid. A vertical syringe was placed at the bottom of the tank.

In another study, Leighton et al. (1991b) used a totally different method, see Figure 2-16. They introduced an additional device that introduced a pump frequency ω_p and image frequency ω_i. In this technique, the bubble is insonated with two frequencies; a high fixed frequency ω_i (called the *imaging* frequency), and a lower frequency ω_p (called the *pump* frequency) *which* is tuned to the resonant frequency of the bubble. This coupled frequency can be detected when the pump frequency is at (or close to) the bubble resonance. When the bubble is driven by a sound field of slightly greater amplitude, a *subharmonic* at $\omega_p/2$ is the most prominent.

This method combined subharmonic emissions with an imaging frequency. For their experiment, a continuous-wave imaging signal was generated by a Therasonic 1030 ultrasound generator through an acoustic window. The pump signal was produced in the water tank by a submerged Mylar cone speaker which was driven by the signal generator. The audio pump frequency was measured directly using a frequency counter. The bubble was blown underwater by a drawn glass pipette, then was held on a vertical wire (insulated with wax). They used a needle hydrophone (Dapco NP10-3) with a frequency range up to 5 kHz to detect the scattered megahertz acoustic signal. The signal was then processed by a spectrum analyser. It was found that the scattered signal of frequency $\omega_i \pm (\omega_p/2)$ tended to be sharper than the $\omega_i \pm \omega_p$ signal, making it a better tool for the resolution and sizing of bubbles. The plot in Figure 2-17 shows the distinctive peak signal of the combination of subharmonic emissions with imaging frequency (Phelps and Leighton, 1996). A similar plot from using this subharmonic technique can be found in Leighton, 1994b.

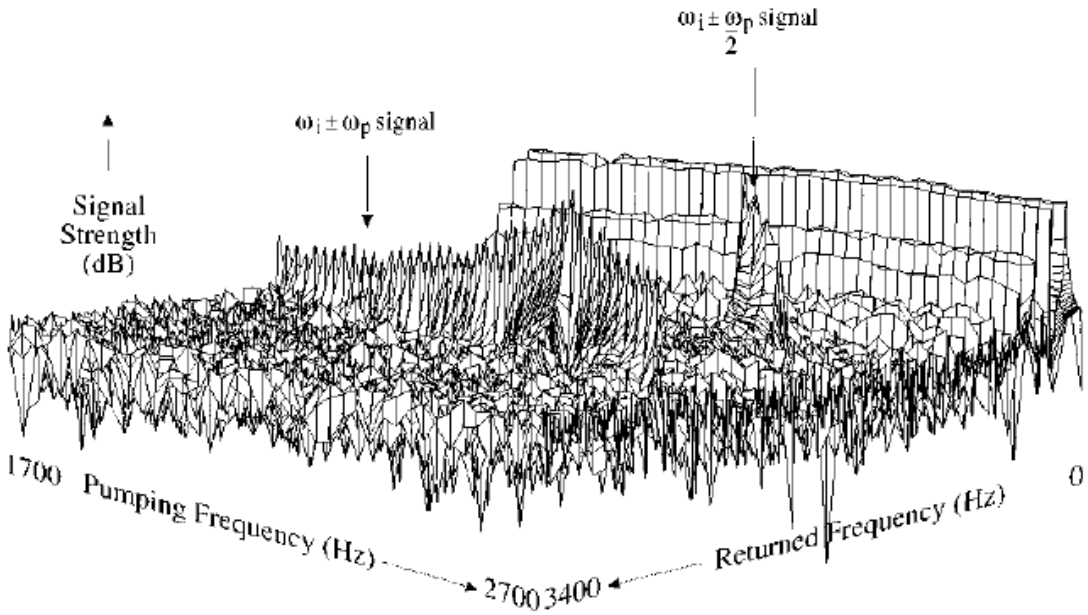

Figure 2-17: Mesh plot of returned signal strength through a bubble's resonance using the combination of subharmonic emissions with imaging frequency (Phelps and Leighton, 1996).

Phelps and Leighton (1996) showed a typical sweep across the resonance of a single tethered bubble, see Figure 2-17 (page 34). The plot shows the heterodyned output from the high frequency receiver between 0 and 3400 Hz for a bubble insonated between 1700 and 2700 Hz in discrete 25-Hz steps. The direct coupled $\omega_i \pm \omega_p$ *ridge* is present over the entire 41 pumping tones, which rises up to a maximum at the bubble resonance and then falls away again. Every peak has a sum of the $\omega_i+\omega_p$ and the $\omega_i-\omega_p$ signals as a result of the heterodyning process (Heterodyning is a radio signal processing technique where high frequency signals are converted to lower frequencies by combining two frequencies; one is the sum of the two frequencies mixed, the other is their difference). A narrower peak from the $\omega_i \pm \omega_p/2$ signal is clearly visible, due to the bubble's subharmonic output coupling with the imaging signal. This peak has been shown to be a much more accurate indicator of the bubble resonant frequency.

Boyd and Varley (2004), Figure 2-13 (page 32), used a hydrophone placed inside a liquid bath to measure the acoustic signals generated by bubbles created by a liquid jet. The signal from the hydrophone was amplified by a 2 channel Nexus 2692 conditioning amplifier with analogue bandpass filter between 0.1 and 100 kHz. The amplified signal was then acquired by a PC using a National Instruments NI 4551 dynamic signal analyser card with sampling rate 200 kHz and analysed using Labview and Matlab software. For photographic measurements, they used a Panasonic GP-MF66E camera fitted with a monozoom lens which digitally photographed the entrained bubbles. The image of the bubble was assumed to be spheroidal. The equivalent diameter, "size", of this spheroidal bubble was calculated using:

$$d_{eq} = \sqrt[3]{AB^2} \qquad \textbf{(2-7)}$$

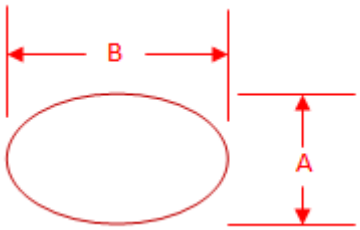

Where A is the smallest chord length and B is the largest chord length in the 2-dimensional photograph.

For the given arrangement Boyd and Varley (2004) found that the acoustic resonance frequency was related to the bubble size, nozzle height and jet flow rate. Leighton et al. (1991a) demonstrated that higher gas flow rates generate a smaller bubble size which gives rise to a high frequency sound. Holler et al. (2003) employed a high speed camera coupled with simultaneous passive acoustic measurements using a hydrophone for local observation and frequency measurement of bubbly flow; they demonstrated that the frequency of bubble swarm formation was a linear function of the superficial gas velocity.

2.6 Conclusion

The bubble size measurement techniques discussed above are intrusive methods employing a hydrophone. However, an intrusive method such as employing a hydrophone is suitable for laboratory and research use only. The methods described above are definitely impractical for on-site application in industrial engineering. No attempt so far has been made using non-intrusive and passive methods such as the application of Acoustic Emission (AE) transducers. Detection and monitoring of bubble activities in two-phase flow non-intrusively contributes to major savings in terms of capital for devices, installation, maintenance and time. This passive and non-intrusive technique offers an alternative to the aforementioned existing methods.

The determination of bubble size from natural frequency bubble oscillation has limitations, particularly in signal detection in real engineering systems which always contain background noise. The signals or pressure pulses from bubble resonance or oscillation are very weak. Furthermore, the presence of a pipeline and the constraints it places on the flow can affect the inertia of the liquid contained within it, complicating the issue considerably. For both tanks and pipes, the reverberation present in the environment means that the results obtained can be misleading and need independent practical verification, therefore allowance must be made for this if the technique is to be used to determine bubble size in pipes. Thus, other bubble activities which emitted stronger signals, such as bubble inception (e.g. formation at nozzle) and burst at the free surface, are worth analysing for their frequency for bubble sizing.

3 ACOUSTIC EMISSION

This chapter provides a brief review of Acoustic Emission (AE) and its applications. The chapter starts with an overview of acoustics followed by the fundamentals of sound transmission in a medium, which focuses on AE. A brief history of AE technology is given, including its working principles, transducer types and signal analysis. Then, the common applications of AE in engineering are enumerated, with particular emphasis on the application of AE technology in gas-liquid systems. The chapter closes by looking into the feasibility of AE technology for bubble/cavitation detection, measurement and monitoring in two-phase flow.

3.1 Introduction

Acoustics methods have been widely applied in many fields of engineering including the monitoring of earthquakes, the propagation of elastic waves through the earth (seismic monitoring), non-destructive testing (NDT), underwater navigation, fault detection and fish finding sonar. The scope of acoustical engineering and frequency range is shown in Figure 3-1, page 39 (Rodney, 1990).

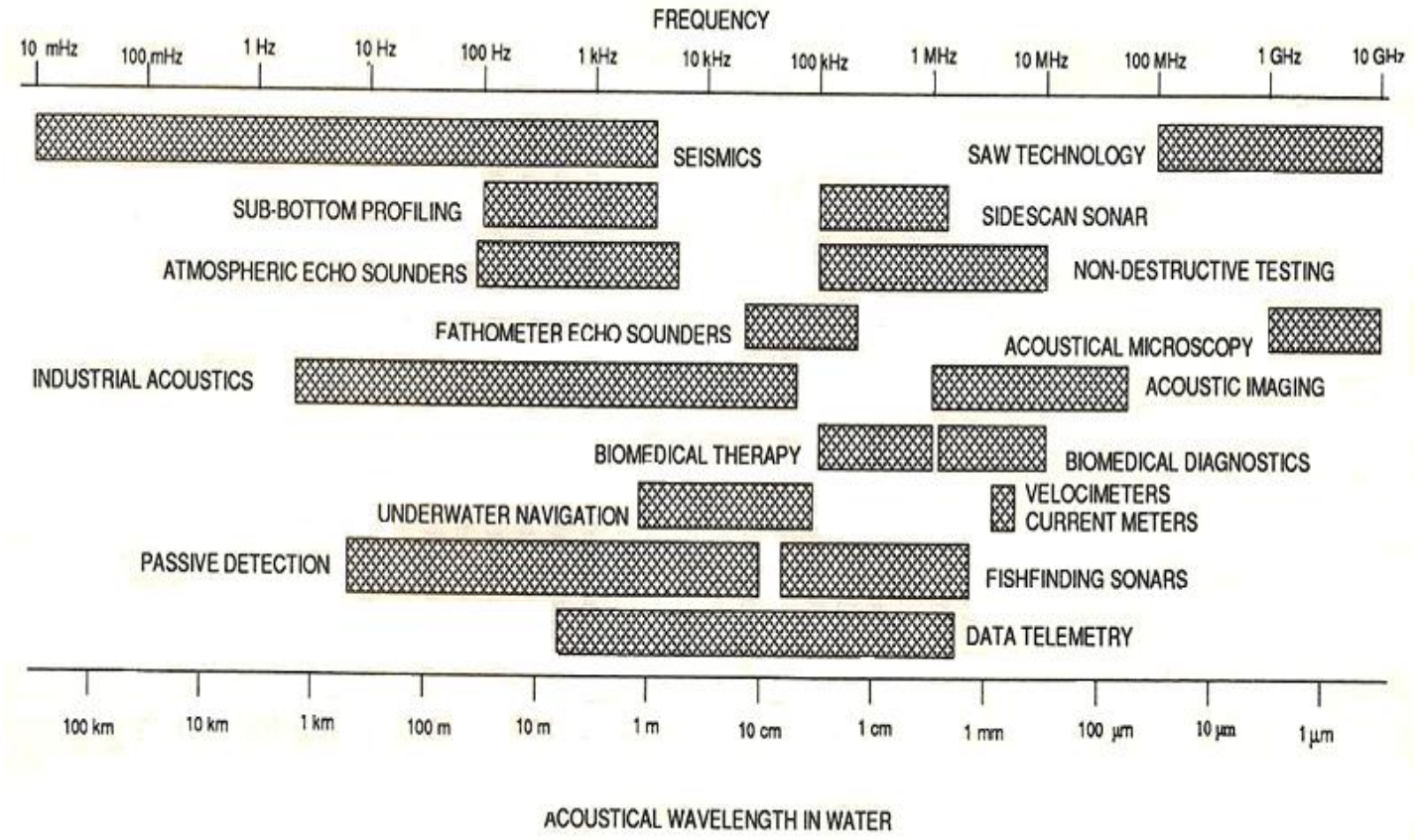

Figure 3-1: Acoustical engineering and frequency range (Rodney, 1990)

3.2 AE Definition

Miller and McIntire (1987, p.12) defined AE as "*acoustic emission is the elastic energy that is spontaneously released by materials when they undergo deformation*", though most researchers use the definition of the American Society for Testing and Materials (1982) "*the class of phenomena where transient elastic waves are generated by the rapid release of energy from localized sources within a material, or the transient elastic waves so generated"* (quoted in Yen and Lu, 2002; and Matthews and Hay, 1983). Although AE is the most widely used term for this phenomenon, in some literatures it has been called *stress wave emission, stress waves, micro-seismic activity* and *rock noise* (Miller and McIntire, 1987). This particular investigation considers the transient elastic waves generated by bubble inception (when it collapses at the 'neck') and/or bursts at a free surface, as AE.

3.3 Brief History of AE

The first use of AE by human beings appears to have been in the manufacture of hard fired pottery about 6,500 BC, the sound of the cracking of cooling clay vessels in the kiln was used by the potters to evaluate the products' quality. The first observation of AE in metals may have occurred when man learned to smelt pure tin, possibly as early as 3,700 BC when the mechanical twinning of pure tin produced an audible emission or "cry" during plastic deformation. However, it is definitely known that in the 8th century, an Arabian alchemist Jabir Ibn Hayyan documented the observation that tin gives off a harsh sound when a bar of tin is bent. He postulated that the crackling sound could be due to crystals in the inner parts of the bar breaking against one another (Miller and McIntire, 1987). In 1950, Joseph Kaiser performed the first comprehensive investigation into AE and suggested that crystalline solids could emit sound when under a mechanical load. Kaiser systematically used high frequency sensors and electrical amplifiers to listen to a range of engineering materials under controlled loadings. These experiments were published in Kaiser's thesis in 1950, in which he stated

"*engineering materials in general emit low amplitude clicks of sound when they are stressed"*. The most significant discovery of his work was the irreversible AE phenomenon which is now known as the 'Kaiser Effect': "*A material does not start to re-emit AE activity until the applied stress exceeds that which it has previously experienced"* (cited in Holroyd, 2000). Kaiser had found a new technique for non-destructive testing.

3.4 Brief Introduction to AE Technology

The frequency range for the AE sensor is usually above the upper limit of human hearing threshold, usually from 25 kHz to 1 MHz. Typically the active element in an AE system is a ceramic piezoelectric transducer, used either as a source or a receiver, converting AE activity into electrical signals.

Transducer output is invariably connected to a pre-amplifier and then to a data acquisition system where the signals are sampled, stored, processed and displayed. The schematic AE instrument is shown in Figure 3-2 (Physical Acoustic Corporation, 2011) where the amplifier and filter are embedded in the circuit of the system.

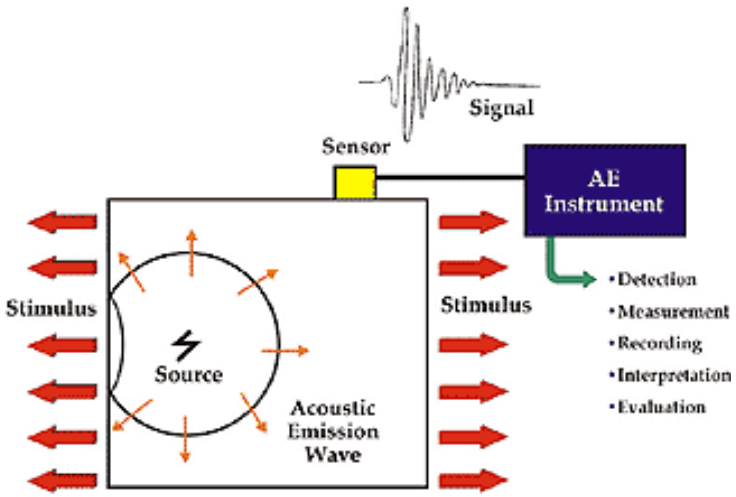

Figure 3-2: Schematic diagram of AE Technology (Physical Acoustic Corporation-http://www.pacndt.com/index, 2011)

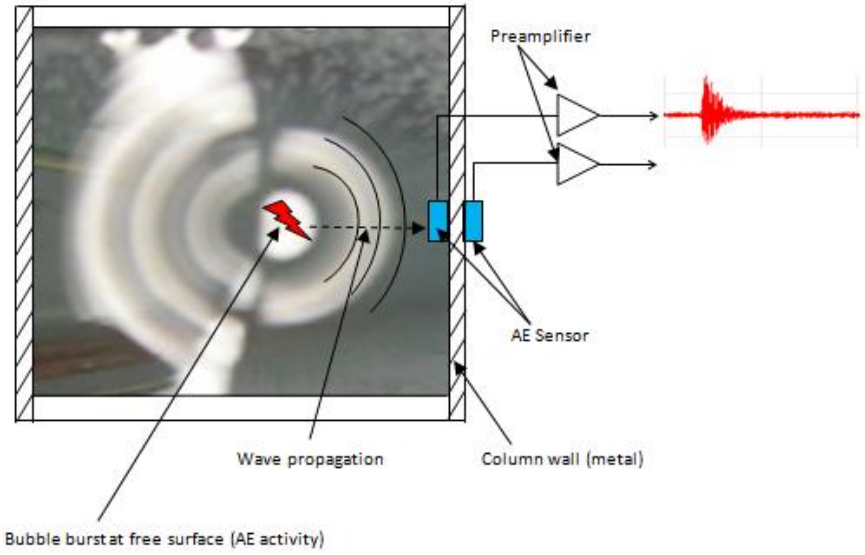

Figure 3-3: Principle of AE process in two phase air-liquid system

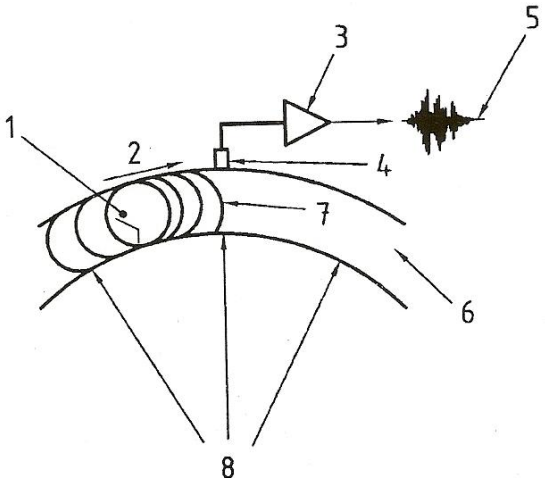

Key

1 Growing discontinuity
2 Surface waves
3 Preamplifier
4 AE sensor
5 Signal out
6 Section view of the component material
7 Wave packet
8 Applied load inducing stress

Figure 3-4: Principle of AE process in solid material (Bearing) [BS EN 13554:2002]

The application of AE technology in metal component such as gears and bearings is common for condition monitoring. However, its application in a two phase gas-liquid system is new and has been attempted for flow monitoring in a horizontal pipeline. The physics of AE generation in these two systems (AE generation in metal e.g. crack and AE generation in liquid e.g. bubble activity) is different and can be compared with illustrations as shown in Figures 3-3 and 3-4 (page 43). Figure 3-3 is an illustration of pressure/shock wave propagation in liquid due to bubble burst at a free surface, while Figure 3-4 is an illustration of the basic principle of the AE process in metal (e.g. bearings).

As shown in Figure 3-3, bubble burst or formation events generate pressure pulse at the instance of the event. This pressure transient, radiated in the liquid, will take the form of a pressure/shock wave. Aitken et al. (1996) defined the shock wave as "*a surface in a fluid through which there are sharp gradients in pressure, velocity, density, etc and such surfaces are considered surfaces of discontinuity*". This pressure transient can be detected by AE sensor both intrusively and non-intrusively mounted.

In metals (see Figure 3-4), the propagation of a defect (crack) can be initiated by crack blunting and local yielding. A crack propagates and it is associated with the rapid release of energy governed by presence of hard particle in the metal structure (Mathews, 1983). The released energy propagates as a stress wave to a free surface which then oscillates producing a pressure which can be detected by an AE piezo-electric sensor.

3.4.1 AE transducer

The piezoelectric transducer (PZT) is the most commonly used AE sensor. This type of transducer uses a piezoelectric material which generates an electrical charge when it is mechanically strained. Lead Zirconate, Titanate and Polyvinylidene Fluoride are amongst the most common piezoelectric materials

for AE transducers. A typical construction of a simple AE transducer is shown in Figure 3-5.

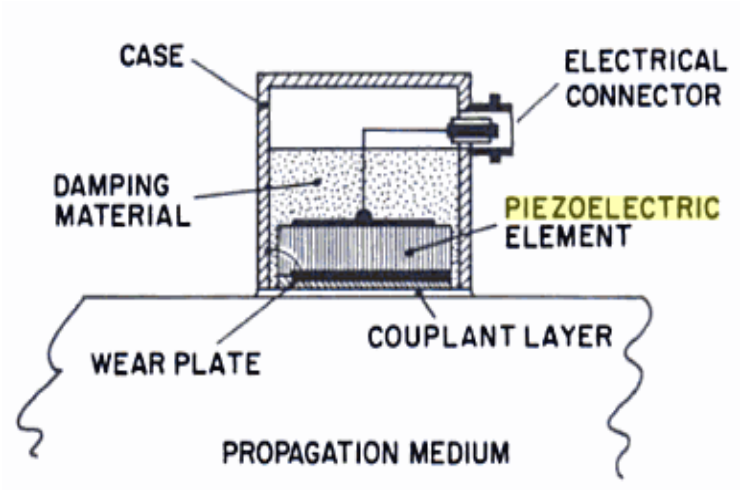

Figure 3-5: Construction of a simple AE transducer (Hardy, 2003 p.105)

There are two types of AE transducer in common usage:

i) Resonant, and
ii) Broadband

The resonant type, also known as a narrow band transducer, is used at frequencies that match the natural frequency of its piezoelectric element. Precisely because of this restriction, resonant type transducers are more sensitive than the broadband type. A broadband AE transducer is used in a frequency range well below the natural frequency of the piezoelectric element and this means the transducer output signal needs to be amplified. The attachment of the transducer to the surface of the test specimen is of paramount importance as it has a substantial effect on the AE output.

The European Standards (BS EN1330-9:2000) method for AE transducer calibration, usually used before any experiment is performed, is the Hsu-Nielsen Test. This is a pulse calibration method which requires breaking a 2H pencil lead of specified diameter and length (see details in the experimental procedure, **Chapter 5**).

3.4.2 Signal types

Three types of AE signals are encountered in practice (Kline, 1983; Miller and McIntire, 1987);

i) Transient (or burst) signals,
ii) Continuous signals, and
iii) Mixture of both burst and continuous.

The transient type signal takes the form of a discrete transient burst. Normally, the source of burst type signals is spontaneous acoustic events generated by local defects in a material, or reflections of transient pulses emitted from a transducer. This type of signal can be separated in time, and different information obtained from the beginning and end of the pulse. A continuous type signal may either be the sum of many emission bursts (e.g. frictional rubbing) or the reflection of a continuous signal emitted by a transducer. Continuous signals will often contain both mechanical and electrical background noise. Because of their continuous nature (statistically stationary) little or nothing is gained by separating these signals in time. The mixed mode type of signal is characterised by burst activity which is superimposed on a background of continuous activity. A typical representation of signals is shown in Figure 3-6 (page 47). The shape of an AE impulse or burst type transient signal is often referred to as a damped sinusoid. There is a rapid rise to maximum amplitude followed by a more gradual decay back to background noise level. Background noise is any signal detected below the threshold of the interest signal. In addition, it is defined as “non-relevant indications; signal produced by causes other than AE, or by AE sources that are not relevant to the purpose of the test”, e.g. electrical noise.

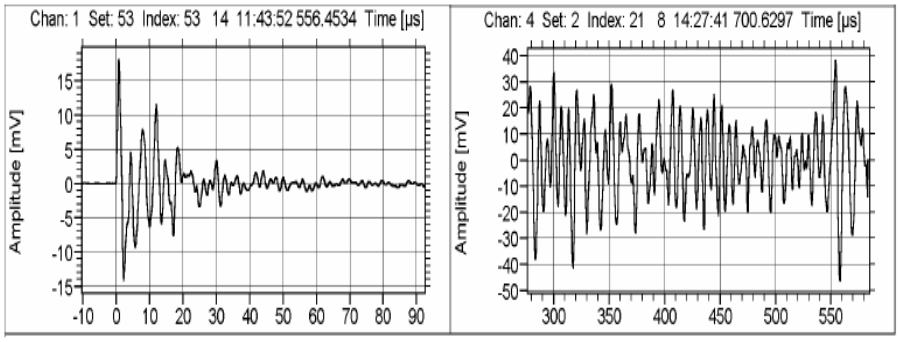

Transient (left) and continuous (right) AE signal

Figure 3-6: Representation of transient and continuous AE signals http://www.vallen.de/zdownload/pdf/sea204E.pdf (April 22, 2011)

The AE amplitude is the maximum (positive and negative) AE signal excursion during an AE hit. The amplitude is expressed in dB using the relationship (AE system user manual, 2007):

$$dB=20 \log (V_{max} / 1\ \mu Volt) - (Preamplifier\ Gain\ in\ dB) \quad \textbf{(3-1)}$$

For example using above equation, 0.61 mV is equivalent to 15.6 dB.

3.4.3 Definitions of AE Parameters

The definition of a number of waveform parameters is represented in Figures 3-7 and 3-8 (page 48).

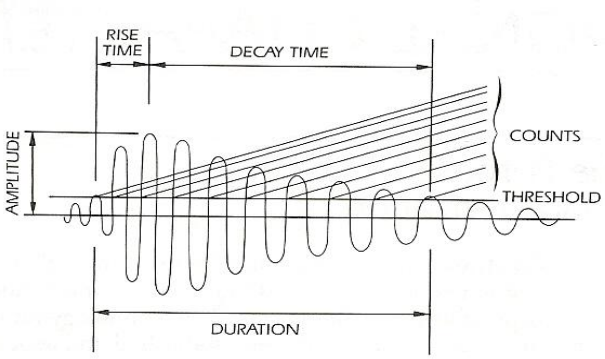

Figure 3-7: Definition of simple waveform parameters (Miller and McIntire, 1987)

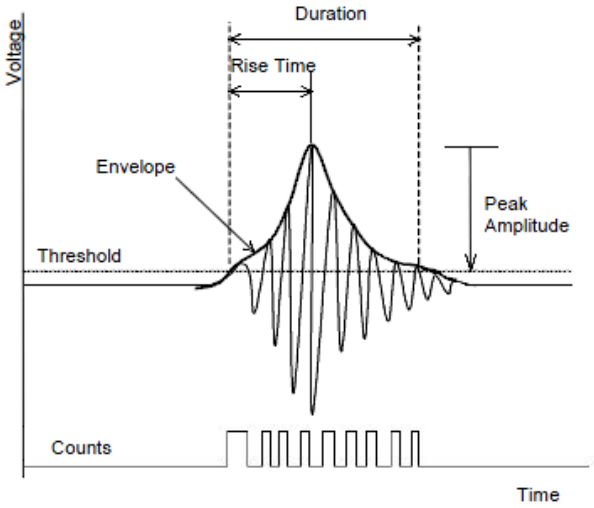

Figure 3-8: Typical AE waveform and main parameters (Physical Acoustic Corporation, AE System User's Manual, 2003)

I. The threshold is a predetermined value, and the AE level must exceed this to be counted as an AE event.

II. An AE hit (event) is defined as the process of detecting and measuring an AE signal on a channel where it depends on the timing parameters of the signal process. There are three timing parameter: Peak Definition Time (PDT), Hit Definition Time (HDT) and Hit Lock Time (HLT). PDT ensures correct identification of the signal peak for rise time and peak amplitude measurements; HDT ensures that each AE signal from the structure is reported as one, and only one, hit; while HLT ensures spurious measurements during the signal decay are avoided (Physical Acoustic Corporation, 2003).

III. AE signal duration: the period between first hit and last event (pulse crossing threshold).

IV. AE ring-down count: the number of the threshold-crossing pulses occurring during the AE signal duration.

V. Peak signal amplitude: the maximum value of the AE signal, a measure of the intensity of the source producing the AE.

VI. Emission signal rise time: The time between the instant the signal first crosses the threshold and time at which the maximum amplitude occurs.

VII. Emission signal decay time: The time between maximum amplitude and the last time that the decaying amplitude crosses the threshold level.

VIII. AE event energy: The true energy is directly proportional to the area under the AE waveform. The electrical energy, U, present in a transient voltage, V, across a resistor, R, has been defined as (Miller and McIntire, 1987):

$$U = \frac{1}{R}\int_0^{\alpha} V^2\,(t)dt \qquad \textbf{(3-2)}$$

3.4.4 AE Signal Analysis

AE signal processing is a very important element in detecting, monitoring, testing and characterisation of any defect present in a structure or particular event in a process (Serrano and Fabio, 1996). This includes time-domain analysis, frequency-domain analysis and joint time-frequency analysis. AE signal analysis can be categorised into two: the *parameter-based AE* (classical) approach and *signal-based* (quantitative) approach (Grosse and Reinhardt, 2002).

Signal parameter-based analysis is a conventional approach for AE source characterisation and overall assessment of the mechanical performance of materials and structures (Spasova and Ojovan, 2008). In this category, the data recorded on a PC hard drive in an ASCII file format for each AE signal consist

of a set of parameters such as duration, amplitude, counts, rise time and absolute energy (Yoon et al., 2000; Maradei et al, 2003; Piotrkowski et al., 2005; Spasova and Ojovan, 2008; Ayorinde, 2009). The type of information for AE parameters analysis is simplified in Table 3-1.

Table 3-1: AE parameters and information to be extracted (Toutountzakis, 2003)

Parameter	Type of Information
Waveform	Gives an indication of movement in the structure
Frequency spectrum (From FFT)	Gives an indication of material behaviour
Amplitude	Gives the strength of the signal
Amplitude distribution	Type of damage occurring
Rate	Rate of damage occurring
Distribution in time (AE HIT: AE HIT is used to describe the AE event that is detected by a particular sensor and can be described by several parameters such as threshold, duration, counts and rise time, refer to page 48)	Type of damage occurring; integrity of specimen
Relative arrival times at several transducers (From Wavelet)	Source location

When analysing AE waveform data, two general signal processing approaches are used:

i) Threshold based

ii) Envelope based

A threshold, or trigger, level can be preset for AE data. Only levels which exceed the threshold are considered, levels lower than the threshold are taken to be background noise, see Figure 3-9.

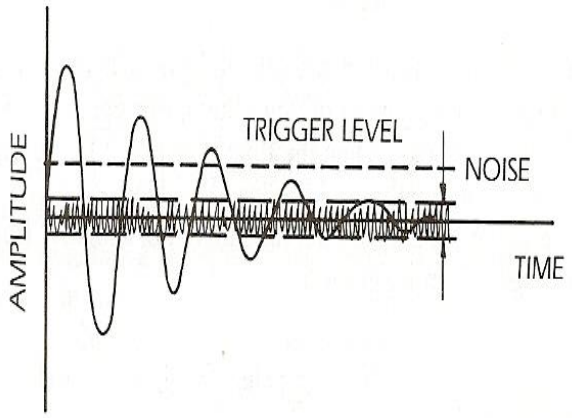

Figure 3-9: Threshold setting to avoid triggering by background noise (Miller and McIntire, 1987)

AE parameters derived from threshold analysis are:

i) AE counts – The number of times the AE level exceeds the threshold is counted.

ii) AE events – Operates on the same principle as AE counts, the number of AE bursts are counted.

Envelope analysis is a technique to extract the modulating function from an amplitude modulated signal. It is a statistical technique for analysing the oscillatory waveform.

Signal-based AE analysis, e.g. fast Fourier Transform (FFT) and wavelet transforms (WTs) are advanced mathematical transformations to facilitate the identification of characteristic features of the recorded acoustic waves (Spasova and Ojovan, 2008).

The Fourier transform (FT) method is based on the assumption that the signal to be transformed (fixed window) is periodic and of infinite length (Zhao et al., 2004). In the FT method, all information about time is lost once the signal is transformed into the frequency domain (Kaplan, 2002), so this method cannot localise faults in time (Alm and Walker, 2002; Zhao et al., 2004) and therefore cannot be sensitive to abrupt changes in an AE signal caused by faults, defects or certain process/events (Pryor et al., 2001).

The wavelet transforms (WT) was developed to overcome the drawbacks of the conventional Fourier transform and Short Time Fourier Transform (STFT) (Suzuki et al., 1996; Pryor et al., 2001). A wavelet is a “small wave”, which has its energy localised in time and provides a tool for the analysis of transient phenomena (Gannam, 2009). Its application in the area of AE research began in earnest in the late 1990s and early 2000s and included non-destructive testing (e.g. cracks and faults detection in gear systems, fracture of composite materials) and process monitoring (e.g. tool insert wear) (Loutas et al., 2004; Pryor et al., 2001; Suzuki et al., 1996; Baulahbal et al., 1999; Wang and McFadden, 1996; Ferlez and Lang, 1998).

The Wavelet transforms (WT) method, which combines measures of time with those of frequency and intensity, is regarded as one of the most advanced and powerful signal processing methods (Ayorinde, 2009). Generally, the wavelet transforms (WT) is defined in terms of basic functions obtained by compression/dilation and shifting of a “*mother wavelet*”; its mathematical structure is expressed as:

$$\psi_{t,s}(t) = \frac{1}{\sqrt{|s|}}\psi^*\left(\frac{t-\tau}{s}\right) \qquad \textbf{(3-3)}$$

Where ψ^* is the complex conjugate of the wavelet function, *s* is the scale variable (*s≠0*), and *t* the time shift variable. The basic function ψ is usually called the "*mother wavelet*" (Grosse and Reinhardt, 2002).

Signal processing with wavelet transform (WT) provides local information about both time and frequency, sensitivity to transient signals and is known as time-frequency analysis (Hess-Nielsen and Wickerhauser, 1996; Suzuki et al., 1996; Pryor et al., 2001; Grosse and Reinhardt, 2002; Zhao et al., 2004; Spasova and Ojovan, 2008; Kim and Lee, 2008). Better precision in the frequency domain, as offered by the WT, is often necessary to characterise the time-frequency phenomenon. Wavelet transform is suitable to be applied to the detection of short time phenomena, discontinuities, or abrupt changes in a signal. The WT technique demonstrates its effectiveness when analysing AE transient data, particularly in characterising AE singularities (Ayorinde, 2009). In addition, the *wavelet coefficients* provide explicit information.

Application of the WT is commonly used in the time domain (Kaplan, 2002) and has been shown to be useful in the detection of a signal in low signal-to-noise applications such as in ultrasonic non-destructive testing and condition monitoring of rotating machinery (Yoon et al., 2000). Typical AE events from mechanical systems generate multiple, short, transient pulses. Information about the time variance of particular events such as cracking or fracture cannot be obtained from waveform or frequency analysis (e.g. FFT) but can be done only with wavelet analysis (Spasova and Ojovan, 2008; Yoon et al., 2000). In addition, information about the frequency content, amplitude, duration and arrival time can all be obtained from a single wavelet transformation (Yoon et al., 2000). Based on these advantages, the WT is now widely used for AE signals analysis.

3.4.5 Review Application of WT for AE Data

Hamstad et al. (2002) examined the application of a WT to identify the characteristics of AE signals from three types of buried point-sources; in-plane dipole, out-of-plane dipole, and crack initiation. They used the AGU-Vallen Wavelet software program to calculate the WT. They noted the extraction of meaningful source identification features by the use of a WT can be used as a direct method of source identification.

Bayray and Rauscher (2006) studied the WT method for AE signals by identifying wave modes in the signals of steel pressure vessels by employing AGU-Vallen. This software calculates the WT of the signal and produces a colour plot on which it presents the WT coefficient against the frequency and time. A 3D plot of WT results shows a clearer WT coefficient on the y-axis. The main parameters they set up with AGU-Vallen software were: maximum frequency 500 kHz, frequency resolution 2 kHz, wavelet size (samples) 200, number of samples 1024, offset samples 0 and scale factor 100.

Matsuo et al. (2006) determined arrival times at three sensors using the time transient of WT coefficient at specific selected resonance frequencies in their study into the proposed source location method of artificial sources on the CFRP plate. The artificial sources they used were: Hsu-Nielsen source, a small AE sensor (a Pico-sensor) as the transmitter, steel-ball drop, pull-off of glued sewing needle. The three sensors, aforementioned, were positioned as a triangle at locations on the specimen surface. They accurately located the AE source of Hsu-Nielsen and PZT transmitter.

Hamstad (2007a) in his studies of using AE for source location in a thick steel plate, employed AGU-Vallen software for WT analysis. WT results were used to enhance the identification of the AE signal Lamb modes and to obtain from WT coefficient peaks the different mode arrival times at key frequencies. The parameters he used in AGU-Vallen were: maxima frequency 500 kHz, frequency resolution 2 kHz, wavelet size 600 samples. Colour scales in the WT figure indicate the intensity region of the WT coefficient. For example, the red

colour indicates the highest intensity region of the WT coefficient. Two types of AE sources Hamstad used in investigating the accuracy of source location, employed WT analysis with AGU-Vallen software and were buried in out-of-plane (2-dimensional) and in-plane (3-dimensional) AE dipole-point-sources at different depths below the top surface of a thick steel plate. In another research, Hamstad (2007b) used the same procedures as previously in investigating the comparison of AE signals generated by monopole (pencil-lead break) with dipole sources at an aluminium plate. His experimental results using WT employed AGU-Vallen software showed that the WT coefficient obtained was higher from the source located near the centre of the plate (buried) compared with the source located on the edge surface of the plate. In addition, the result of the WT coefficient was a function of source depth: WT coefficient increased when the source depth increased.

Laschimke et al. (2004) managed to record AE from transpiring plants. This implies that AE technology is very sensitive. In their study, they used a piezoelectric sensor SE-45 produced by Duncan Engineering Consultants, USA. The AE sensor was attached to the upper side of the leaf (Ulmus glabra), by applying a mild medical contact gel, the mesophyll. They used Wavelet analysis using AGU-Vallen software to observe the frequency pattern and waveform. They noticed a significant change of the signal types where AE was generated during transpiration. They used laser scanning microscopy (CLSM) which showed evidence of an accumulation of gas bubbles at the vessel pits and, due to the effect of illumination, some of those bubbles showed intense light reflection. This is a convincing proof of the existence of gas/water interfaces. Furthermore, their observation under the microscope showed the bubbles intermittently coalesce violently.

3.4.6 Application of AE to Two-Phase Gas-Liquid Systems

The phenomenon of cavitation or bubbles in a two-phase gas-liquid system is common. It has a significant effect on efficiency. In addition, cavitation in

centrifugal pumps can lead to the rapid degradation even destruction of the pump.

More recently, Addali (2010) and Al-Lababidi et al. (2009) in the first ever known attempt to apply AE technology as a tool for gas void fraction (GVF) measurement and slug flow monitoring in a horizontal pipe, have shown a very successful result. GVF is defined as the ratio of the volumetric of the gas to the total volumetric flow-rate. They proved that AE measurement from a two-phase flow has correlation with the gas void measurement obtained from a conductivity ring. A correlation between GVF, absolute AE energy and slug velocities in a two-phase air-water flow regime was established. It was found that the higher the Superficial Gas Velocity (VSG), the higher the absolute AE, while the GVF as measured by a conductivity ring is lower. Superficial Gas Velocity (VSG) is defined as the volumetric flow rate of gas phase divided by the cross-sectional area of the pipe. Addali (2010) concluded that the GVF can be determined by AE measurements. This passive AE technology offers an alternative to the intrusive ultrasonic methods.

3.5 Bubbles Activities in Slug Flow

Slug flow phenomena encompass a single bubble, a cluster of bubbles, coalescence and collapse which might be caused by the turbulent flow and pressure drop. The gradual increase in liquid velocity in a horizontal pipe will result in converting the wavy flow to what is described as "*slug flow*" (Addali, 2010) where large waves of liquid form a slug that can fill the whole cross-section of the pipe leading to blocking of the downstream gases. Slugs are usually not intentional and can be disruptive to flow as well as liquid transfer efficiency. Slug flow is commonly found in long-distance piping which may be caused by leaks in the pump (McAllister, 2009). Liquid flow in pipes is highly intricate due to the existence of various interfaces between the two phases, gas and liquid (Yen and Lu, 2002). In slug flow, the dynamics of bubbles including

their formation, oscillation, coalescence and burst (destruction) contribute to AE (Addali, 2010).

Bubble oscillations can create underwater noise and its amplitude is dependent on the bubble size. Normally, bubble oscillations give only a small pressure pulse. While bubble coalescence and burst give a higher pressure pulse and this can be detected by transducer (Strasberg, 1956). In the case of slug flow in the pipeline, the elongated bubble (EB) induces greater interfaces (film region) where bubbles commonly collapse/burst in this region. In addition, the concentration of bubbles at its nose and tail due to the dragging force provided by the EB would increase the rate of coalescence, see Figure 3-10. Bubble activities, particularly coalescence and burst, are prevalent in this region. This phenomenon is one of the reasons why in the presence of slug flow, the AE generated is higher (Addali, 2010).

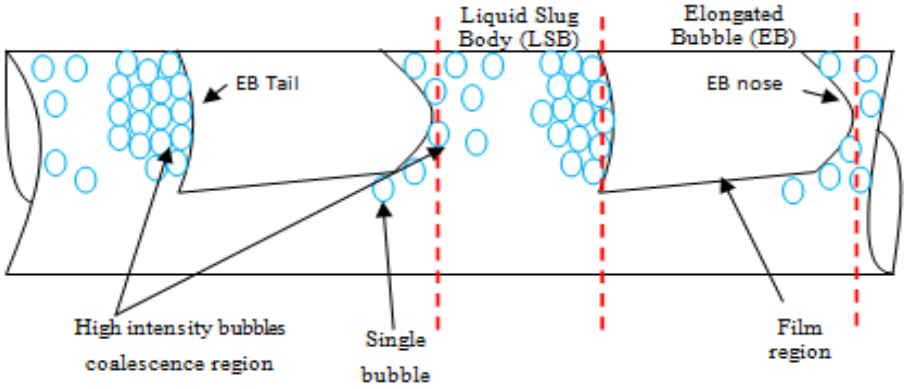

Figure 3-10: Illustration of the Elongated Bubble (EB) and Liquid Slug Body (LSB) of liquid flow in a horizontal pipe (Al-Lababidi et al., 2009)

High pressures arise from the bubble activities (formation, coalescence and collapse) radiated in the form of a shockwave (Benjamin and Ellis, 1966). This shock wave propagation can be detected by transducers such as the hydrophone, microphones and AE transducers.

Based on the evidence from the background survey and in particular previous works carried out at Cranfield University (Addali, 2010; Husin et al., 2010;

2011), it is evident that the AE technology can be employed for detecting gas bubble activities: formation, coalescence and collapse. Furthermore, it is strongly believed that pressure pulses associated with the bubble activities are potential sources for AE. Therefore, an investigation into single bubble activity would provide a basis for the acoustic measurement or energy presence in slug flow which would lead to the extension of the application of AE technology for correlation work with gas void fraction (GVF) in horizontal pipelines.

3.6 Advantages of the AE technique

Based on the research into AE methods and applications carried out at Cranfield University and referred to above, the advantages of AE are:

i) AE is non directional where the surface waves propagate within a material. Therefore, AE sensor can be placed anywhere in the vicinity of AE sources.

ii) The AE signal is less affected by mechanical background noise, and the high signal to noise ratio (SNR), giving a clearer and direct indication of fault mechanisms.

iii) AE technology is very sensitive and capable of detecting incipient failures (or event) since the sources are usually produced at a microscopic level of the material.

iv) Structural resonances have no effect on the AE signal generated.

v) Applicable to all machines irrespective of operating speed.

vi) Provides good trending parameters.

vii) Localisation of measurements to the machine being monitored.

3.7 Disadvantages of the AE technique

i) Requires highly specialised sensor and signal processing.

ii) Sensitive to other ultrasonic sources (other high frequency sources, e.g. turbulence, etc), therefore AE technique requires sensor(s) to be placed closer to the investigated AE source.

iii) AEs are characterized by low amplitude signal; therefore, require AE sensors to be located close to the sources of emission.

iv) AE results are more qualitative, and need correlation and calibration to be done. Both data interpretation and decision making require a very experienced and skilled person.

v) Analysis of AE results need highly skilled and experienced employees.

3.8 Conclusion

AE technology is very sensitive, it can detect high frequencies from an event above human ear threshold (>20 kHz). One of its significant advantages over other techniques is that AE technology provides a passive and non-intrusive technique in which it offers a practical inspection particularly for the monitoring of two phase gas-liquid systems such as liquid flow in pipelines and columns where the bubble phenomenon cannot be avoided. This technique is practical and efficient with respect to set up and inspection time, considerably reducing cost (Mathews, 1983).

4 APPARATUS AND EXPERIMENTAL SETUP

This chapter explains in detail the experimental setup for the two stages of the research programme; stage one was the initial investigation to assess the capability of AE technology for the detection of bubble activities, whilst stage two was a detailed test programme designed for a deeper understanding of the effect of the selected parameters on the AE from bubble activities.

The experimental setup can be divided into two parts: the bubble test rig and the Data Acquisition (DAQ) system. The bubble test rig includes the column filled with liquid, and the nozzle and syringe for artificially generating gas bubbles. The DAQ can be subdivided into hardware and software. Hardware includes AE transducers and amplifier. Commercial software packages used were AEWin to acquire AE data during the test and WaveView to play the waveform acquired from AEWin.

4.1 Bubble Test Rig Used in Preliminary Test (1st Test)

The initial investigation (1st test) was to assess the feasibility and capability of AE sensors to detect AE from bubble activities, particularly bubble inception and burst. The schematic diagram of the initial test is shown in Figure 4-1 (page 61). The apparatus employed for AE measurement is shown in Figures 4-2, 4-3 and 4-4 (page 62 and 63). The core of the rig was a transparent vertical column (Perspex) filled with tap-water. The column filled with liquid needs to be transparent for video recording which was used to determine the exact times that AE was generated by bubble activities or events. The column was a Perspex tube 150 mm in diameter, height 1500 mm and wall thickness 10 mm. AE sensors were positioned at three locations within the column of fluid, see Figures 4-1 and 4-2 (page 61 and 62). The end of a plastic hose was positioned at the bottom of the column to act as a single nozzle from which an artificial single gas bubble could be released, see Figure 4-3 (page 62). A syringe was

connected to the other end of the hose which was outside the column. When its plunger was gradually depressed it would create single gas bubbles at the nozzle. Various internal diameter hoses were used to generate different sized single gas bubbles, see Figure 4-5 (page 63).

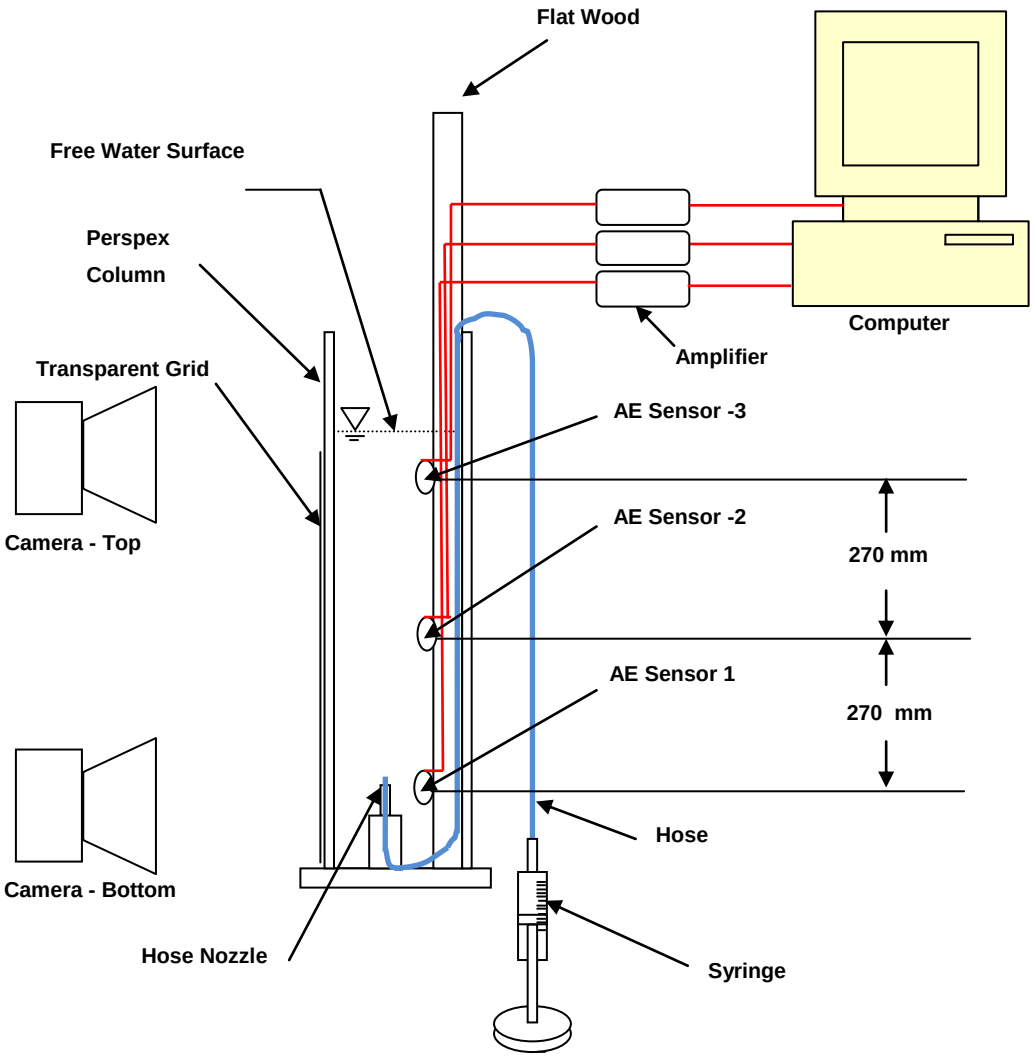

Figure 4-1: Schematic diagram of preliminary experimental arrangement

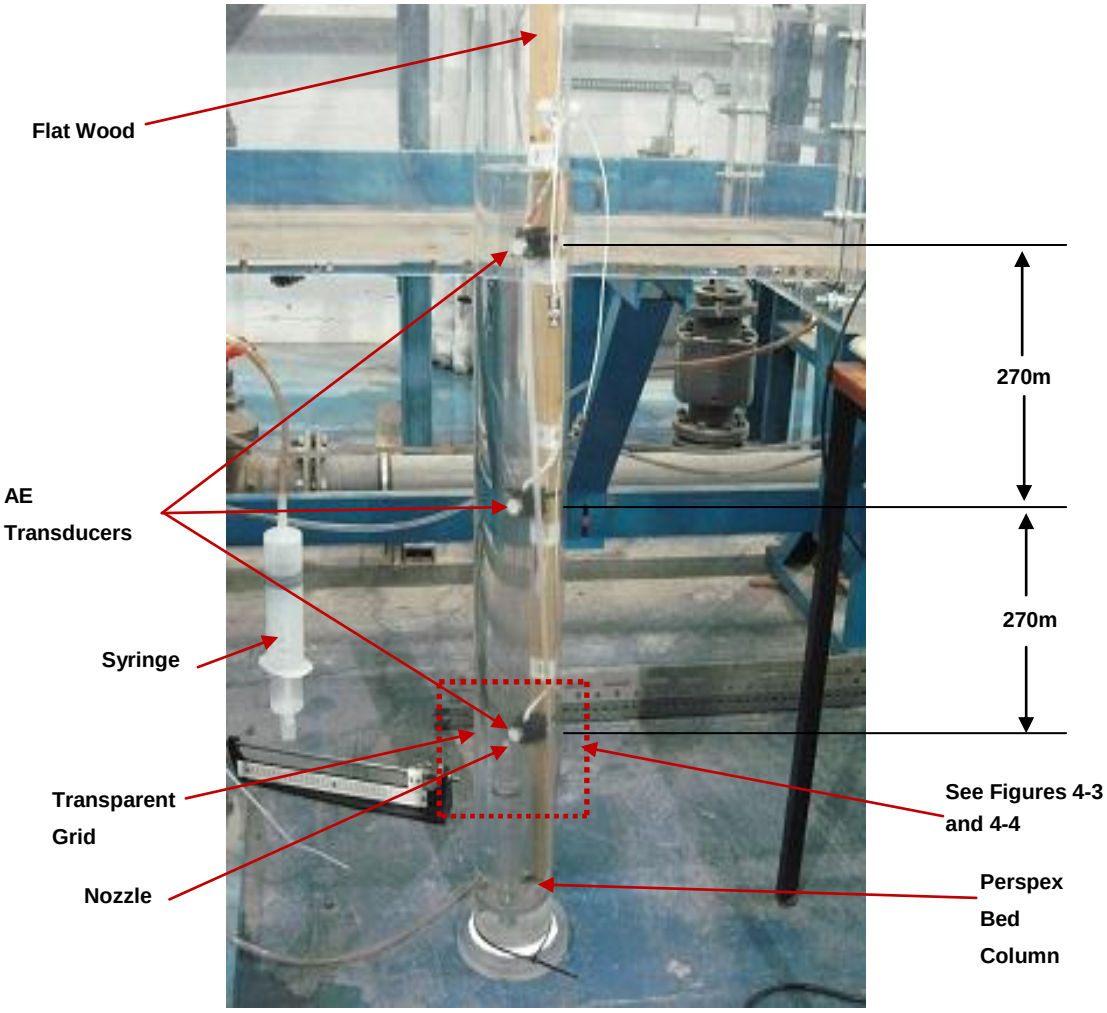

Figure 4-2: Transducer locations in the main column

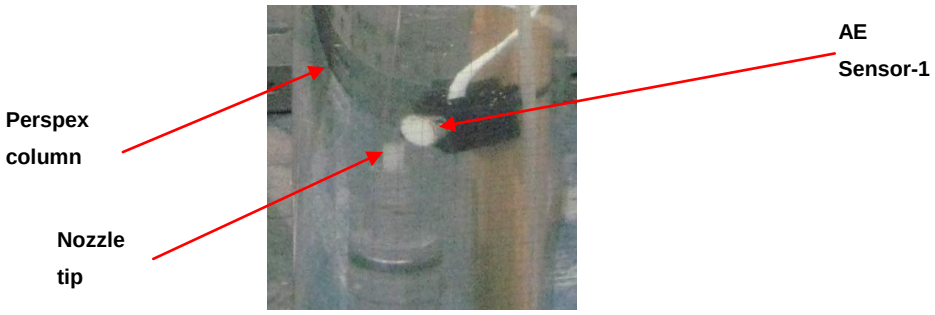

Figure 4-3: Picture of nozzle and AE sensor-1

Figure 4-4: Zoom picture at nozzle

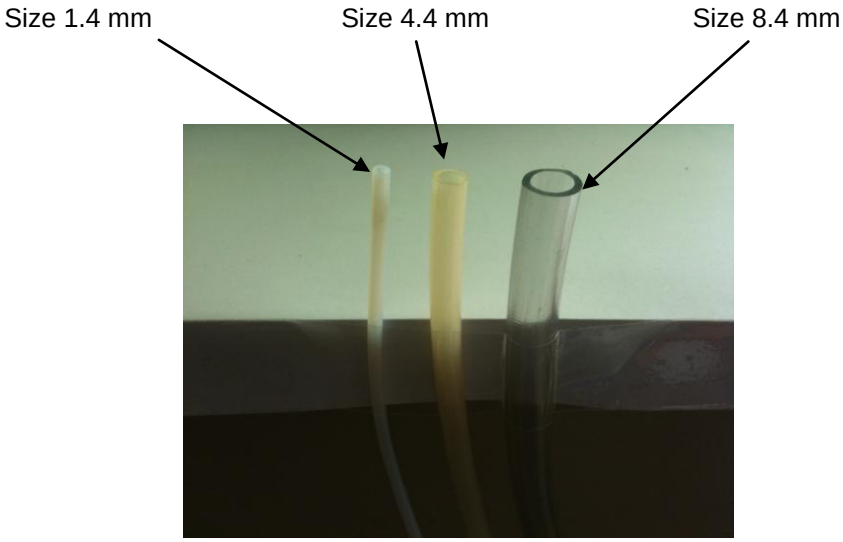

Figure 4-5: Three difference sizes of plastic hose (internal diameters) used in the initial test apparatus as a nozzle

4.1.1 Liquid

In this research programme, the liquid medium selected must be transparent for visualisation purposes. In this initial investigation, tap water was chosen as the liquid because a large volume was required for each experiment. The generation of AE from bubble activities was investigated for two liquids; plain tap water with a viscosity of 1 cP, and a dissolved salt solution with a viscosity of 2 cP. This latter liquid is simply referred to as saltwater. Table 4-1 shows the properties of the liquids used: viscosity and surface tension.

Viscosity is a measure of a fluid's resistance to flow. The viscosity of these solutions was measured using a rotational BROOKFIELD, DV-I *Prime* viscometer, see Figure 4-6. The Brookfield Viscometer is a precise torque meter which is driven at discrete rotational speeds. Its working principle is that resistance to the rotation of the spindle produces a torque that is proportional to the shear stress in the fluid.

Table 4-1: Liquid properties (Kihm, 1996; Trefethen, 1969)

	Tap Water	**Saltwater**
Viscosity	1 cP (measured)	2 cP (measured)
Surface tension	0.72 dyne/cm (literature)	0.75 dyne/cm (literature)

Figure 4-6: Tap water measured by BROOKFIELD, DV-I *Prime* viscometer

4.1.2 Nozzle and syringe

The submerged end of the hose situated at the bottom of the water column was used as a nozzle from which a single bubble was released when the syringe at the other end of the hose was manually and gradually pressed. Three sizes of internal diameter hose were used for the initial investigation:

i) 1.4 mm diameter,
ii) 4.4 mm diameter, and
iii) 8.4 mm diameter.

4.2 Data Acquisition System

As stated above, the DAQ system for the initial test consisted of AEWin and WaveView. The AE parameters were acquired automatically using AEWin software, whilst the waveforms were acquired manually with a preset duration at certain times during the test.

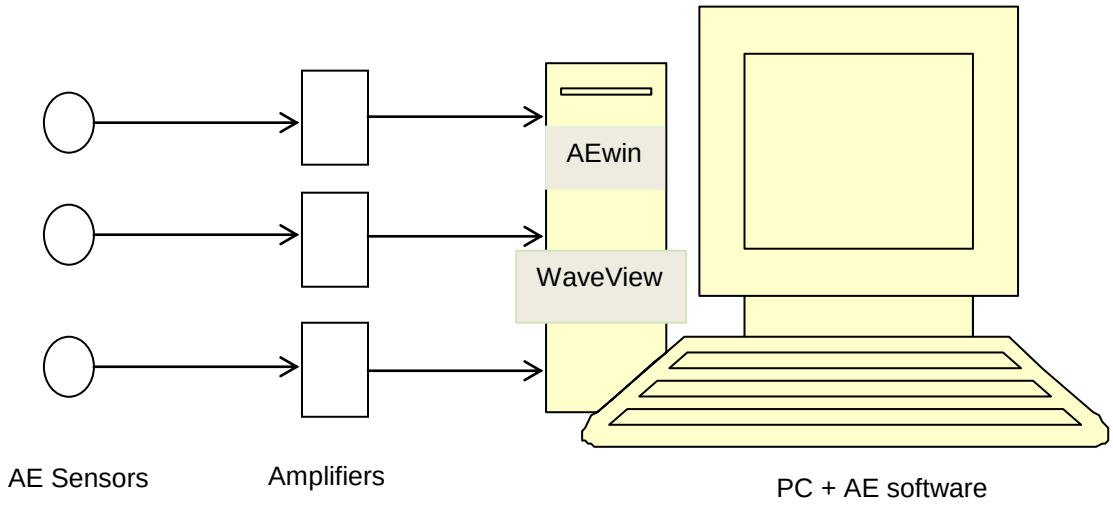

Figure 4-7: Schematic diagram of the data acquisition systems

4.2.1 AE sensors

Three broadband piezoelectric transducers (Physical Acoustic Corporation type WD) were rigidly attached to the inside of the Perspex column ensuring the active sensor face was positioned to measure any AE source. The sensor calibration by Physical Acoustic Corporation (PAC) is shown in Appendix C (page 179). In this initial test, the AE sensors attempted to detect AE from bubble activity intrusively. The transducer leads were sealed with heat-shrink tubing and silicone sealant to prevent damage when submerged in the solution. This insulation technique had been successfully employed by Wentzell et al. (1991) in their investigation using AE for quantitative chemical analysis of solutions.

In this initial investigation, sensor-1 was placed a few millimetres above the location of bubble inception, sensor-2 was placed midway up the liquid column, whilst sensor-3 was placed just beneath the free surface of the fluid. The distance between each adjacent sensor was 270 mm. The transducer had an operating frequency of 100 kHz - 750 kHz and pre-amplification at 60 dB was applied. The sampling rate for acquisition of AE waveforms was set at 2 MHz.

4.2.2 DAQ software

The AEWin version 3.2 software package from the Physical Acoustic Corporation (PAC User's manual, 2007) was used to record the AE parameters (AE amplitude (dB), AE duration, AE absolute energy (atto-Joules) and AE rise time). The software can record the waveform at a maximum sampling rate of 5 MHz. The waveforms captured by AEWin can be viewed using WaveView.

4.3 Bubble Test Rig Used in Second Test (2nd Test): Water (1 cP)

A good correlation of AE with bubble size and liquid viscosities that were used in the preliminary test led to the decision for an advanced test with higher liquid viscosities and nozzle size ranges.

The setup of the apparatus in the second test used to measure and detect the acoustics of bubble activities was the same in principle as the initial test apparatus. The apparatus (2nd test) used sheets of material to construct a larger rectangular column of internal dimensions 100 mm x 300 mm x 2000 mm (D x W x L), see Figure 4-9 (page 69). The number of nozzle sizes used in the advanced experiment was increased to four, see Table 4-2. In this advanced test rig, the nozzles were made from brass and each nozzle's tip was sharpened to a cone shape, see Figure 4-8 (page 68).

Table 4-2: Nozzle sizes used in advanced test

Size	Nozzle diameter
Size 1	1.4 mm
Size 2	2.8 mm
Size 3	5.6 mm
Size 4	8.4 mm

Figure 4-8: Four difference sizes of nozzle used in the advanced test rig made of brass and cone-shaped at each nozzle's tip

The side-walls of the second test rig were made of aluminium, see Figures 4-10, 4-11 and 4-12 (page 70-71), of thickness 50 mm to investigate signal transmissibility from bubble activities to a metal wall to which certain of the AE sensors were attached non-invasively (AE sensor mounted on the outside of the aluminium sheet). In this experiment, a three-way valve was used where a combination of gas released from an air compressed cylinder and syringe facilitated the process of gas injection for bubble creation.

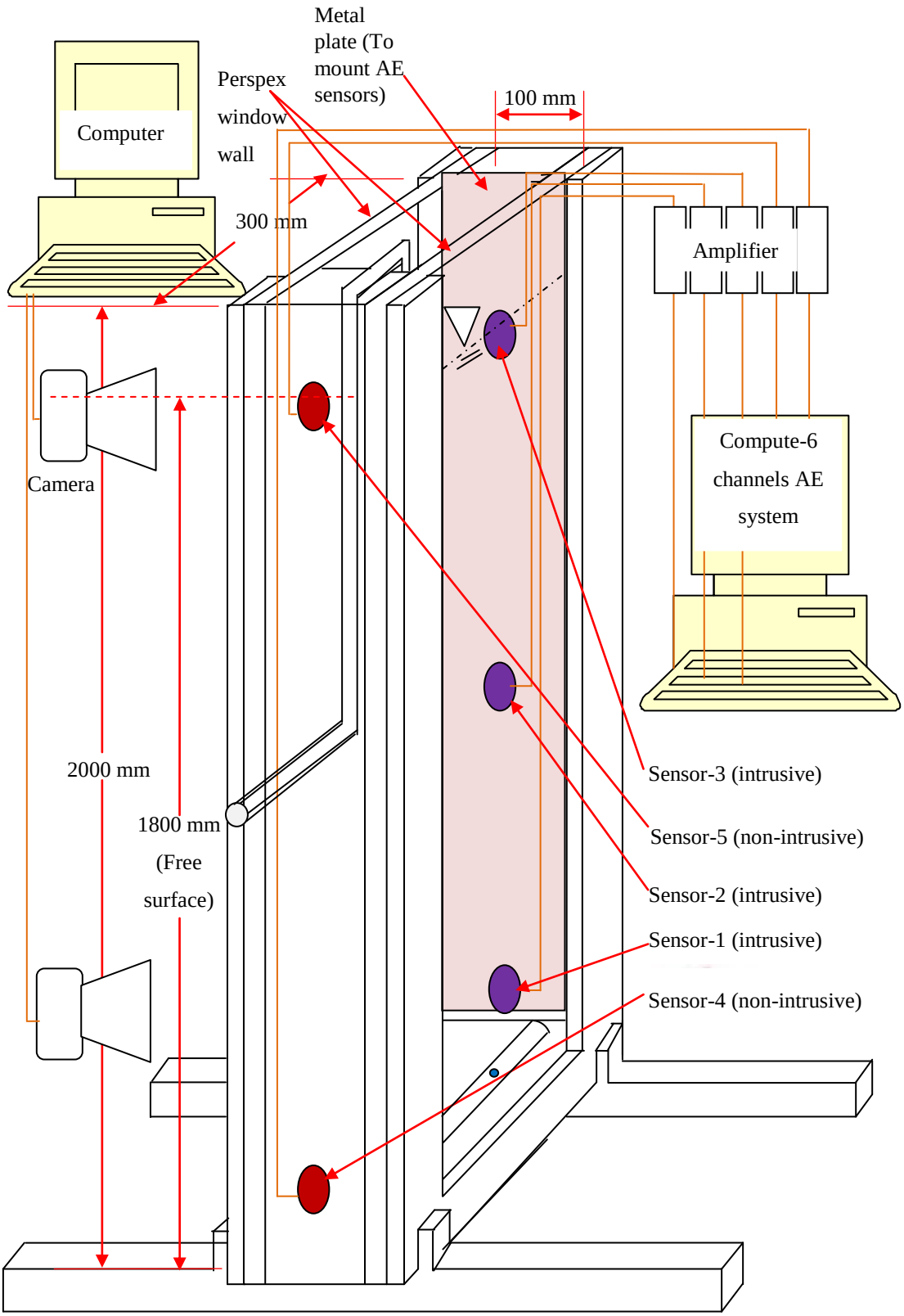

Figure 4-9: Schematic diagram of advanced experimental arrangement

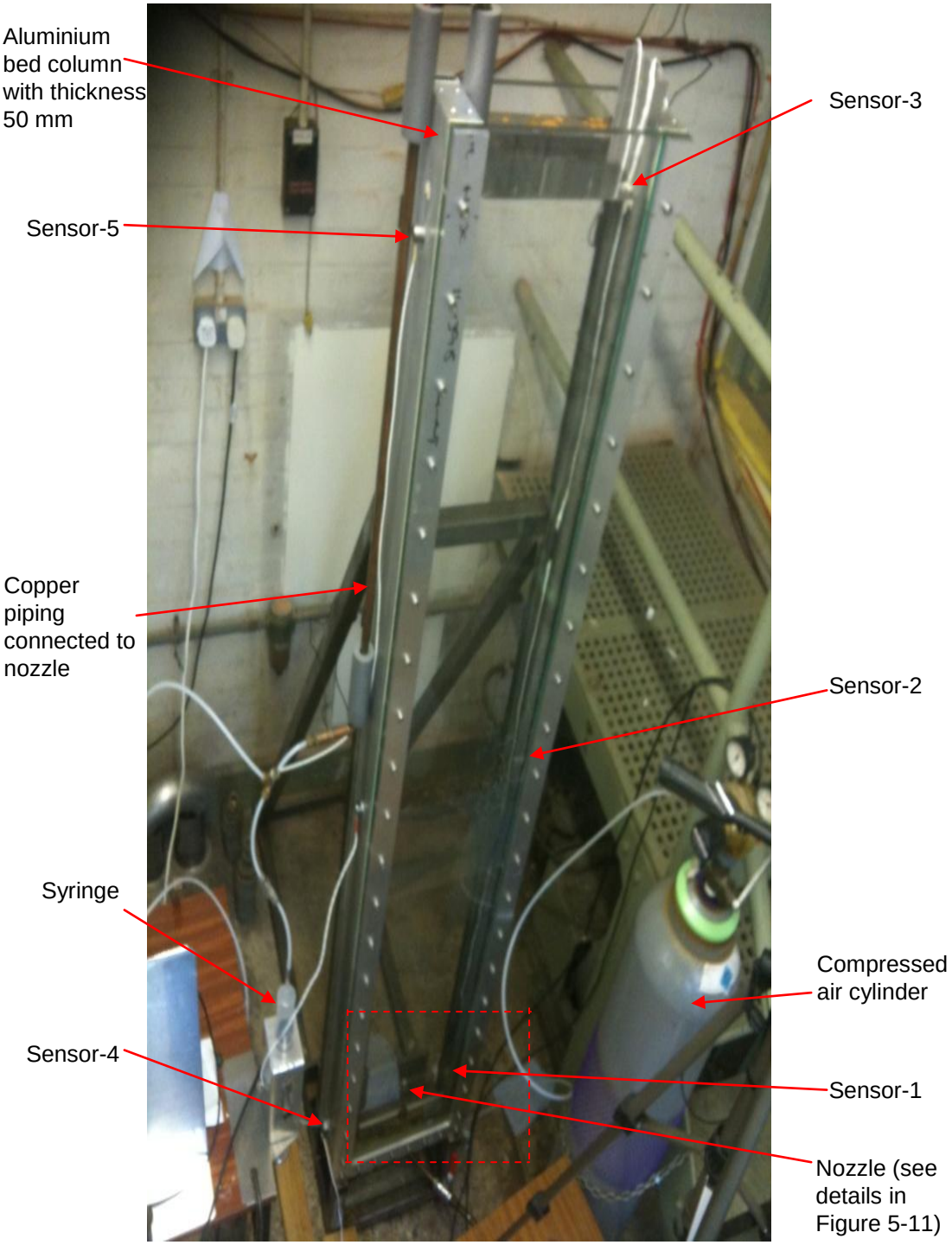

Figure 4-10: Advanced bubble test apparatus

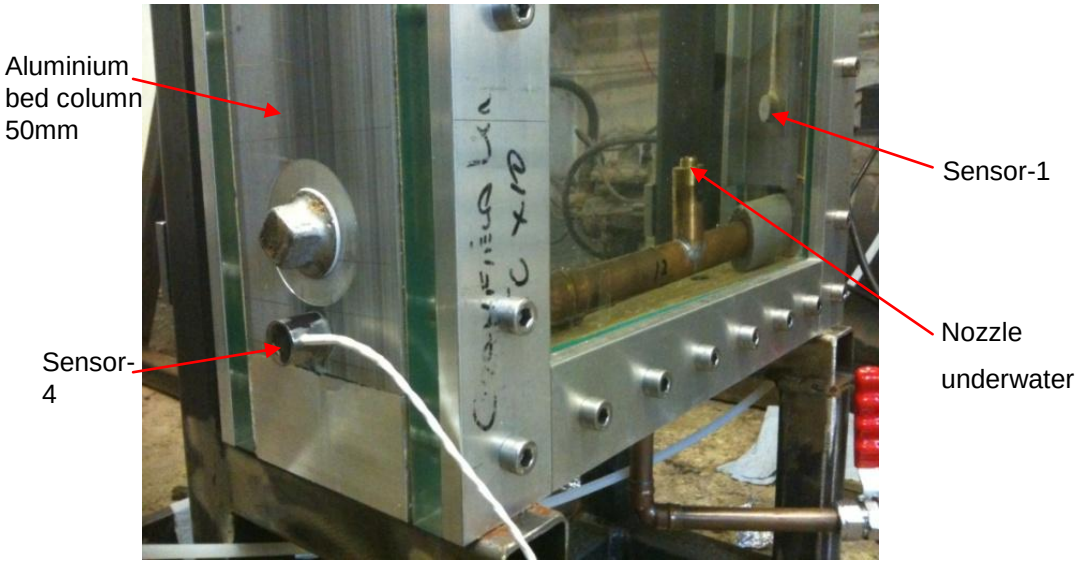

Figure 4-11: Nozzle at the bottom of bubble-column test rig

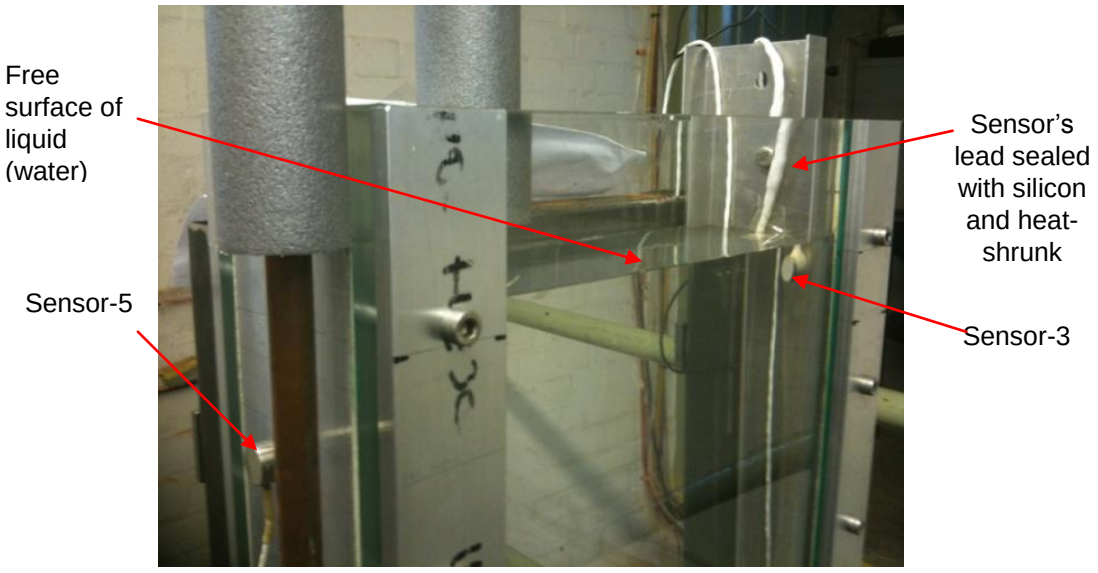

Figure 4-12: Intrusive sensor-3 and non-intrusive sensor-5 mounted at top of bubble rig

4.4 Bubble Test Rig Used in Third Experiment (3rd Test): Glycerine (10 cP)

Further modification was made to the bubble test rig that was employed in the second experiment to avoid the surface degradation (chemical reaction) experienced in a previous test (test 2). The surface degradation process (oxide formation or corrosion), see Appendix D, page 180) on the aluminium surface generated gas bubbles caused interference to the acquisition and identification of bubble activity from the injected bubble. Therefore, the aluminium sheet (thickness 50 mm) was replaced with stainless steel (thickness 10mm), see Figure 4-13.

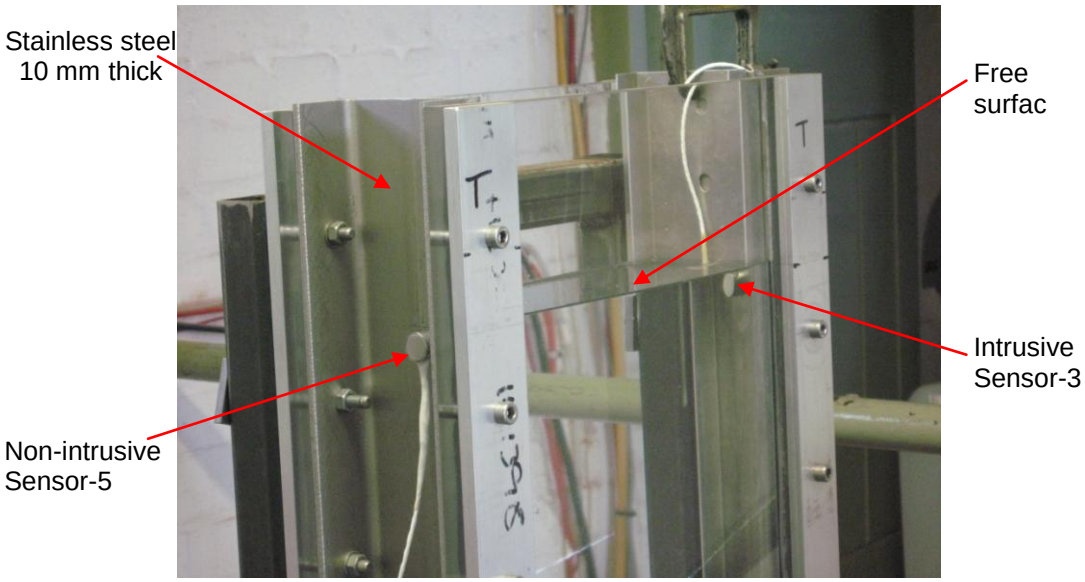

Figure 4-13: Bubble wall replaced with stainless steel, thickness 10 mm

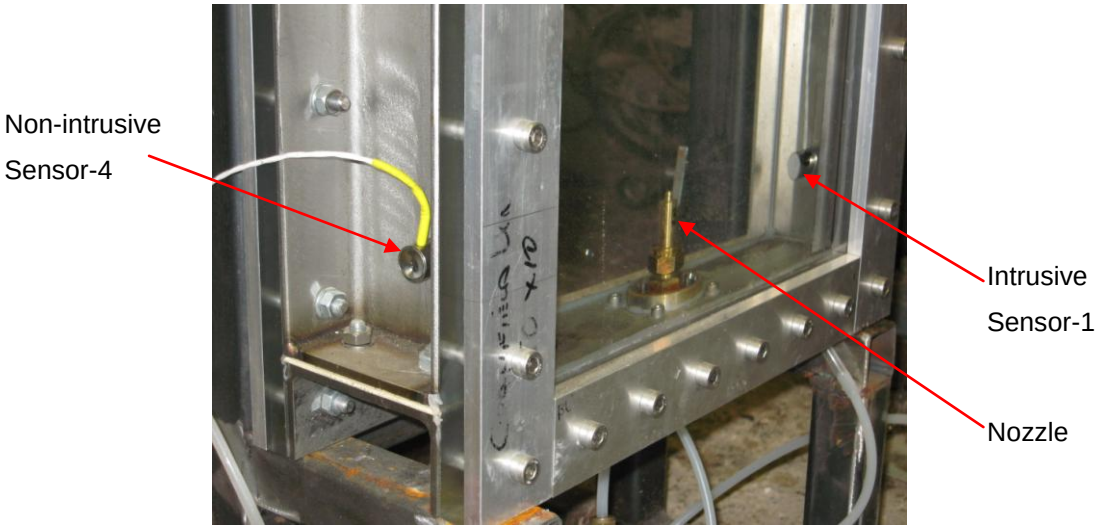

Figure 4-14: Direct gas injection to the nozzle from the bottom of the bubble column

In addition, direct gas injection through the nozzle at the bottom was introduced instead of the long length of tube as used in the test rig in the second experiment, see Figure 4-14. The shorter direct injection at the bottom of the column provided better control for continuous single bubble generation.

4.5 Conclusion

Basically, two different test rigs were used in this investigation. First, the column of the test rig was made of non-metal (core column - perspex). This initial test rig provides free-oxide formation at the perspex column (tube). Second, the column of the test rig was made of metal (aluminium) where AE sensors attempted to detect bubble activity non-intrusively. Various nozzle sizes and liquid viscosities were used to investigate the effect of bubble size generated and viscosity on the AE from bubble inception and burst. A single bubble created with the syringe technique was chosen since this technique produce repeatability of bubble size and gas injection through a nozzle is more commonly encountered in industry, compared with other techniques such as laser (Leighton, 1994).

5 EXPERIMENTAL PROCEDURES

All experimental procedures for the first, second and third tests are described in this chapter.

5.1 General

The preliminary (first) experiment was to assess the capability of AE technology to detect sound pressure emissions from bubble activities, particularly bubble formation, oscillation during rising and bursting at a free surface.

The second and third experiments were carried out after the results from the preliminary (first) test confirmed that AE sensors detected AE signals from a single bubble inception at bubble pinch-off from the nozzle and burst at a free surface. In the second and third experiments, greater numbers of nozzle diameters were tested to observe the effect of bubble size on AE generation from its activities. (Note the range was the same, i.e. 1.4 mm to 8.4mm). Figure 5-1 (page 77) shows the diagram of the experimental strategy for this study programme. Table 5-1 (page 75) shows the parameters for both tests.

Table 5-1: Comparison of the test parameters between 1st, 2nd and 3rd experiments

Test parameter	Initial/preliminary apparatus (First Test)	Advanced apparatus (Second and Third Tests)
Nozzle diameter	1.4, 4.4 and 8.4 mm	1.4, 2.8, 5.6, 8.4 mm
Liquid depth	540 mm	1800 mm
Liquid viscosity	1 cP (Water) 2 cP (Saltwater)	1 cP (Water) – Second Test 10 cP (Glycerine Solution) – Third Test
AE sensor type	Physical Acoustic Corporation type WD	
Sensor number and position	Sensor-1 (intrusive- bottom) Sensor-2 (intrusive- middle) Sensor-3 (intrusive- top)	Sensor-1 (intrusive- bottom) Sensor-2 (intrusive- middle) Sensor-3 (intrusive- top) Sensor-4 (non-intrusive- bottom) Sensor-5 (non-intrusive- top)

The Hsu-Nielsen test was used prior to the laboratory tests to verify the sensitivity of the sensors to an AE source and calibrate them relative to each other to ensure that the relative strength of AE from different bubble activities could be accurately compared.

Liquids of different viscosities were used; in the initial (1st) experiment, water and saltwater were used and here the two viscosities were quite close; 1 cP for tap water and 2 cP for saltwater. Whilst in the second (2nd) and third (3rd) experiment a glycerine solution with a viscosity of 10 cP and tap water were used.

In the 2nd and 3rd experiments, an attempt was made to detect AE from single bubble activities using a non-intrusively mounted sensor fixed onto the metal sheet forming one wall of the liquid column, see Figures 4-11, 4-12, 4-13 and 4-14 (page 71-73).

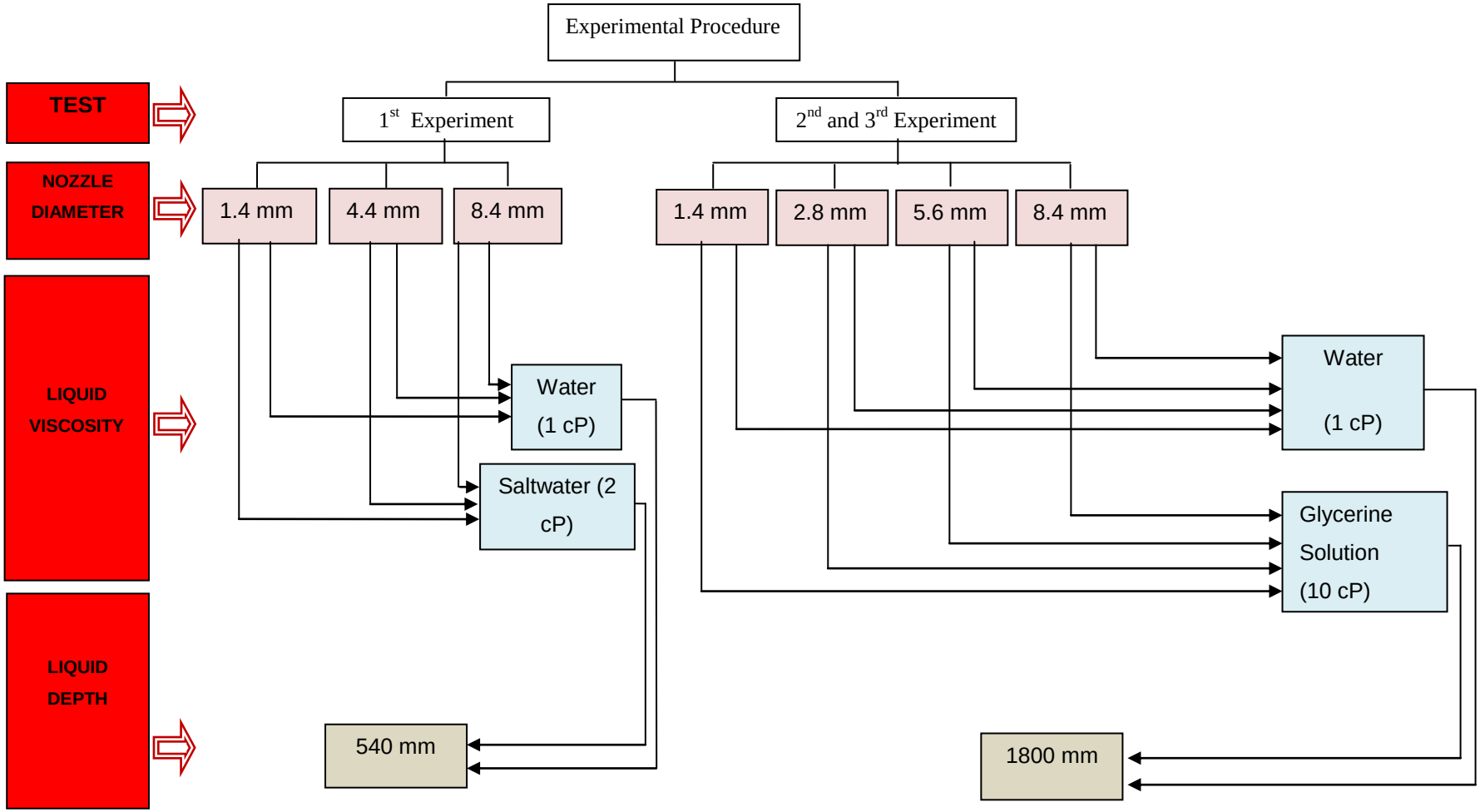

Figure 5-1: Schematic diagram of the experimental strategy

5.2 Hsu-Nielsen Test

The Hsu-Nielsen pencil lead break test is a well established procedure for verification of the sensitivity of AE sensors (BS EN 1330-9:2000). This procedure was adopted for this experiment; see Figure 5-2 for an illustration of Hsu-Nielsen source test technique. A 2H pencil lead with a length 3 mm and diameter of 0.5 mm (see Figure 5-2) is broken (snapped) at each of the three sensors' faces to check the sensitivity level of each sensor to an identical AE source. This procedure also verified that the AE acquisition systems were functioning properly.

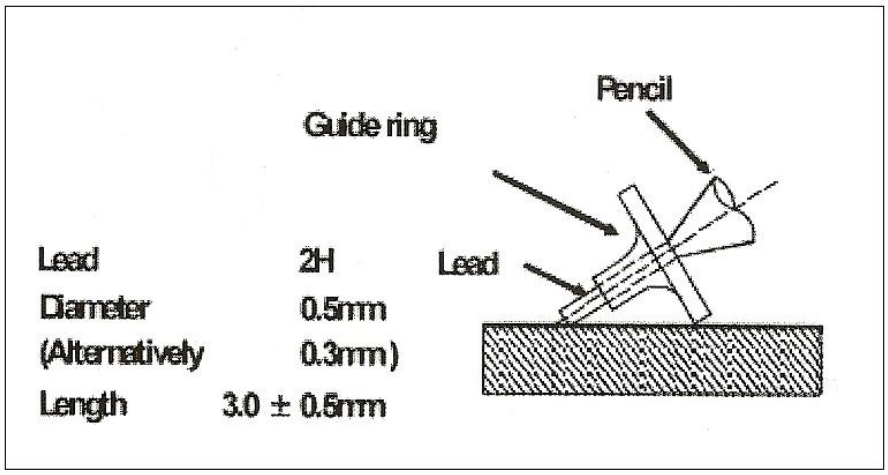

Figure 5-2: Hsu-Nielsen source test technique and the standard dimension (BS EN 1330-9:2000)

The test was performed on each sensor face with pre-amplified gain at 60 dB and 40 dB. The results are shown in Table 5-2 (page 79), where it can be seen that all sensors had the same sensitivity level 78 dB for both levels of gain. Figure 5-3 (page 79) shows the example of hit data from the pencil lead breaking test for a gain at 60 dB. The pencil lead break test on each sensor's face was performed three times to check reliability and repeatability of sensor sensitivity.

Table 5-2: Pencil lead attenuation test results

Gain Amplifier used	Hsu-Nielsen result: Sensor 1	Hsu-Nielsen result: Sensor 2	Hsu-Nielsen result: Sensor 3
60 dB	78 (dB)	78 (dB)	78 (dB)
40 dB	78 (dB)	78 (dB)	78 (dB)

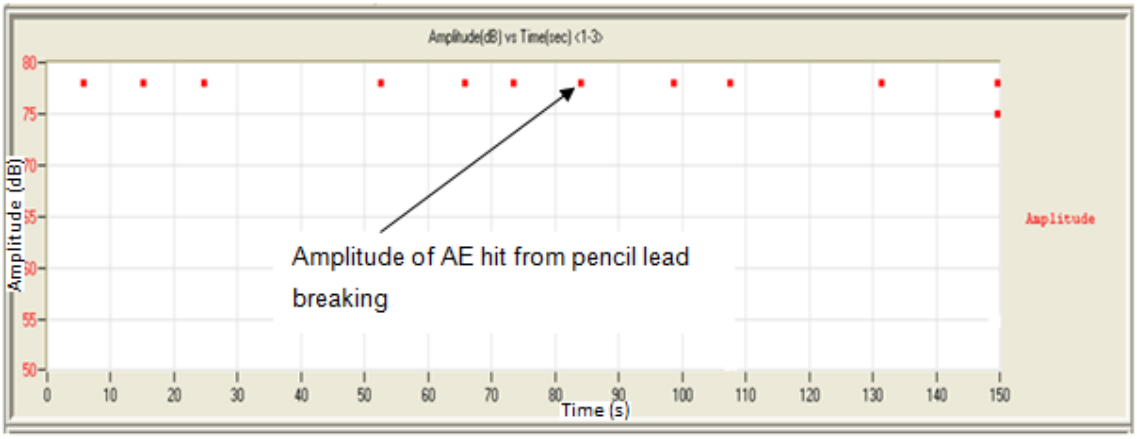

Figure 5-3: Hit driven data from pencil lead break test on every sensor's face with gain amplifier setup at 60 dB

5.3 Preliminary Experiment (First Test) and Procedures

Sensor-1 was positioned near to the nozzle purposely to detect bubble formation/incipience. Sensor-2 was positioned at the mid-depth of the liquid column to detect bubble oscillations as the bubble rose up to the free surface. Sensor-3 was placed very near to the free surface to detect AE from bubble burst at a free surface.

The sensors/transducers had an operating range of 100 - 750 kHz and a pre-amplification at 60 dB was applied. The sampling rate for the acquisition of AE waveforms was set at 2 MHz and the threshold level for hit data acquisition was set at 24 dB to eliminate background noise. Whenever AE sources from bubble

activities exceeded this level, data from all three sensors were acquired simultaneously.

A single bubble was created with a syringe as gas (air) was forced through different sized nozzles (diameters of 1.4, 4.4 and 8.4 mm) placed at the bottom of the water column. Throughout the experiment it was assumed that the diameter of the nozzle was equivalent to the diameter of bubble. Various nozzles, as shown in Table 4-2 (page 67), were used to produce gas bubbles of different sizes in order to investigate the effect of bubble size on AE released from bubble activities. In the initial investigation (1st experiment) two liquids with difference viscosities (tap water - 1 cP and saltwater - 2 cP) were used to investigate the effect of viscosity on AE from bubble activity. In addition the two cameras continuously recorded the motion of every bubble throughout the test.

In this initial experiment, the parameter-based AE (classical) approach: AE amplitude, AE average count, AE absolute energy and AE rise time, were directly obtained from the system. However, the focus of the test programme was the burst signal from bubble activities (see Figure 5-4, page 81). The background noise level could have affected the statistical results because the AE system takes the entire signal data (continuous signal) or the whole process, which includes the background noise. Hence, certain AE parameters, particularly AE absolute energy and AE duration, needed to be calculated carefully for transient waveforms. Waveform was obtained from hit driven data which determined by three timing parameters; the HIT definition time (HDT), HIT lockout time (HLT) and peak definition time (PDT). These were set at 200 µsec, 800 µsec and 1000 µsec respectively. Correctly setting the PDT will result in an accurate measurement of peak amplitude while the appropriate definition of HDT will ensure that each signal generated from the structure is reported as one HIT, as it defines the period over which a HIT can be acquired. With an accurate setting of HLT spurious measurement during the signal decay will be avoided; essentially it defines the period between successive HITs.

AE burst duration is obtained by the duration from the point at which the AE response was above a specified underlying threshold level (value of the tested

background noise that has been setup as threshold value) to the point at which it returned to that threshold level. The start and end of each burst on the waveform curve needed to be defined in order to obtain the AE duration. Figure 5-5 shows the procedure for transient waveform analysis; AE burst duration is the duration between the points at which the AE response was higher than the underlying threshold level to the point at which it returned to the underlying threshold level, see Figure 5-5 (page 82). The threshold set for this calculation procedure on the waveform plot as shown in Figure 5-5 was 0.61 mV.

The total energy release from the bursting event can be estimated by measuring the bubble's potential energy which is proportional with bubble size. In this investigation, it was assumed that bubble size generated was equivalent to nozzle size and the size was maintained until it burst at the free surface. Assuming pressure constant (isobaric) collapse, the bubble energy E_b available for each burst at the free surface is equal to the work W done by the liquid on the bubble during its collapse/burst, and is obtained by multiplying the pressure by the initial maximum bubble volume (Buogo and Cannelli, 2002):

$$E_b = W = \frac{4}{3}\pi R_{max}^3 (P_\infty - P_v) \qquad \textbf{(5-1)}$$

Where E_b is bubble energy; W is work done; R is radius of bubble; P_∞ is hydrostatic pressure at the outside of bubble; and P_v is vapour pressure in the bubble.

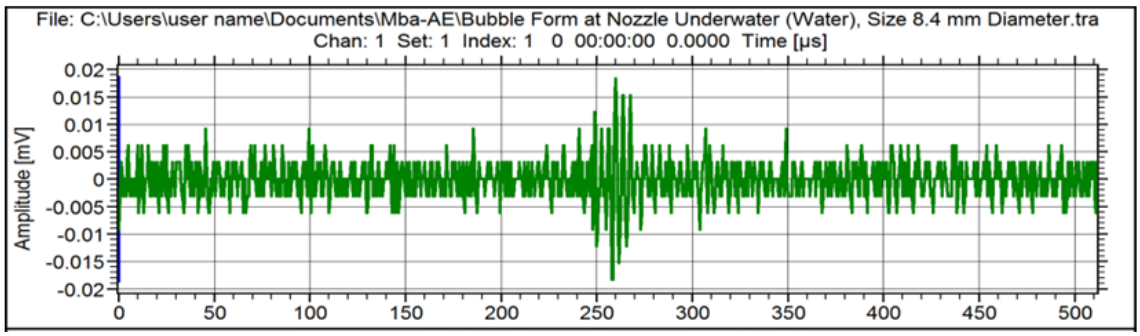

Figure 5-4: Example of AE transient signal from bubble formation

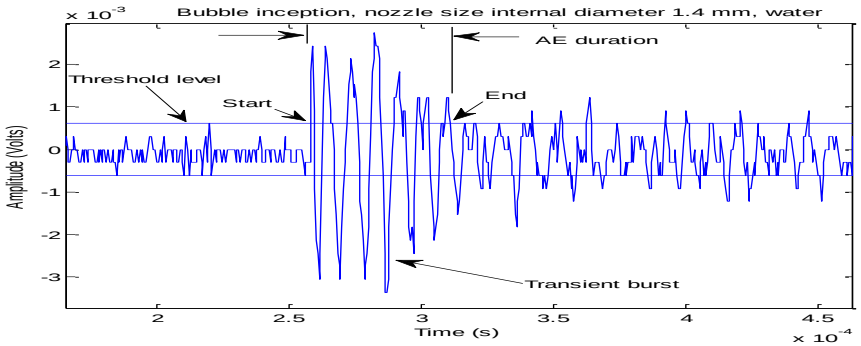

Figure 5-5: AE transient burst duration

5.4 Second and Third Experiments and Procedures

In the second experiment, a different bubble rig with a completely new design (rectangle column, metal nozzle) was used. The test rig was also moved to a different location. The apparatus used for AE detection in this experiment is shown in Figures 4-10 to 4-12 (page 70-71), and described in Chapter 4. The rig consists of a 50 mm thickness aluminium column filled with water. A continuous single bubble in the column was produced with very slow air release from the air compressor by controlling the needle valve.

To compare the AE signal acquired intrusively and non-intrusively, a broadband piezoelectric transducer (Sensors-1 and 3) was fitted in the liquid column with the active sensor face to the fluid (see Figure 4-11, page 71) and a second AE piezoelectric transducer (Sensors-4 and 5) was non-intrusively mounted onto the column test rig aluminium wall (see Figures 4-11 and 4-12). Here broadband Physical Acoustic Corporation type WD AE transducers with an operating range of 100-750 kHz and a pre-amplification at 40 dB were used. The sampling rate for the acquisition of AE waveforms was set at 2 MHz. A level of 26 dB was set as the threshold level for the acquisition system.

In the third experiment, a glycerine solution with a viscosity of 10 cP and tap water were chosen for the test programme. Four nozzle sizes of internal diameters: 1.4, 2.8, 5.6 and 8.4 mm made of brass were used and were fitted

vertically onto the copper pipe, as can be seen in Figure 4-8 (page 68). The tip of each nozzle was chamfered to prevent irregular bubble inception resulting from the adhesion of the meniscus to the material of the nozzle between the bore and the outer diameter (Leighton, 1994a).

The Hsu-Nielsen pencil lead test was repeated prior to the tests to ensure the transmissibility of the AE signal from the source to the sensor and to verify that the AE acquisition systems were functioning properly. All sensor tests had the same sensitivity level at 78 dB at 40 dB gain pre-amplified.

Air was gently released through the four different sized nozzles to obtain four different bubble sizes. Again, in this experiment it was assumed that the diameter of the nozzle was equivalent to the diameter of each bubble. Physically, the size of bubble generated by gas injection through a nozzle is attributed to the size and shape of the nozzle. There is a range of nozzle size for the size of bubble generated where it is attributed to the bubble meniscus development as explained in Section 2.2, Figure 2-5 (page 22). The shape of the nozzle's tip, for instance a flat shape, contributes to irregularity of the size and shape of the generated bubble due to cohesion force between the interface of the bubble and metal surface area (nozzle end/tip). AE Sensor-1 (intrusive sensor which had its active plate facing the nozzle) and AE Sensor-4 (non-intrusive sensor mounted onto the outside aluminium wall at 50 mm) were positioned for capturing AE as the bubble pinched-off at its inception and detached from the nozzle. The waves travelled through two media: water and metal (aluminium), before being picked up by Sensor-4.

The same procedure for transient waveform analysis as used in the 1st and 2nd tests was applied; the threshold used in the procedure analysis waveform for AE duration was 0.61 mV, see Figure 5-5 (page 82). This methodology was also applied to calculate the AE energy within the burst by determining the area of the waveform and dividing by the reference resistance (10 kΩ), see Eq 3-2 (page 49). The energy was calculated using the trapezoidal numerical integration which allows a direct energy analysis to be performed (Mba et al., 2004).

In addition, a fast Fourier analysis (FFT) was performed to show the frequency content of the signal. Also presented was a corresponding time-frequency plot employing a Gabor wavelet which was generated with the AGU-Vallen software tool.

5.5 Conclusion

In this investigation on the energy released from a single bubble inception and burst, waveform analysis at the transient waveform with a threshold was proposed for AE energy measurement. The area under curve within the duration of transient waveform was calculated; presenting the energy of a single bubble activity. The procedure proposed did not take into account the average background noise which would show a more accurate result compared with the result obtained directly from the AE system (AEwin). This is because the statistical result obtained directly from the AE system considers the average value of the whole waveform.

Time-frequency analysis with wavelet transforms (WTs) was chosen for this singularity and transient event as this method localises the frequency or energy of the event with time. Wavelet transforms with AGU-Vallen software were chosen for energy analysis. This software was used as a tool for AE data analysis.

6 RESULTS, OBSERVATION AND DISCUSSION

This chapter presents and discusses the results obtained from a series of experiments performed in this study programme. Discussion will also be presented on the statistical analysis of the AE output parameters: AE amplitude, AE rise time, AE duration and AE absolute energy. From this analysis, the best AE indicators will be determined. Post-processing for AE waveforms was further analysed for AE duration and AE energy at a predetermined threshold condition. Signal processing of AE waveforms using Gabor wavelet transform is also presented.

6.1 First Experiment; tap water (1 cP) and saltwater (2 cP)

The first experiment used a simple bubble test rig that consisted of a vertical Perspex pipe of diameter 150 mm, with water depth of 545 mm. Three sensors were placed intrusively with a separation of 270 mm between consecutive sensors. The nozzles were constructed from the ends of plastic hoses and all three sensors were attached to a length of wood fixed into the column.

6.1.1 AE Detection from a Single Bubble Activity: inception, oscillation, hitting free surface and burst

It was observed that at pinch-off, as the bubble closed during its inception and detached from the hose, an AE event was captured by AE Sensor-1, closest to the nozzle. A typical waveform associated with pinch-off is shown in Figure 6-1 (top) (page 86) where a transient AE event is evident above the electronic background noise level of the acquisition system. A corresponding time-frequency plot (WT) is also presented in Figure 6-1 (bottom).

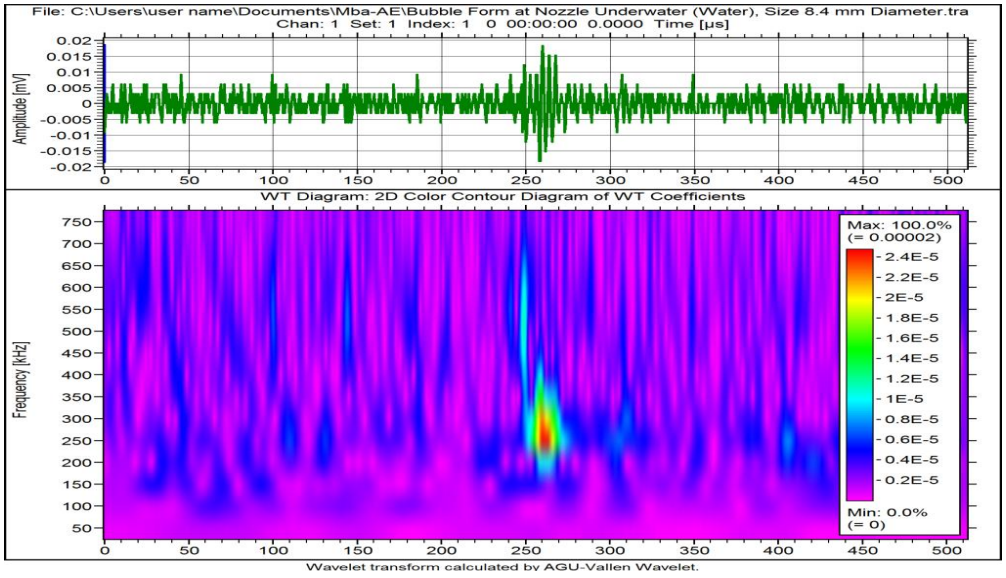

Figure 6-1: Time-domain waveform (top) and time-frequency plot (bottom) associated with bubble inception (nozzle size 8.4 mm in tap water (1 cP))

The bubble travelled up the fluid column and burst at the top of the fluid (free surface), and the resulting AE waves were captured during this burst event by Sensor-3, closest to the top of the fluid. Figure 6-2 (page 87) shows the waveform and WT from the burst event. The higher frequency content was noted at the start of the AE event, typically within ~10 µs, see Figure 6-2. Similar observations were noted for the AE associated with inception; see Figure 6-1. A transient at the waveform is associated with the pinch-off when the bubble is released from the nozzle (see Figure 6-1(top)) and collapses/bursts at the free surface (see Figure 6-2 (top)).

The frequency range of bubble burst inception is up to 670 kHz, while for bubble burst a lower frequency range of up to 570 kHz was shown. In addition, the WT plot (see Figure 6-1 (bottom) and Figure 6-2 (bottom)) clearly shows that the intensity of frequency range (red colour) for bubble burst is lower than bubble inception, i.e. up to 340 kHz and up to 130 kHz respectively. Comparison of the rate of change of intensity of frequency parameter between these two events (inception and burst) therefore is about 38%. In this investigation, the

comparison of the rate of change of intensity of frequency parameter between bubble inception and burst is defined as a relative increase or decrease of the signal strength in terms of frequency from a time-frequency plot of wavelet transforms analysis.

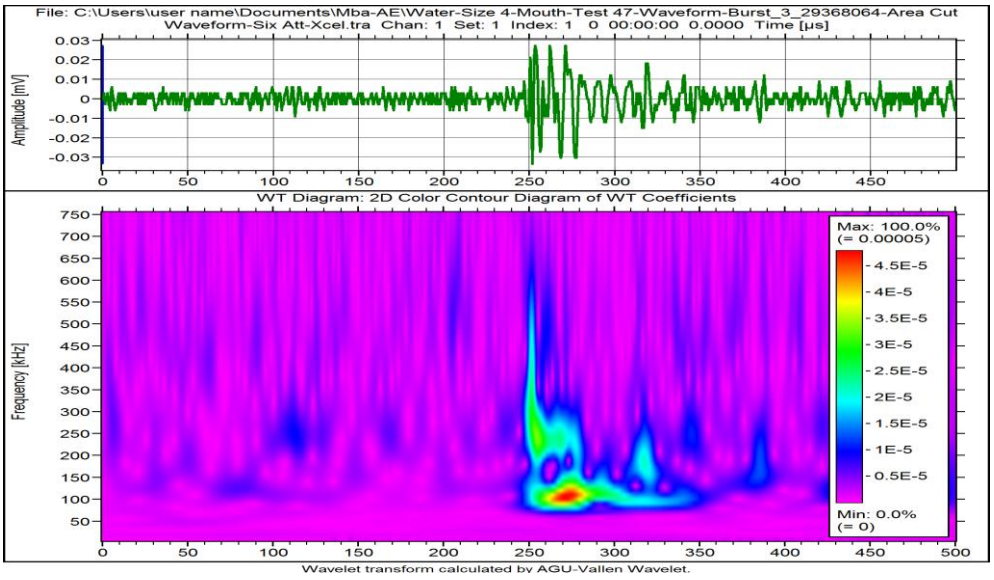

Figure 6-2: Typical time-domain waveform (top) and time-frequency plot (bottom) of a bubble burst at the free surface, nozzle size 8.4 mm in tap water (1 cP)

In some instances, dependent on the amount of energy released from the bubble during its burst at the free surface, Sensors-3, -2 and -1 would detect the emissions associated with the bubble burst, see Figure 6-3 (page 88). Thus AE waves from a burst will be detected by sensors further away from the source but there will be an associated time delay equal to the time taken for the signal to travel to the sensor, relative to the sensor closest to the AE source.

In Figure 6-3, the time-frequency plot of the AE measured at Sensor-2 and -1 showed a reduction in the higher frequency content compared with Sensor-3 which was closer to the source of AE. This observation implied attenuation of the AE signal as it travelled through the water. The average amplitude

attenuation rate with distance travelled in tap water in this experiment was 22 dB/m.

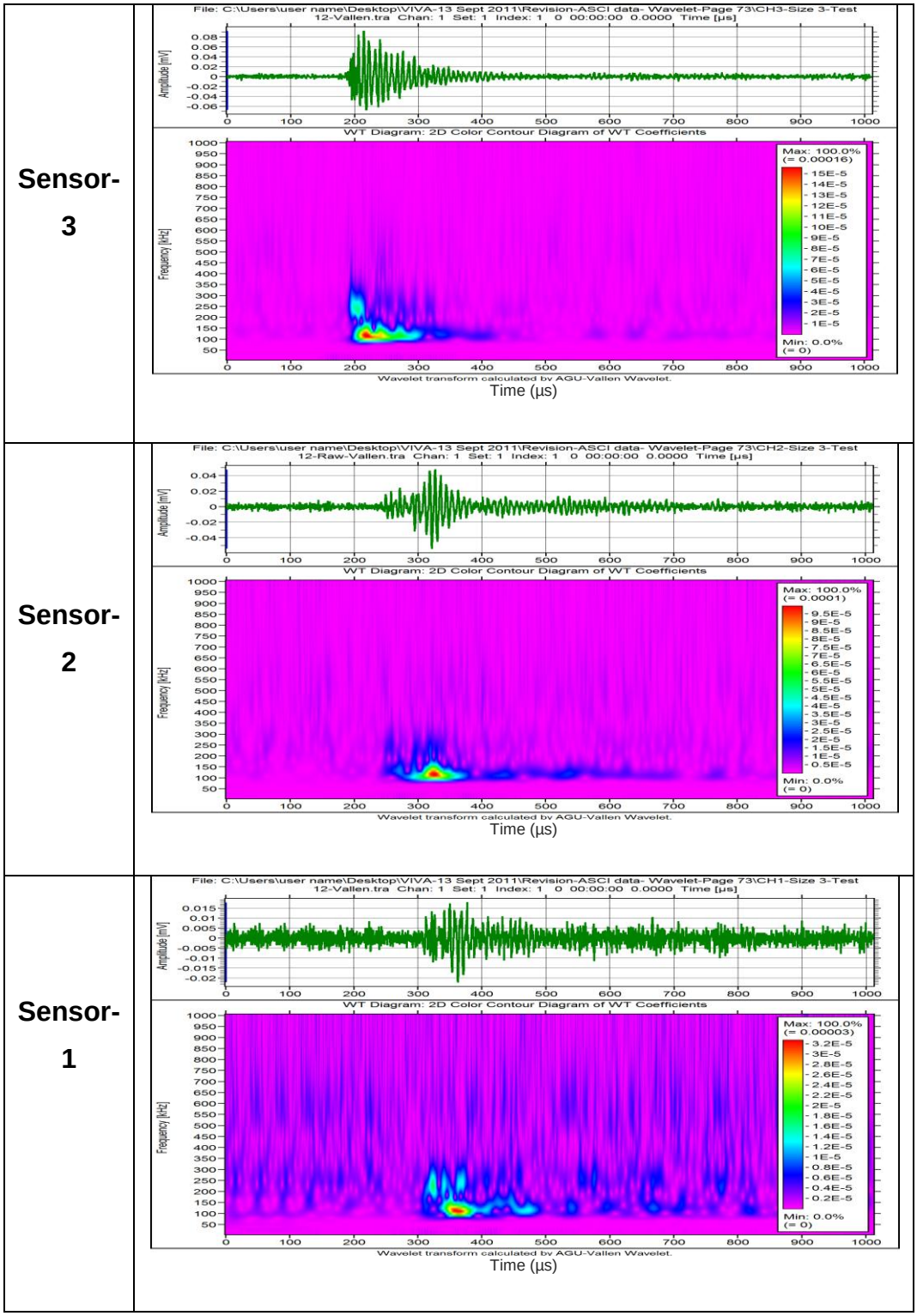

Figure 6-3: Time and frequency plots of a bubble burst at the free surface (nozzle size 8.4 mm in water)

The waveforms presented in Figure 6-3 (page 88) are plotted from raw data obtained from bubble burst to show time delays and the arrival time of AE signals between sensors. The plots show that the signals' arrival times are in order: Sensor-3, Sensor-2 and then Sensor-1. It was noted that the signal intensity decreased as the sensor distance from the AE source increased. In Figure 6-3, it can be seen that the signal strengths which are depicted by the maximum WT coefficient obtained from the waveform of the bubble burst detected by Sensors-3, -2 and -1 are $15x10^{-5}$, $10x10^{-5}$ and $3.2x10^{-5}$ respectively.

The time-frequency plot (wavelet) from AE data obtained from Sensor-1 (the farthest sensor from the bubble burst point at the free surface) shows a lower wavelet energy compared with Sensors-2 and -3. However, signal intensity of the burst event detected by Sensor-1, as can be seen in the wavelet plot (the bottom of Figure 6-3) can still be differentiated from the background noise.

Figure 6-4 (page 90) shows a comparative view of the AE arrival time differences between the sensors-3, -2 and -1 for bubble burst event signal detection. The black vertical lines are provided to determine the starting point of the bursting event and to show the time delay of the signal detected between sensors. The transient waveform from bubble burst at the free surface detected by the closest Sensor-3 shows relatively higher amplitude compared with the farthest Sensors-2 and 1. This demonstrates that waves from bubble activity (burst) are propagating and can be detected by sensors located away from the AE source. In other words, the energy is spread and decreases (attenuation) as the distance increases. The waveform shows that energy before and after the transient occurrence is relatively lower; it is a background noise. A higher signal to noise ratio (SNR) of AE technology, as indicated in Figure 6-4, provides an effective detection and monitoring of the fault (defect) or particular event in an investigated system.

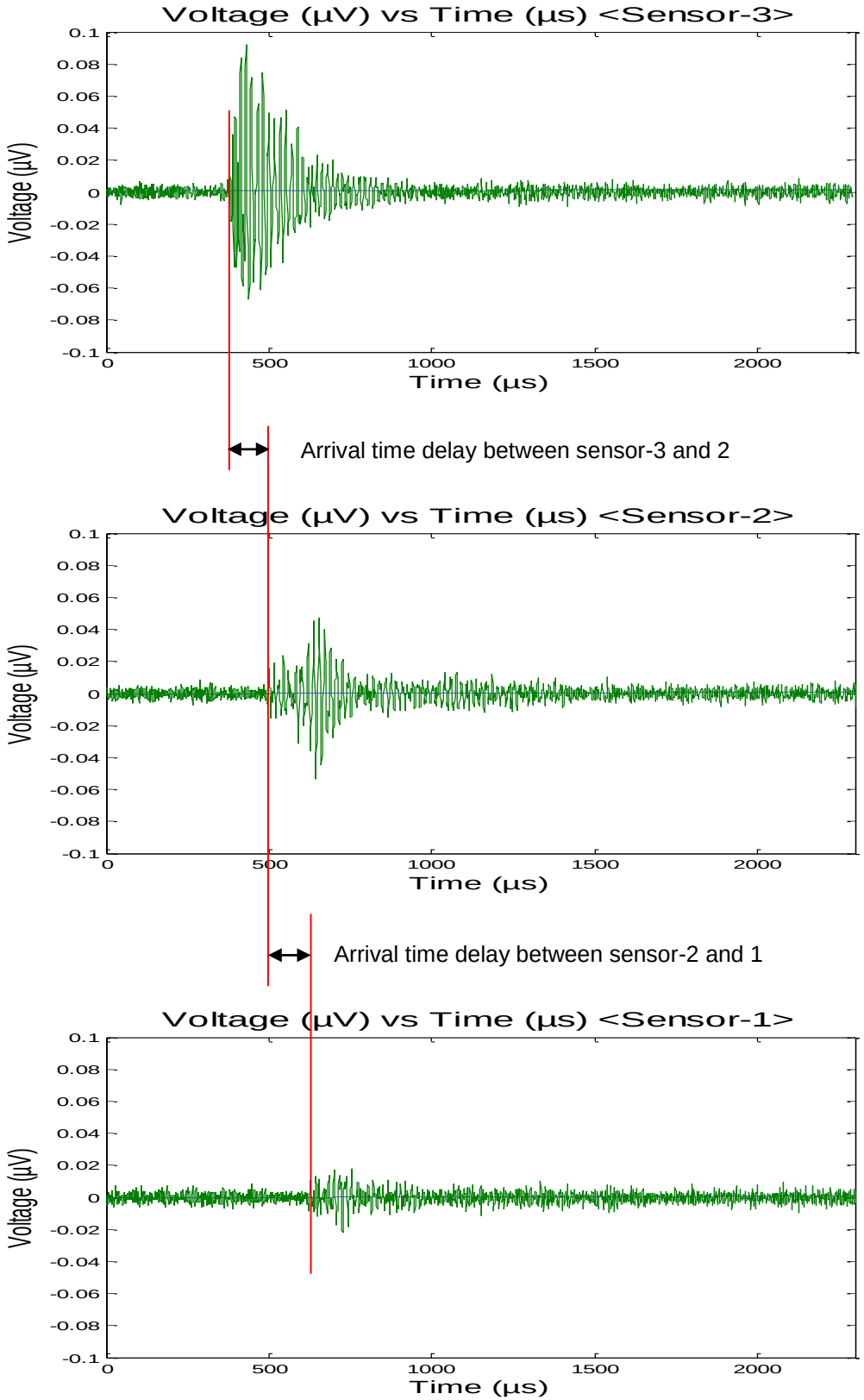

Figure 6-4: Difference in arrival time of AE waves at Sensors-1, -2 and -3, from bubble burst event at the free surface, size 8.4 mm

In this experiment it was found that no signal was picked up by Sensor-3, the closest to the free surface, when the bubbles hit the free surface. This was confirmed by analysing the hit data and occurrence time checking with the video camera. Figures 6-5 and 6-6, and Table 6-1 (page 92) justify the observations and conclusions made for a bubble hitting the free surface.

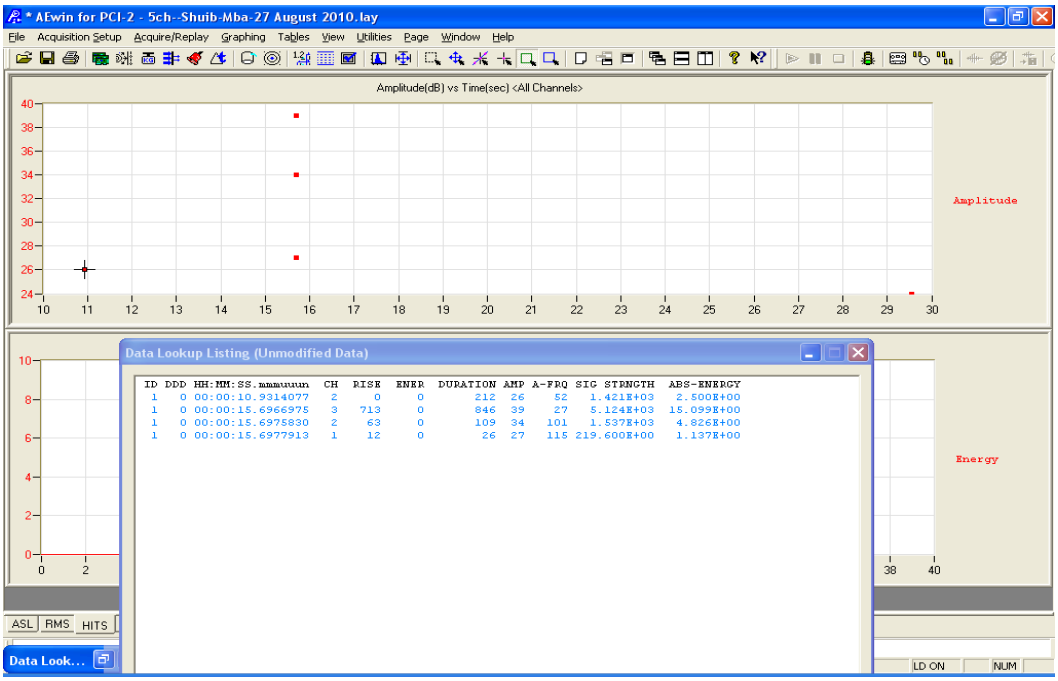

Figure 6-5: AE hit signal output

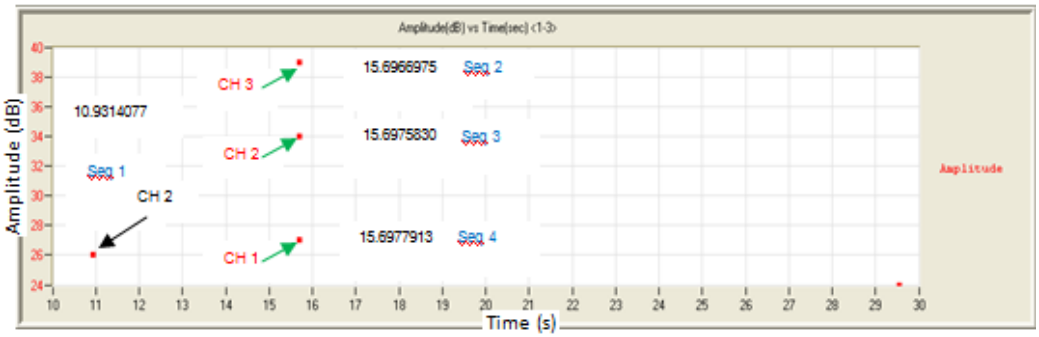

Figure 6-6: Example of hit signal output from bubble activity; Size 8.4 mm in tap water

Table 6-1: AE observation on bubble activities; inception, oscillation, hitting the free surface and burst

Sequence	Channel (Sensor)	Event Occured at Time (s)	Event
1	2	10.9314077	Other AE activity
2	3	15.6966975	Burst Event; Sensor-3 pick up
3	2	15.6975830	Sensor-2 pick up
4	1	15.6977913	Sensor-1 pick up

Note: the accuracy as presented in Table 6-1 was from the system. The time recorded reflects the sensor picking up the signal from the event. This accuracy is needed to differentiate the arrival time of signal picked up by Sensors-1, -2 and -3 on the AE activity (bubble burst).

The sequence in the first column refer to the time of the event (AE source) detected by AE Sensors-1, -2 and -3. Figure 6-6 (page 91) shows AE HITs output from the system where time or event sequence can be seen. In some cases, dependent on the amount of energy released from the bubble during burst at the free surface, Sensor-3, 2 and 1 would pick-up the signals; see Figure 6-6 and Table 6-1. Sequence no 2 is the event of bubble burst at the free surface and was first detected by the nearest Sensor-3 followed by Sensor-2 and 1 with some arrival time delay. Sequence no 1 had occurred 4.8 sec earlier than the burst event. Therefore, the hit of sequence no 1 was confirmed not from the oscillation when the bubble rise-up to the free surface since time taken for a bubble in this experiment to reach the free surface after being detached from the nozzle is approximately 3 sec; signal from bubble oscillation should be detected at ~1.5 sec before the bubble burst occurrence. Therefore, refer to Figure 6-6 and timing analysis (sequences) as shown in Table 6-1, it is concluded that in this experiment there was no bubble oscillation frequency detected by the AE sensors as the bubble rose through the liquid after pinch-off. In particular Sensor-2, which was placed at the middle of the column, did not detect the shape oscillations observed during the bubble rise up, as they passed Sensor-2. Moreover, Figure 6-6 shows that no signal for bubble

inception event was detected by Sensor-1 most likely because the signal strength was probably below the set threshold value of 24 dB.

6.1.2 Statistical analysis on AE parameters of bubble burst

The bubble burst at the free surface is independent of parameters other than for bubble size and liquid viscosity. Thus the bubble burst events were statistically analysed to determine the critical AE parameter indicator for bubble activity detection. Table 6-2 (page 94) shows the average and standard deviations for comparison between classical AE parameters from the AE system (AE Amplitude, AE Count, AE Average Frequency, AE Absolute Energy and AE Rise Time) from Sensor-3 (bubble burst). These statistical parameters were obtained directly from the AE system (AEWin).

The average and standard deviation calculation set out in Table 6-2 was taken from 25 test samples. These results are based on the raw data taken from the AE system (AE count, AE frequency, AE absolute energy and AE rise time). Only AE amplitude (dB) shows a standard deviation that is not over the mean value (13 % of mean value). This suggests that this could be the most useful measure for further analysis; and careful consideration is needed on how to minimise the background noise in the waveform analysis. One recommendation could be the use of waveform analysis for the transient signal instead of taking data from the whole waveform (statistical AE parameters from the AE system).

Table 6-2: Comparison of average AE parameter of free surface bubble burst for all nozzle sizes

	Size 1.4 mm				Size 4.4 mm				Size 8.4 mm			
	Water		Saltwater		Water		Saltwater		Water		Saltwater	
	Ave	Stdev	Ave	Stdev	Ave	Stdev	Ave	Stdev	Ave	Stdev	Ave	Stdev
AE Amp (dB)	26	3	30	5	30	3	37	6	35	4	38	5
AE Count	3	2	5	4	5	4	8	9	16	10	18	11
AE Freq (KHz)	0.263	0.284	0.341	0.351	0.239	0.301	0.236	0.269	0.105	0.117	0.124	0.74
AE Abs Energy (atto-Joule)	0.7	0.3	1.3	0.9	1.3	1.9	4.9	15.4	4.4	3.6	10.2	13.7
AE Rise Time (µs)	17	57	11	29	93	221	54	111	130	192	63	134

The results show that the bigger the bubble size, the higher the AE amplitude, AE Absolute Energy, AE Count and AE Rise time, see Figures 6-7 to 6-10 (page 95-97) respectively. Figure 6-7 (page 95) suggests that for saltwater, a small increment of amplitude for the size of bubble generated from the nozzle size beyond 8.4 mm is due to the size of bubble, not equivalent to the nozzle size. In this experiment, bubble diameters (Figures 6-7 to 6-11, page 95-97) are assumed equivalent to nozzle size (internal-hole diameter). In addition, the bubble size is difficult to control with the gas injection technique. This is because the bigger the nozzle size, the lower the incipient fluidization rate (U_{mf}) for bubble/void forming at the end of the nozzle. However, a comparison of bubble burst in saltwater and water, as shown in Figure 6-7, shows a significant effect of viscosity and bubble size on the AE generated. The closer the molecules of a material which is associated with material properties such as

density and viscosity, the higher the AE propagation and transmission that will take place. Moreover, it will give a higher amplitude of the AE event.

In contrast, Figure 6-11 (page 97) shows the AE Frequency decreases with increasing bubble size. Larger bubbles are louder and contribute more to sound power when bursting at the free surface (Manasseh and Chanson, 2001; Husin and Mba, 2010), and generate a lower wavelength (λ) compared with smaller bubbles. Therefore, by applying the sound field equation, the frequency produced from a larger bubble burst at the free surface is lower compared with the frequency produced from a smaller bubble.

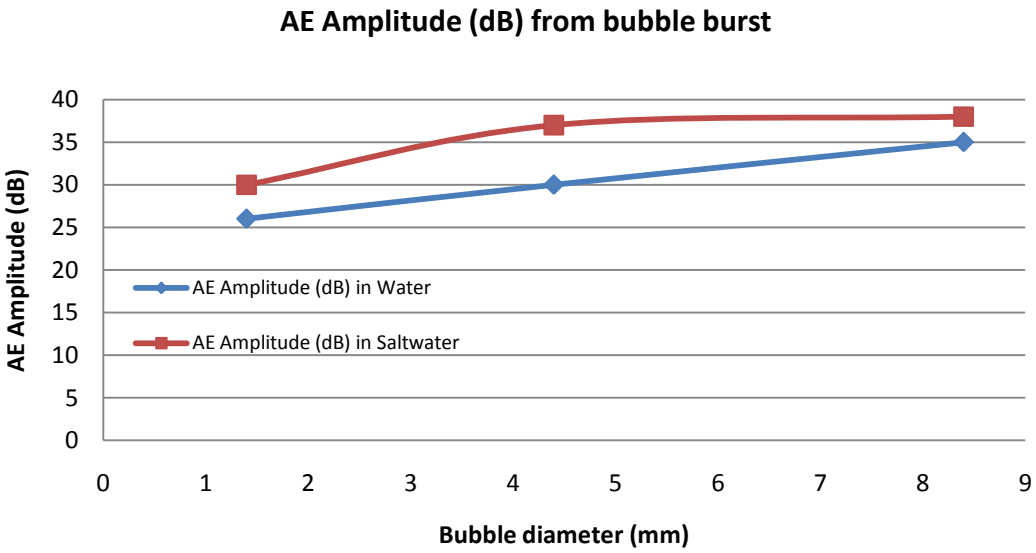

Figure 6-7: AE Amplitude from bubble burst as a function of bubble size and viscosity

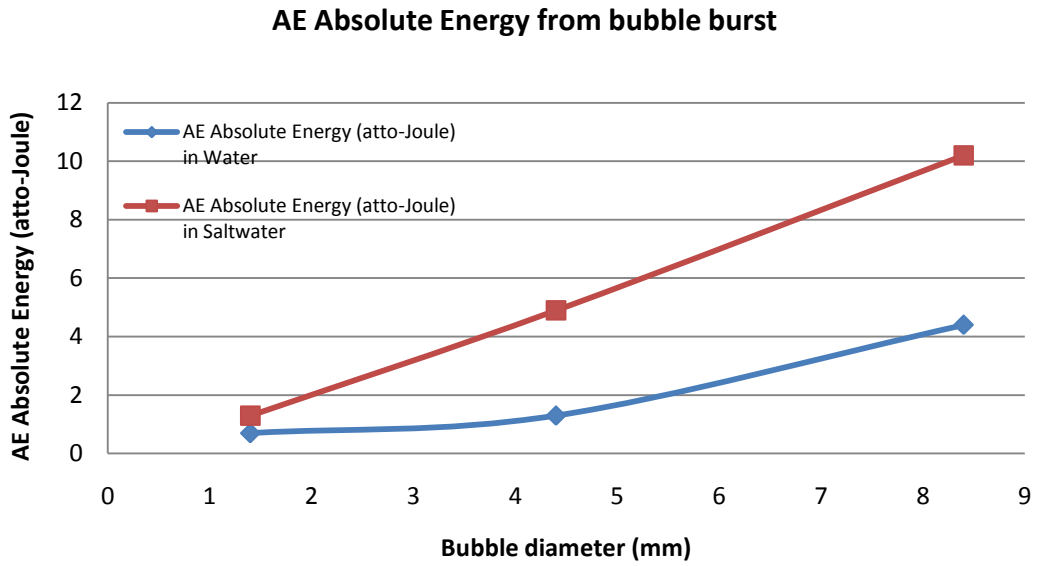

Figure 6-8: AE Absolute Energy (atto-Joule) from bubble burst as a function of bubble size and viscosity

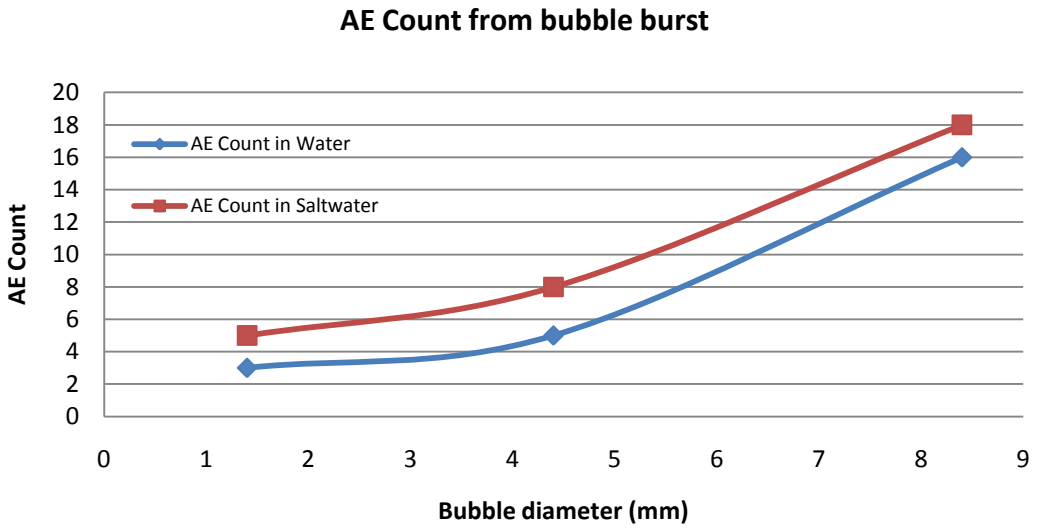

Figure 6-9: AE Count from bubble burst as a function of bubble size and viscosity

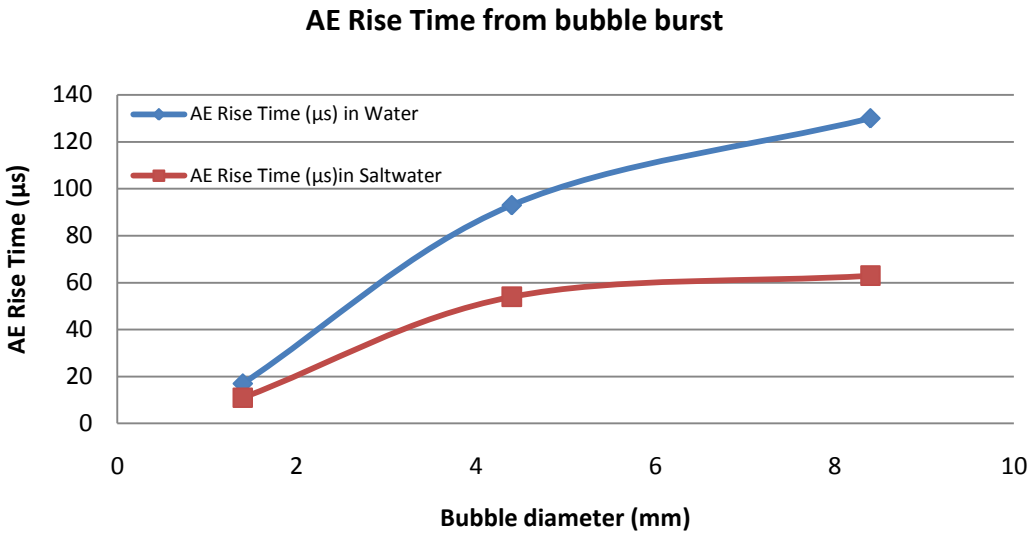

Figure 6-10: AE Rise Time from bubble burst as a function of bubble size and viscosity

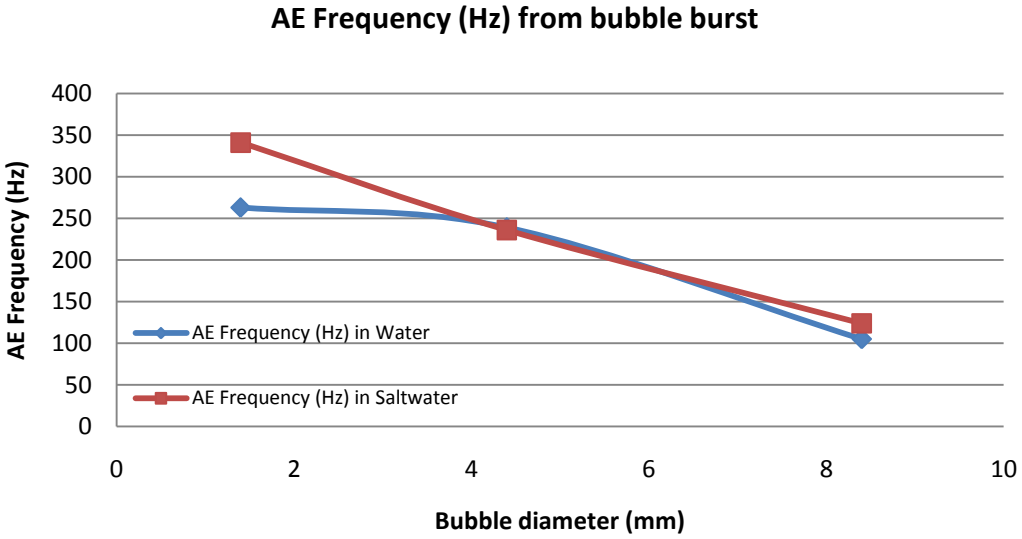

Figure 6-11: AE Frequency from bubble burst as a function of bubble size and viscosity

The increase in AE bubble burst amplitude with bubble size was also seen in saltwater. Table 6-2 (page 94) also shows that there is a clear and consistent increase in AE amplitude between tap water and saltwater. Doubling the

viscosity from 1 cP (tap water) to 2 cP (saltwater) increased the AE amplitude as shown in Table 6-3; 4 dB, 7 dB and 3 dB increased for respective size 1.4mm, 4.4 mm and 8.4 mm. This is because media properties such as density and viscosity affect the wave's propagation and will give stronger signal when detected by transducers.

Table 6-3: Comparison of average AE parameter of free surface bubble burst for all nozzle sizes

	Size 1.4 mm		Size 4.4 mm		Size 8.4 mm	
	Water	**Saltwater**	**Water**	**Saltwater**	**Water**	**Saltwater**
Average AE Amp (dB)	26	30	30	37	35	38
Difference of the Average AE amplitude in Water and Saltwater	4		7		3	

AE rise time shows a similar trend with AE amplitude in water and saltwater, where AE rise time increases with the size increase. However, AE rise time in saltwater is less, compared with water. This is associated with wave propagation in higher viscosity media is faster than lower viscosity media (in this case the duration taken to reach to maximum peak at the waveform). But, the standard deviations are so large that comparison of these rise time readings is meaningless. The system (AEwin) considers the whole waveform for statistical analysis; therefore for AE data from a transient waveform (see Figure 6-4, page 90) will give a big standard deviation.

The parameter-based AE (classical) results as directly obtained from the system, it was noted that AE amplitude shows greater consistency and is taken as the best AE indicator among the AE traditional parameters for bubble activity detection obtained for this system. This indicates that amplitude which is always associated with the signal strength is the most appropriate parameter to be considered for the case of the detection of bubble strength activity. AE amplitude is always associated with AE energy; therefore the result of AE energy from post-signal processing of waveform definitely will give the similar trend as AE amplitude.

6.1.3 Waveform analysis of AE Duration and AE Energy

The duration of AE transient bursts associated with the collapse of each bubble size was obtained by calculating the duration from the point at which the AE response was higher than the underlying threshold level to the point at which it returned to the underlying threshold level. The average value of burst duration for the nozzle sizes are plotted in Figure 6-12 for both liquids. The average AE burst duration increases with increasing bubble size and viscosity. The strength of signal (from potential energy of the bubble burst) increases as the size of bubble increases ($E_b \, \alpha \, R_{max}^3$) (Rayleigh, 1917; De-Bosset et al., 2007; Shangguan et al., 1987; Buogo and Canneli, 2002). The average bubble burst duration in saltwater was higher than in pure water which implies that media properties such as density and viscosity affect the wave propagation.

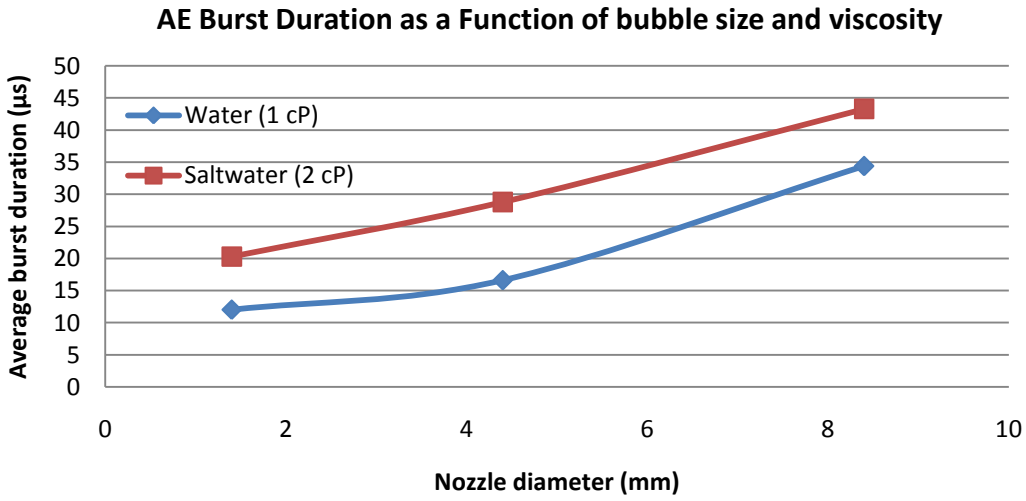

Figure 6-12: Comparison of average AE bubble burst duration in tap water and saltwater

The same methodology of waveform analysis as used in the AE duration analysis has been employed to determine the AE energy which was found by calculating the area within the emission (under curve within the duration stipulated) divided by the reference resistance (10 kΩ). The energy of bubble burst event associated with each bubble size at the free surface energy is

shown in Figure 6-13. The AE burst energy increases with increasing bubble size and viscosity. Waterfall plots in Figure 6-14 shows correlations AE energy with bubble size and liquid viscosity at burst event.

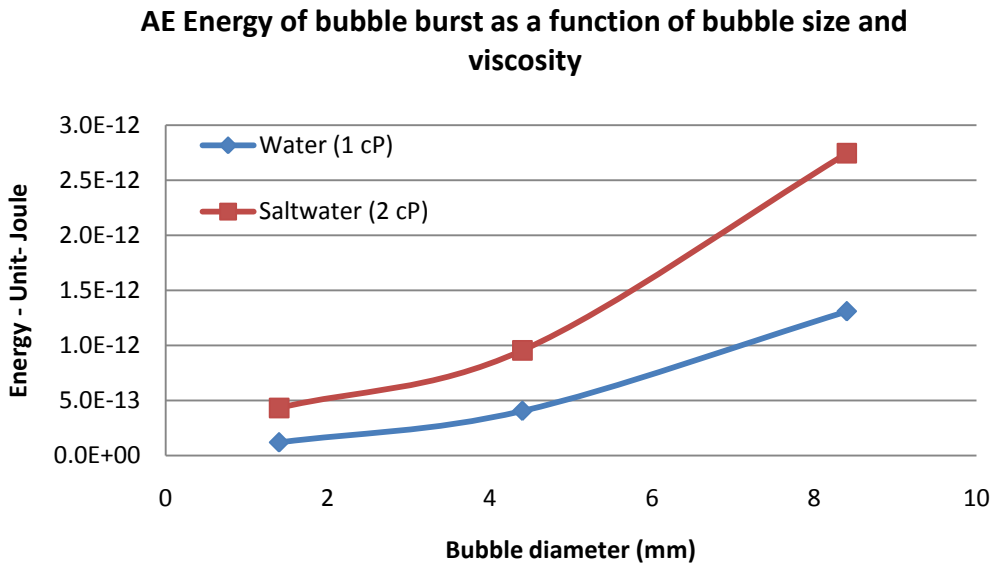

Figure 6-13: Comparison of average of energy of bubble burst in tap water and saltwater

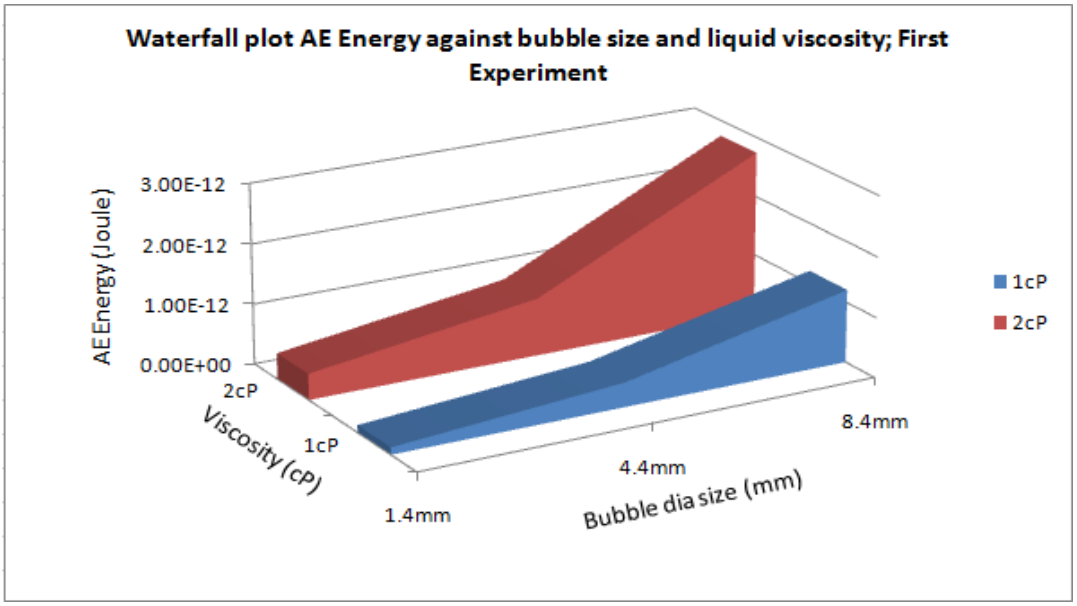

Figure 6-14: Data from the first experiment; water (1cP) and saltwater (2cP)

6.1.4 Velocity of the Acoustic Emission Wave

With the known distances between the sensors in the column and the time difference of AE travelling waves detected between two sensors, the velocity of the AE wave in the liquid was determined (*v*=distance/time). The results of velocity are shown in Table 6-4 for water and saltwater respectively.

Table 6-4: Average velocity of the acoustic wave in water

Size (mm)	Ave Velocity of AE wave in Tap Water (m/s)	Ave Velocity of AE wave in Saltwater (m/s)
1.4	1284	1456
4.4	1351	1535
8.4	1483	1576

In tap water, the average velocities of the AE wave obtained were 1284 m/s, 1351 m/s and 1483 m/s for nozzles size 1.4, 4.4 and 8.4 mm respectively, while, the corresponding average velocities of the AE wave in saltwater were 1456 m/s, 1535 m/s and 1576 m/s. The velocity of sound in liquid is influenced by density of media and pressure (Urick, 1993), but the phenomenon of bubble burst is extremely complicated, involving motion of the liquid, compressibility, viscosity, surface tension, heat conduction, gaseous diffusion and thermodynamic effects (Ross, 1976). These results confirm the well known fact that the speed of sound is faster in saltwater than in tap water, but they also appear to show that the velocity of the AE wave increases with the increasing size of bubble. This finding would be a new reference, associating AE wave velocity with the size of the bubble bursting at the free surface. This is because the bigger the bubble size, the higher the potential energy the bubble possesses. This implies that the results obtained were contributed by the liquid properties (e.g. viscosity and density) and bubble properties (e.g. bubble size). This is because the energy radiated as sound depends entirely on the potential energy of the bubble collapse/burst and it is proportional to bubble size

(Rayleigh, 1917; De-Bosset et al., 2007; Shangguan et al., 1987; Buogo and Canneli, 2002).

The wave propagation in the system was non-linear because the speed of a wave will vary depending on the frequency (Kim and Lee, 2008). Also, the pressure pulse emitted by a collapsing bubble is sufficient to produce non-linear effects in the medium, leading to shock waves (Ross, 1976). In this experiment, these non-linear effects contributed to the difference of AE wave velocity as a function of the size of bubble burst and liquid viscosity. However, the results obtained from this experiment showed that AE wave velocity was very close to the value as stated by Leighton (1994a) and Wissler and Del Grosso (1951) for water and saltwater/sea water respectively: the longitudinal wave velocity of sound in water, 1480 m/s (Leighton, 1994a) and 1543 m/s in sea water at 30^0C (Wissler and Del Grosso, 1951).

6.1.5 Frequency domain analysis; Bubble Burst

Fourier analysis revealed the frequency characteristics for all bubble sizes in both liquids, see Figure 6-15 (page 103).

Frequency domain analysis, as the plot in Figure 6-15 shows, reveals that there are many peak frequencies associated with bubble burst. However, in this experiment, peak frequency at 120 kHz which is the first peak of frequency components was chosen just to show changes in amplitude on the respective bubble sizes used in the experiment. The averaged frequency spectra (taken from 10 test-samples) of AE events associated with differing bubble sizes showed an increase in amplitude with size over the frequency range. This was noted for both fluid types.

Nozzle Size	Frequency Spectra in Water	Frequency Spectra in Saltwater
1.4 mm	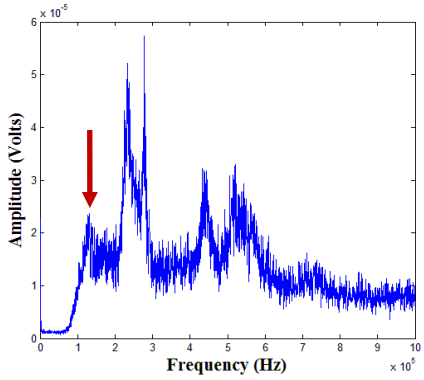	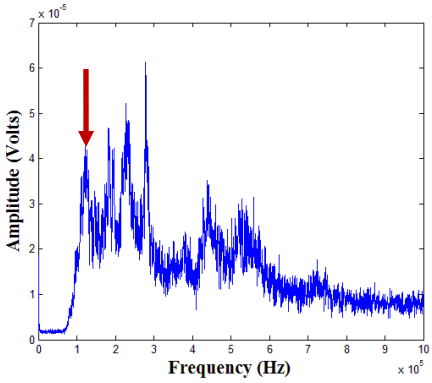
4.4 mm	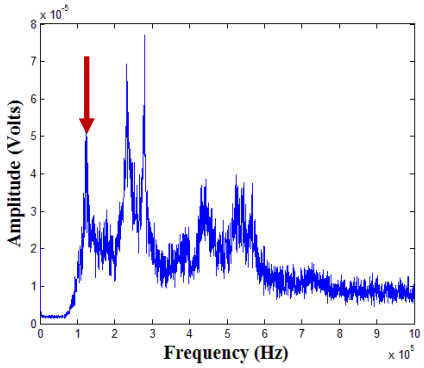	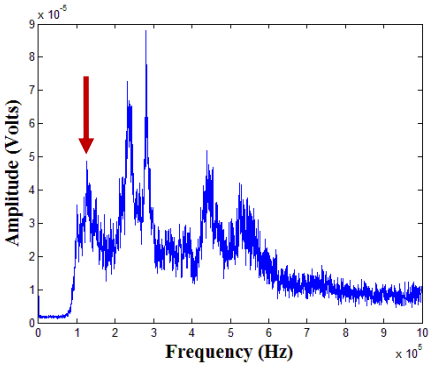
8.4 mm	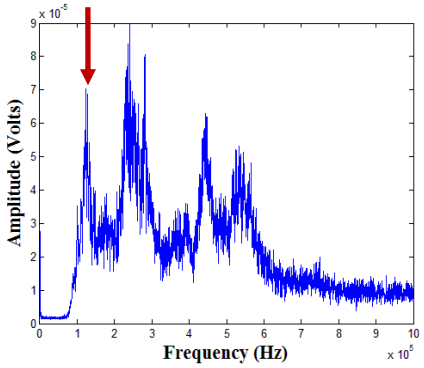	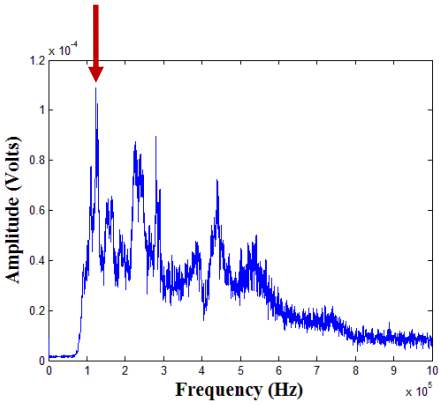

Figure 6-15: Average frequency spectra for bubble bursts

Table 6-5: Comparison of peak amplitude at frequency 120 KHz for all sizes in Water and Saltwater

	Size 1.4 mm	Size 4.4 mm	Size 8.4 mm
Peak amplitude at 120 kHz in Water	2.5×10^{-5} Volts	5.5×10^{-5} Volts	7.0×10^{-5} Volts
Peak amplitude at 120 kHz in Saltwater	4.3×10^{-5} Volts	4.8×10^{-5} Volts	11.5×10^{-5} Volts

The results from FFT show that the bigger the size, the higher the amplitude frequency spectra. Table 6-5 shows the comparison of peak amplitude at frequency 120 kHz for both liquid conditions: water and saltwater. It is noted that peak amplitude at a higher viscosity (saltwater, 2 cP) is higher than for lower viscosity (water, 1 cP). For nozzle sizes 1.4 and 4.4 mm, peaks occur at the same frequency, i.e. 280 kHz for both liquids. However, for nozzle size 8.4 mm, it is found to shift to the left to a lower frequency; in water the peak frequency shifts to 220 KHz, while in saltwater it shifts to 120 KHz. Shifting is apparent at the bigger nozzle size, e.g. 8.4 mm apparently produces a bigger bubble size compared with the other two nozzle sizes.

6.2 Second experiment; tap water (1 cP)

In the second experiment, a comparison of AE amplitude, frequency content, AE duration and AE energy as a function of nozzle size and the sensor used (intrusive or non-intrusive) for AE bubble inception detection was performed.

Figure 6-16 shows a scatter plot of AE amplitude (dB) from bubble inception obtained intrusively (sensor-1). It was found that the bigger the bubble size, the higher the AE amplitude at pinch-off. The average AE amplitude of 10 test samples plotted in Figure 6-16 is shown in Table 6-6 for each nozzle size. The average amplitude from bubble inception at nozzle 1.4 mm, 2.8 mm, 5.6 mm and 8.4mm were 32.3 dB, 33.3 dB, 36.2 dB and 40.9 dB respectively.

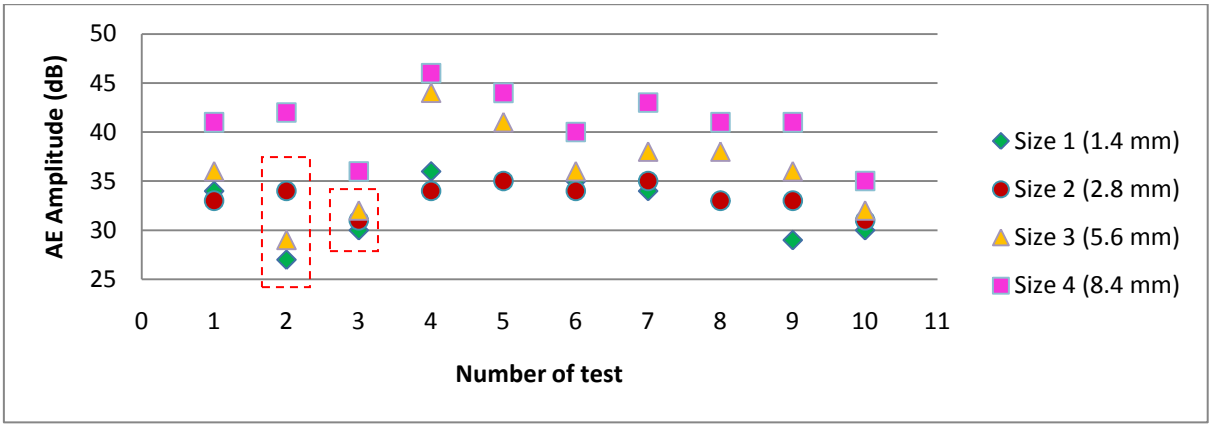

Figure 6-16: AE Amplitude of bubble inception as a function of nozzle size (Sensor-1)

The general trend suggests that as bubble size increases, AE amplitude increases. However, there are certain cases (e.g. number of test-2) where this is not observed. For example, number of test-2 in Figure 6-16 shows AE amplitude from bubble size-2 (nozzle diameter 2.8 mm) is higher than bubble size-3 (nozzle diameter 5.6 mm) which is contradicted with the assumption that the bubble size generated is equivalent with the nozzle size. The result of scatter plot randomly from the number of tests as shown in Figure 6-16 indicates that it is hard to control a consistent size of bubble inception at nozzle's end. However, statistical average analysis shows a distinctive trend as a function of bubble/nozzle size (see Table 6-6).

Table 6-6: Average values and standard deviation of AE amplitude of bubble inception as a function of nozzle size (Sensor-1)

Nozzle size	1.4 mm	2.8 mm	5.6 mm	8.4 mm
Ave (dB)	32.3	33.3	36.2	40.9
Stdev (dB)	3.1	1.4	4.4	3.3

The result of AE amplitude obtained non-intrusively (sensor-4) for bubble inception is shown in Figure 6-17 (page 106). The average AE amplitude of 13 test samples plotted in Figure 6-17 is shown in Table 6-7. For Sensor-4, the average AE amplitude due to the AE signal released at pinch-off was lower than the result obtained from Sensor-1 for each nozzle size. The average amplitude from bubble inception at nozzles 1.4 mm, 2.8 mm, 5.6 mm and 8.4mm obtained non-intrusively were 26.9 dB, 29.6 dB, 32.3 dB and 37.2 dB respectively.

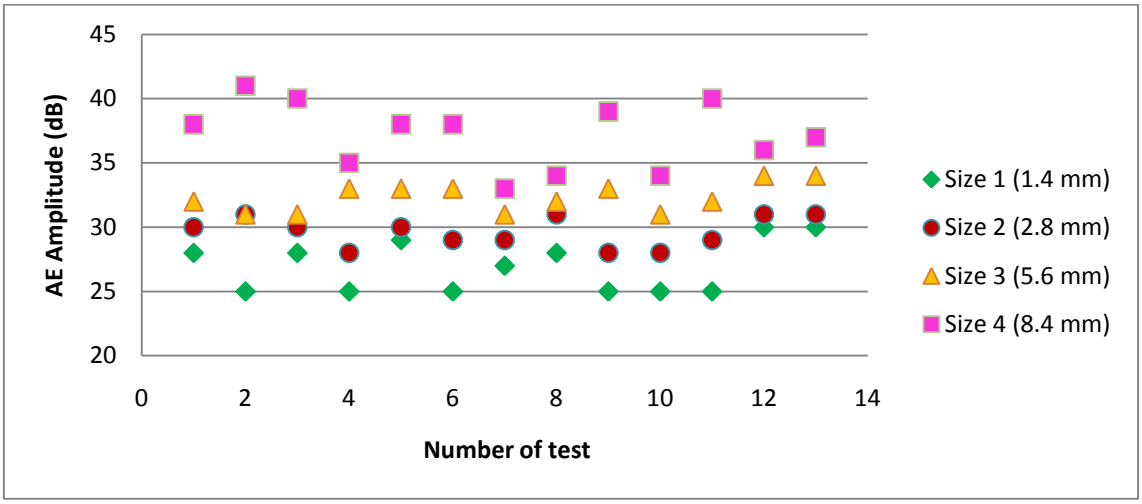

Figure 6-17: AE Amplitude of bubble inception as a function of nozzle size detected (Sensor-4)

Table 6-7: Comparison of average and standard deviation of AE amplitude of bubble inception as a function of nozzle size (Sensor-4)

Nozzle size	1.4 mm	2.8 mm	5.6 mm	8.4 mm
Ave (dB)	26.9	29.6	32.3	37.2
Stdev (dB)	2	1.2	1.1	2.6

The statistical comparison between intrusive and non-intrusive method showed that the average value of AE amplitude (dB) of Sensor-4 was less than the average value of Sensor-1. This is because the AE signals originating from the bubble inception at the tip of nozzle underwater incurred significant attenuation prior to reaching the receiving Sensor-4. This attenuation can be a function of

the number of media, and media properties such as bonding structure, thickness and viscosity. Attenuation and transmissibility of AE waves across the media or component has been demonstrated by Mba and Hall (2002) in their case study on monitoring the rubbing surfaces of the rotor and stator in large-scale power generation turbines with Acoustic Emission (AE).

The comparison of average amplitude (dB) detected by Sensor-1 inside the bubble test rig near the nozzle with that from Sensor-4 mounted outside the column is shown in Figure 6-18. The amplitude difference between intrusive and non-intrusive methods is about ~4 dB which is statistically significant, considering the distance of intrusive Sensor-4 from the point of AE activity (bubble inception at the nozzle) and the thickness of the aluminium column (50 mm).

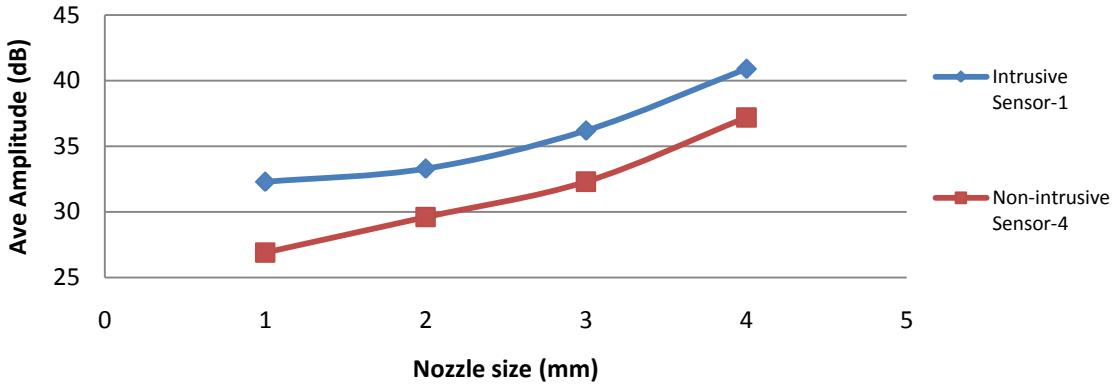

Figure 6-18: Comparison of Average Amplitude (dB) from bubble inception detected intrusively (sensor-1) and non-intrusively (sensor-4)

In this experiment it was confirmed that no signal was picked up by Sensor-3, which was closest to free surface, when the bubbles hit the free surface. Figures 6-19 to 6-21 (page 108) show the recorded still picture of bubble rising up, bubble arriving at the free surface causing surface distortion and the shockwave resulting from bubble burst at the free surface, respectively.

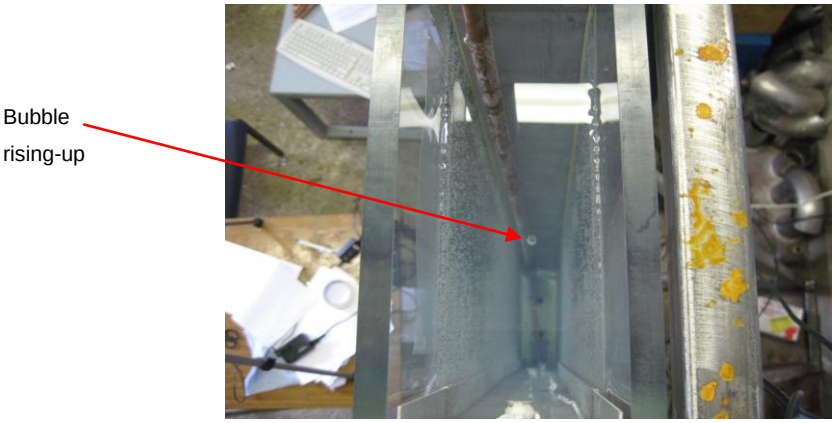

Figure 6-19: Bubble rising up in the column test rig, seen from the top

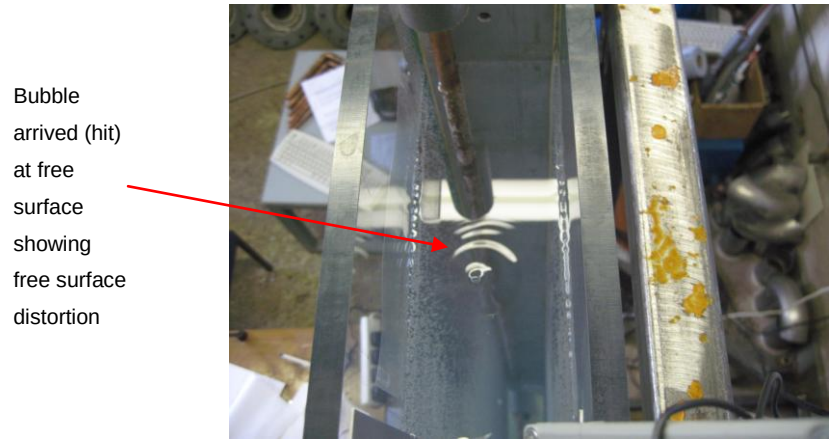

Figure 6-20: Free surface distortion when bubble hits the free surface

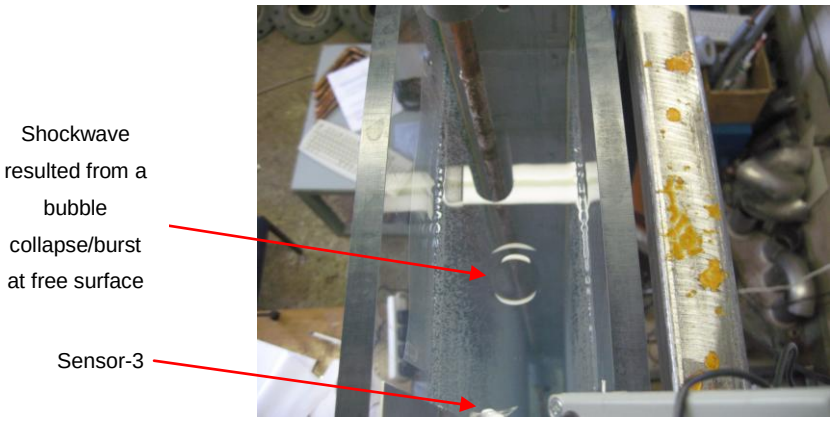

Figure 6-21: Shockwave just after bubble burst at free surface

It was observed that an AE signal was captured by the AE Sensor-3 (intrusively placed near to the free surface) as the bubble bursts at the free surface. However, Sensor-5 (non-intrusive sensor mounted onto the outside wall) did not detect any AE from the bubble burst occurrences; it is postulated that in the burst event at the free surface, only a small fraction of energy is transferred to liquid; most of the rest of the energy (acoustic) is lost to the open space at the free surface. Contrarily, bubble formation process is surrounded by liquid; energy of the bubble formation is considerably transmitted to liquid where the Sensor-4 detected the signal from the event.

Analysis of the AE amplitude, frequency content, AE duration and AE energy for bubble burst at the free surface as a function of nozzle size was undertaken. It was found that the bigger the bubble size, the higher the AE amplitude. The test samples and the corresponding results for respective nozzle sizes are presented in Figure 6-22. The average AE amplitude of bubble burst from the four nozzles is shown in Table 6-8.

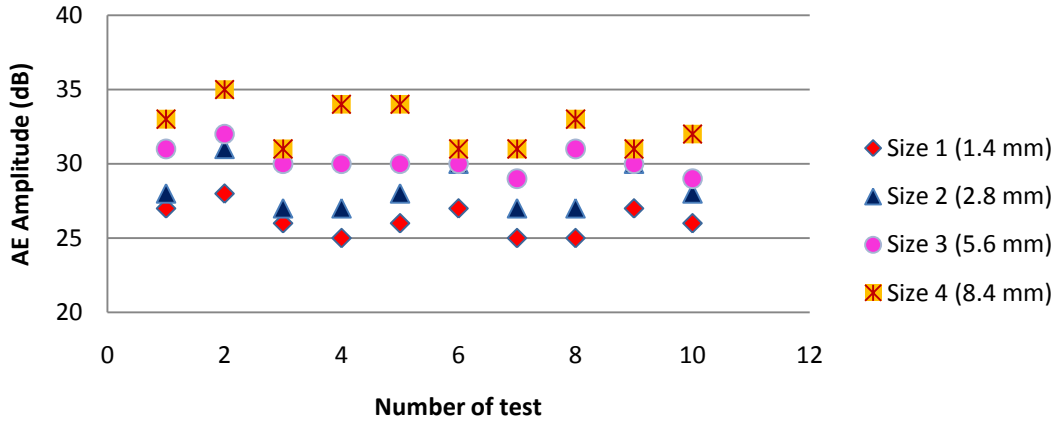

Figure 6-22: AE Amplitude of bubble burst at the free surface as a function of nozzle size detected by Sensor-3

Table 6-8: Comparison of Average and standard deviation of AE Amplitude of bubble burst at the free surface as a function of nozzle size (Sensor-3)

Nozzle size	1.4 mm	2.8 mm	5.6 mm	8.4 mm
Ave amp (dB)	26.2	28.3	30.2	32.5
Stdev (dB)	1	1.5	0.9	1.5

It can be summarised that AE technology is very sensitive and capable of detecting a delicate single bubble inception and burst events intrusively and non-intrusively. Its sensitivity is evident where a distinctive result was obtained from the different bubble sizes. Interestingly, the AE sensor was capable of picking up the signal from the bubble inception non-intrusively through a very thick aluminium wall, i.e. 50 mm. These provide evidence of the applicability of AE technology for bubble measurement and monitoring within hostile environments where non-intrusive methods offer more advantages than intrusive techniques. Its application is predicted for oil and gas product transportation in pipelines.

In such a complicated two-phase flow, measurement and monitoring of flow conditions such as aerations and flow patterns should not depend only on one AE parameter, e.g. AE amplitude. Therefore, other parameters which can be obtained from waveform analysis, such as AE duration and AE energy would give greater accuracy and reliability of the results to monitor or characterise the bubble phenomenon (Addali et al., 2010; Addali, 2010). These parameters can be correlated with critical gas-liquid flow parameters such as Gas Void Fraction (GVF) and Superficial Gas Velocity (VSG).

6.2.1 Waveform analysis: bubble inception

Table 6-9 (page 111) shows a typical example of a waveform obtained from the same source (bubble inception) for nozzle sizes 1.4 mm, 2.8 mm, 5.6 mm and 8.4, as detected by Sensor-1 and Sensor-4. The time when the sensor detected the bubble inception event is shown at the top of each waveform figure, and the amplitude (dB) is given in the brackets. It shows time delays between Sensor-1 and Sensor-4 to be about 0.0001 s.

Table 6-9: Comparison of AE signals for the same event obtained from intrusive and non-intrusive sensors

Nozzle Size	Sensor-1 (Intrusive)	Sensor-4 (Non-intrusive)
1.4mm	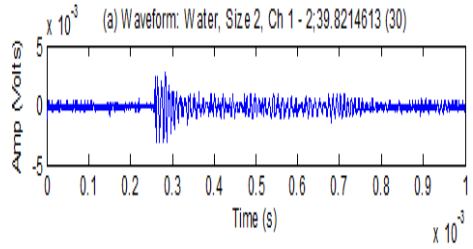	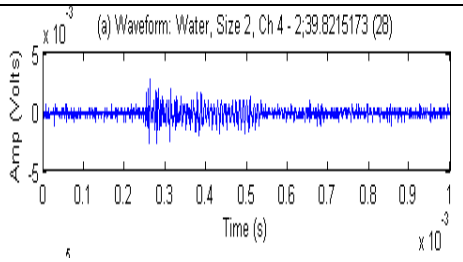
2.8mm	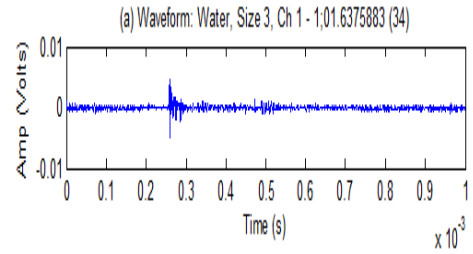	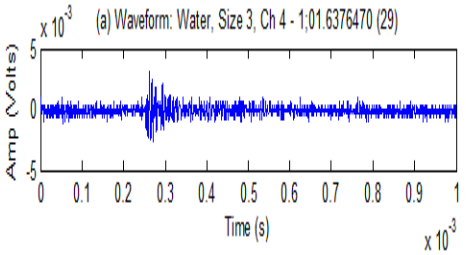
5.6mm	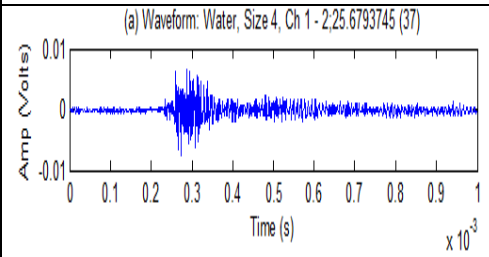	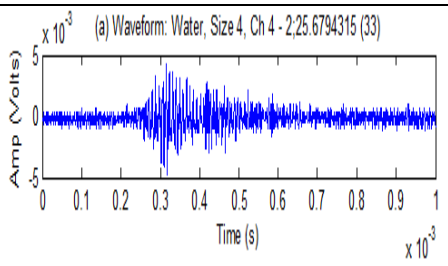
8.4mm	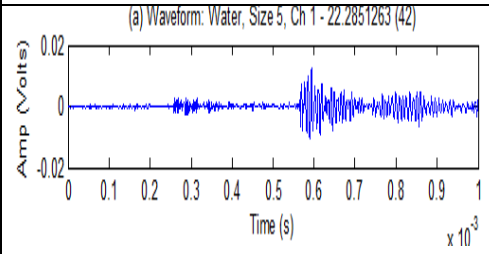	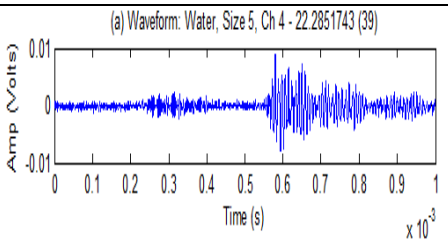

The amplitude of the waveform obtained from Sensor-1 was higher than that obtained by Sensor-4. Furthermore, it was noted that the duration of the AE transient burst waveform obtained by Sensor-4 was longer than the duration of the waveform obtained from Sensor-1. Waveform parameters such as

amplitude and duration are affected by the distance of sensor from the AE source, as well as the media through which the wave is transmitted. Relatively, as can be seen from the signals in Table 6-9 (page 111), the duration of the transient waveform (indicated with a red arrow) from the bubble inception obtained from Sensor-4 is approximately three times longer than the duration of the transient waveform obtained from Sensor-1. This is attributed to the material/media through which the waves propagate; waves propagate longer in duration in solid material than in liquid (Leighton, 1994a).

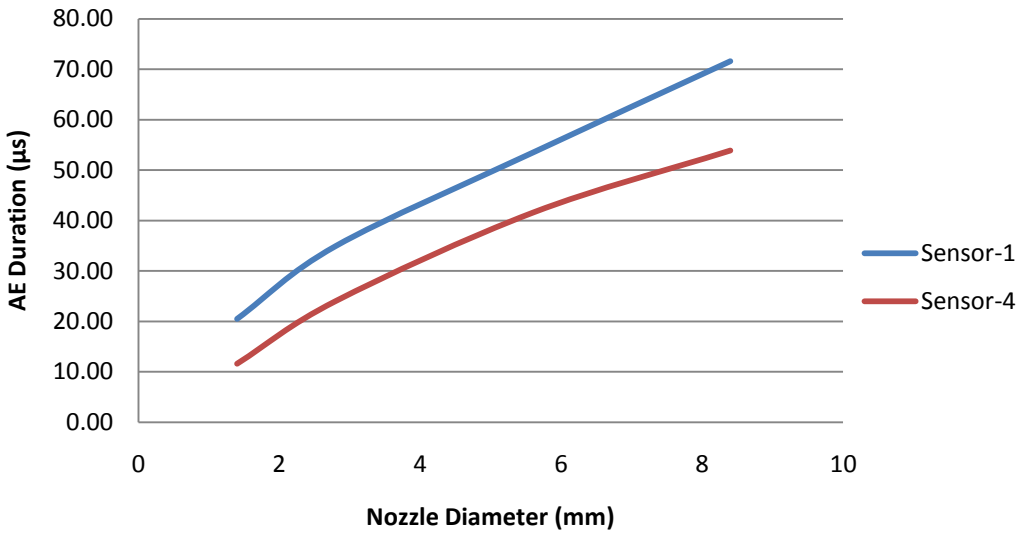

Figure 6-23: Comparison of average AE duration from bubble inception in water detected by sensors-1 and -4 as a function of nozzle size

The transient burst of waveform, as shown in Table 6-9 (page 111), for all sizes of nozzle was further analysed for AE duration and AE energy using the procedure explained in Section 5.3, Figure 5-5 (page 82). The results for the average duration of an AE signal at bubble inception as a function of nozzle size are shown in Figure 6-23. The average was calculated from 7 test samples. The average AE duration of bubble inception increases with the increase of bubble size.

The waveform from the same test samples that were used in the AE duration were further analysed for average AE energy where it was determined by the area under the curve. The results for average AE energy are shown in Figure 6-24. It was found that AE energy associated with the bubbles' inception generally increases with the increase of bubble diameter at the nozzle tip. An abrupt increase of AE energy apparently began at a nozzle diameter of 5.6 mm. It was concluded that nozzle diameters 1.4 and 2.8 mm did not produce bubbles that had a large enough pressure pulse to be able to generate AE's. This is reflected in the plot in Figure 6-24 where there is a very small increment of AE energy from the 1.4 mm size to the 2.8 mm size.

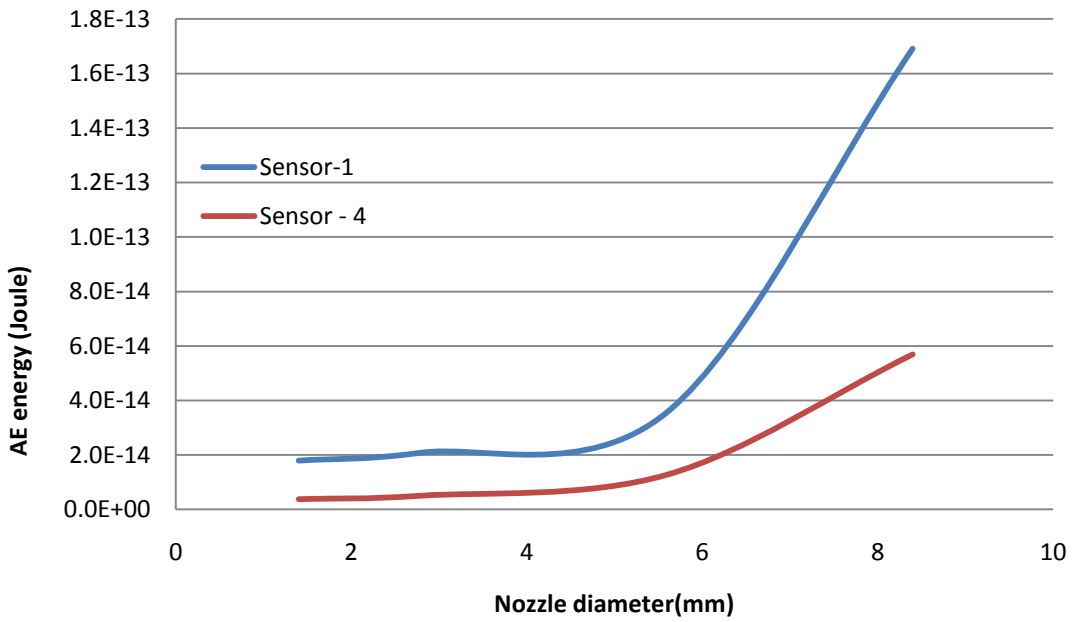

Figure 6-24: Plot of comparison of average energy of bubble inception in water as a function of nozzle size and sensors

6.2.2 Time-Frequency analysis: bubble inception

Table 6-10 (page 115) shows an example of a single plot of analysis containing (a) time-domain waveform, (b) spectrogram/STFT and (c) FFT for signal from bubble inception through the four nozzle sizes. The spectrogram here gives a plot of the intensity of the frequency content of the signal over the time, see (b). The spectrogram shows that frequencies with the most energy occur at the start of the AE event. It can be clearly seen that the duration of signal intensity (red colour) is longer for the waveform obtained from Sensor-4 compared with the signal obtained from sensor-1, while in the FFT analysis, the plots in (c) show that the energy at the primary/main frequency component of 120 kHz grew with increasing bubble size. The amplitude peaks between 100 and 300 kHz, and 400 to 500 kHz were noted though their relative increase in amplitude with increasing bubble size was lower than at 120 kHz. Table 6-11 (page 116) gives the summary of peak amplitude at a frequency of 120 kHz of the average FFT analysis from the waveform data detected by intrusive and non-intrusive sensors for respective sizes. A lower result of the parameters obtained, as discussed above, was noted from Sensor-4 compared with Sensor-1.

This experiment demonstrated that an AE Sensor-4 mounted onto a 50mm thick aluminium wall has the capability to capture an AE signal from bubble inception at a nozzle underwater. This shows the high sensitivity of AE sensors.

Table 6-10: Single plot presenting results containing time-domain, joint time-frequency and frequency-domain of analysis from waveform data (bubble inception) acquired by intrusive and non-intrusive sensors

Nozzle Size	Intrusive (Ch 1)	Non-intrusive (Ch 4)
1.4 mm	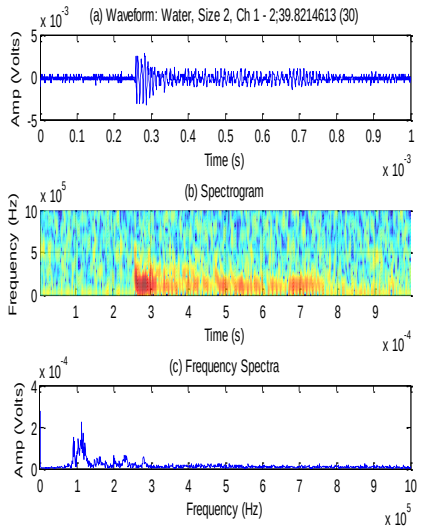	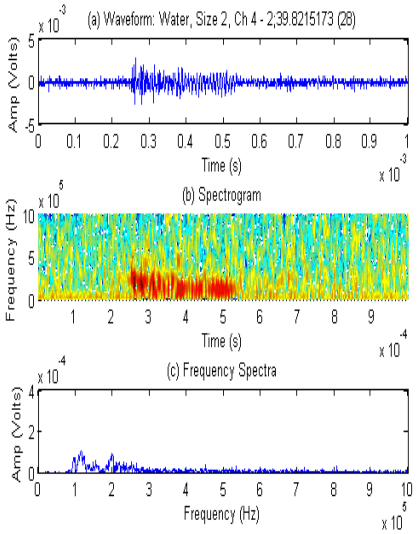
2.8 mm	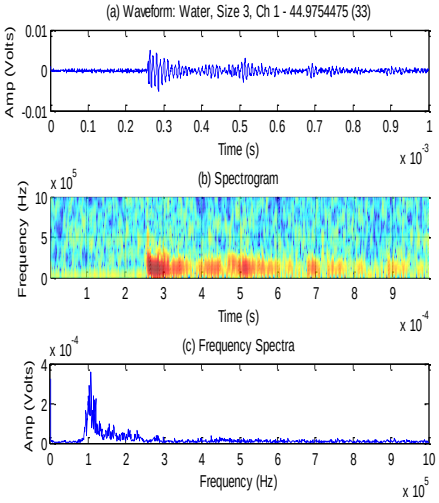	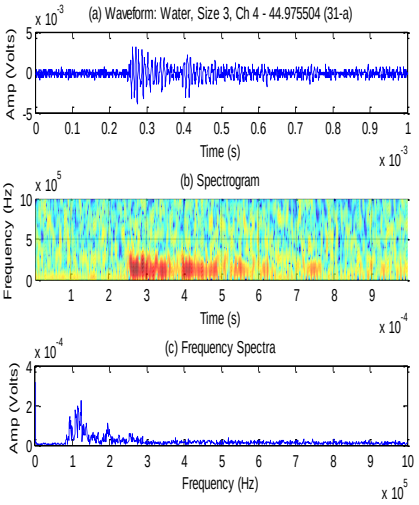

5.6 mm	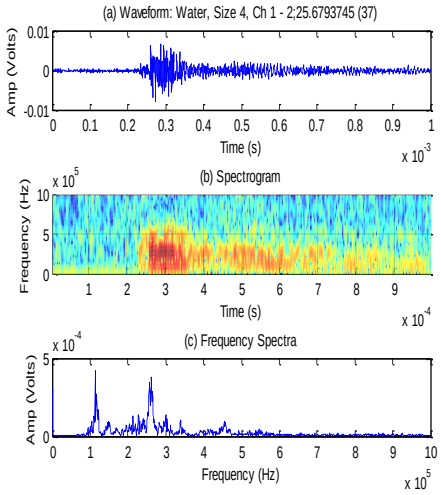	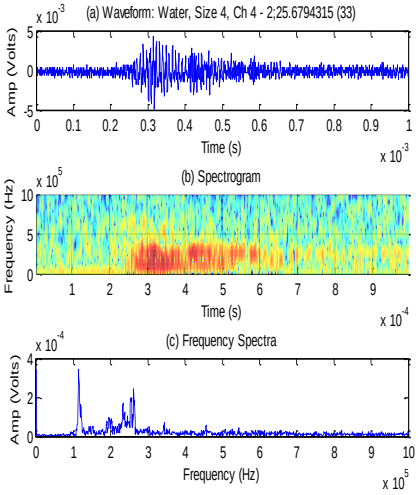
8.4 mm	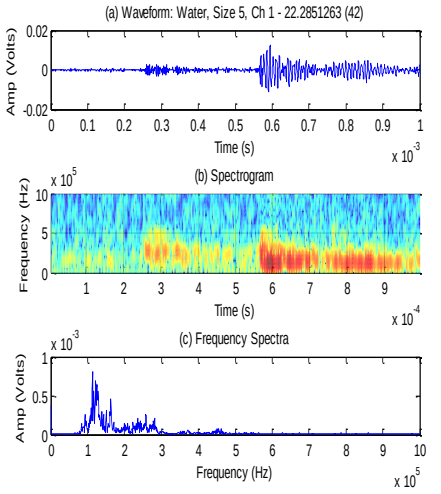	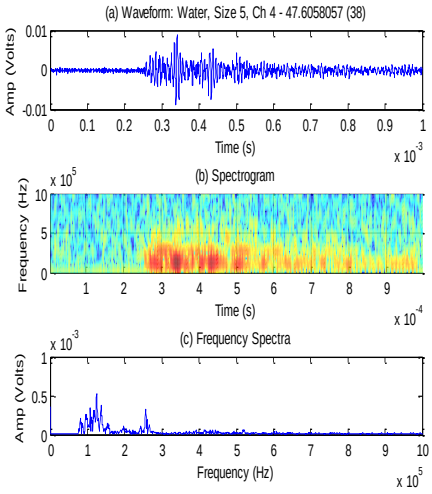

Table 6-11: Peak amplitude at frequency 120 kHz

	Size 1.4 mm	Size 2.8 mm	Size 5.6 mm	Size 8.4 mm
Peak amp (volts): Sensor-1	2.5×10^{-4}	3.8×10^{-4}	4.8×10^{-4}	8.0×10^{-4}
Peak amp (volts): Sensor-4	1.0×10^{-4}	2.0×10^{-4}	3.8×10^{-4}	5.0×10^{-4}

6.2.3 Waveform analysis: Bubble burst

Figure 6-25 (page 118) presents the comparison of the waveform of bubble burst at the free surface as a function of bubble size. A transient at the waveform from a bubble burst released from a bigger nozzle size is more apparent, assuming that the bubble size generated through the nozzle is equivalent to the nozzle size. It is associated with the energy at the bubble burst occurrence. As highlighted by Eq 5-1 (page 81), the bigger the bubble size, the more bubble potential energy (E_B) which causes a larger sound pressure when it bursts at a free surface (Rayleigh, 1917; Sathyam et al., 1995; Shangguan et al., 1997; Xu et al., 2004; Blake and Gibson, 1981; Yasuda et al., 2008; Robert et al., 2007; Obreschkow et al., 2006; Buogo and Canneli, 2002; De-Bosset at al., 2007). The sound magnitude produced by bubble burst is reflected by the amplitude of the signal as recorded in Figure 6-25 (page 118).

The average AE duration of bubble burst as a function of bubble/nozzle size is shown in Figure 6-26 (page 119). The average was calculated from the same 10 test samples. AE duration was determined by taking the time difference between the start and end of the waveform crossing the threshold value. The threshold value set in this calculation was 0.61 mV as shown at the waveform in Figure 5-5 (page 82). The average AE burst duration increases with the increase of bubble size.

Nozzle size	Sensor-3
1.4 mm	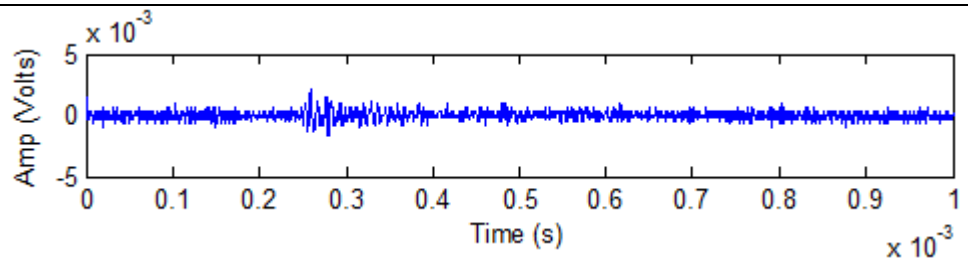
2.8 mm	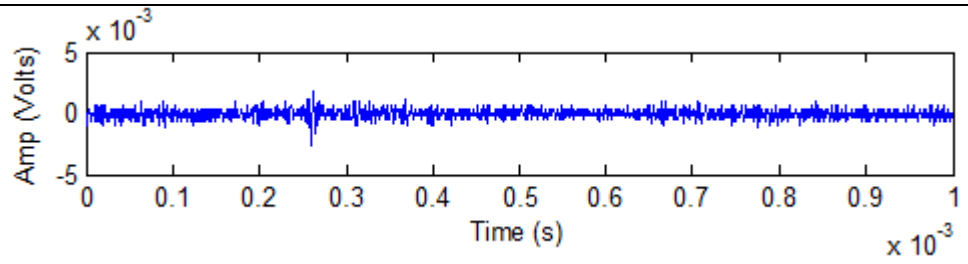
5.6 mm	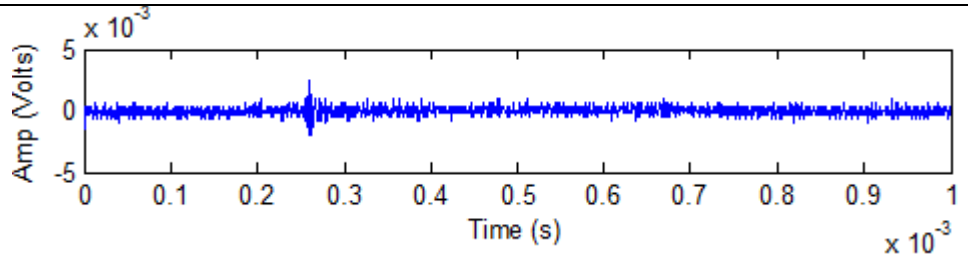
8.4 mm	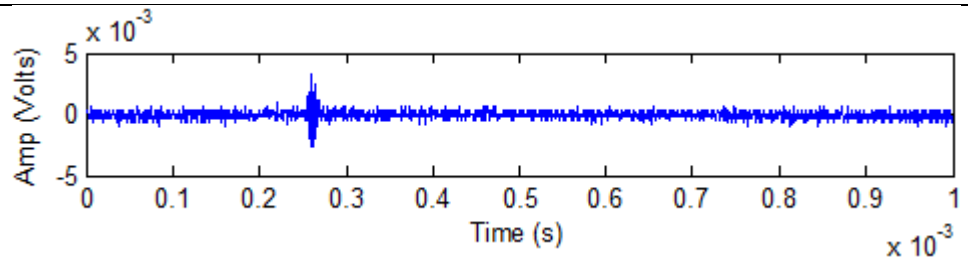

Figure 6-25: AE waveforms from bubble burst as a function of nozzle size detected by Sensor-3.

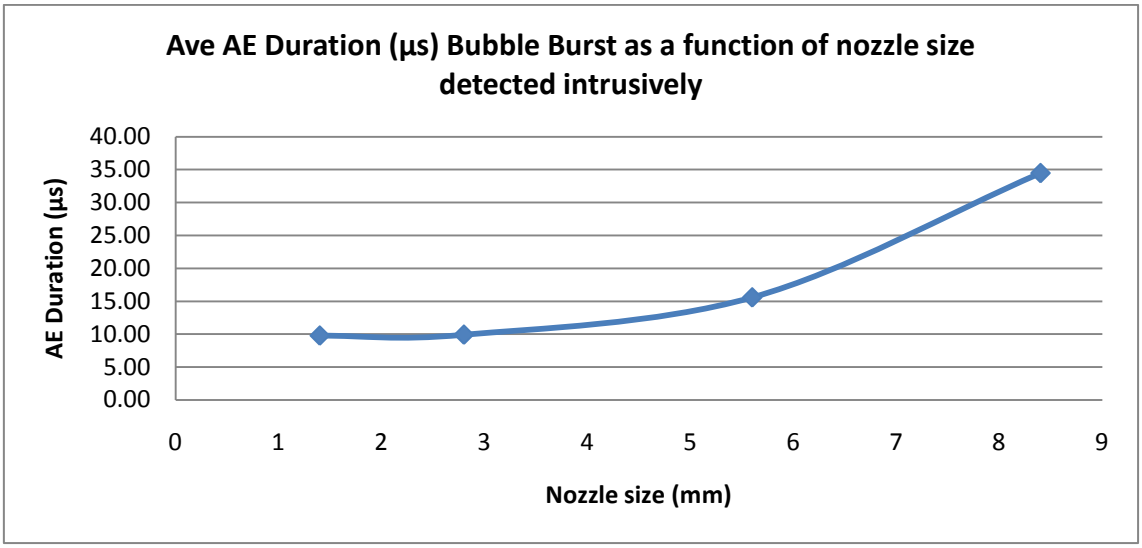

Figure 6-26: Average AE bubble burst duration at free surface of water as a function of nozzle/bubble size detected by Sensor-3

Table 6-12: Comparison of average and standard deviation of AE duration of bubble burst (tap water 1 cP) as a function of nozzle size detected by Sensor-3

Nozzle size	1.4 mm	2.8 mm	5.6 mm	8.4 mm
Ave AE duration (µs)	9.79	9.93	15.6	34.5
Stdev (µs)	4.68	4.80	7.51	22.3

The results of the average AE duration of bubble burst at the free surface as a function of nozzle size 1.4 mm, 2.8 mm, 5.6 mm and 8.4 mm are 9.79 µs, 9.93 µs, 15.6 µs and 34.5 µs respectively. The first two nozzle sizes (1.4 mm and 2.8 mm) show very similar results for both average and standard deviation. The AE duration obtained from the burst event of bubbles generated from nozzle sizes 5.6 mm and 8.4 mm show relatively obvious differences as plotted in Figure 6-26. Average and standard deviation of AE duration is shown in Table 6-12. There was the same trend as for previous results; the bigger the nozzle the higher the average AE duration and standard deviation obtained. In Figure 6-22 (page 109), the scatter plot shows that the data points from the bigger nozzle

size, 8.4 mm, are spread out over a large range of values compared with the smaller nozzle sizes of 1.4 mm, 2.8 mm and 5.6 mm. The data points (amplitude), particularly from nozzle size 8.4 mm, are dispersed from the average value. This indicates that the bigger the nozzle size, the more varied in size the bubble generated. Physically, it can be explained by saying that, in terms of the meniscus of air bubble emerging from a vertical nozzle (see Figure 2-5, page 22), the wider the opening of nozzle (nozzle internal hole diameter) the higher the sensitivity to the forced air volume at the bubble development (meniscus). The volume injected is not proportional to the curvature (radius) of the developing bubble (Longuet-Higgins et al.,1991).

Figure 6-27 (page 121) presents an AE energy plot as a function of nozzle size. The average was calculated from the same 10-test samples used in deretmination of the AE duration, see Figure 6-26 (page 119). The plot shows a very small increment from nozzle size 1.4 mm to 2.8 mm indicating that there is little difference in energy generated from the two nozzles. In contrast, the results of AE energy from nozzle sizes 5.6 mm and 8.4 mm show a clear difference with increasing energy associated with increasing nozzle size. This would imply whilst energy is emitted from the bubbles at burst the level of energy detected by the transducer is influenced by the transmission medium, which in this instance is water. Therefore, the exponential relationship between nozzle size and AE energy is thought to be greatly affected by the attenuation of the medium through which the elastic waves propagate.

The statistical analysis of average and standard deviation is presented in Table 6-13; the results of the average AE energy of bubble burst at the free surface as a function of nozzle sizes 1.4 mm, 2.8 mm, 5.6 mm and 8.4 mm are 10.7×10^{-16} J, 1.24×10^{-16} J, 15.1×10^{-16} J and 179×10^{-16} J respectively. Standard deviation (see Table 6-13, page 121) for AE energy was found to be the same trend as AE duration; the bigger the bubble size, the higher the standard deviation. The same reason for higher standard deviation at the bigger bubble size has been explained as for Table 6-12 (page 119).

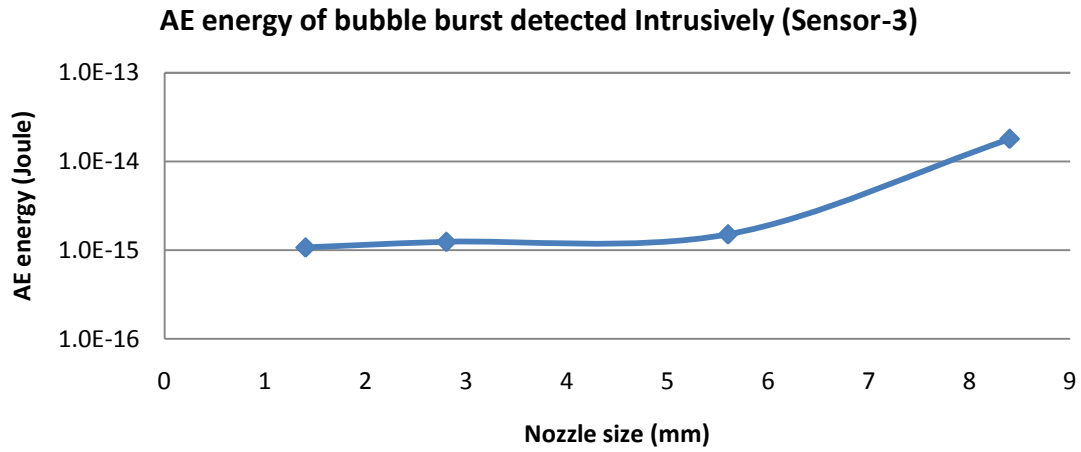

Figure 6-27: Plot of comparison of averages of energy of bubble burst at free surface as a function of nozzle size

Table 6-13: Comparison of Average and standard deviation of AE energy (J) of bubble burst (tap water 1 cP) as a function of nozzle size detected by Sensor-3

Nozzle size	**1.4 mm**	**2.8 mm**	**5.6 mm**	**8.4 mm**
Ave AE energy in bubble burst (J x 10^{-16})	10.7	12.4	15.1	17.9
Stdev (J x 10^{-16})	6.04	6.88	6.87	19.9

6.2.4 Time-Frequency plot (Wavelet plot) of bubble burst

Time-frequency analysis has also been performed on the waveform data by employing a Gabor wavelet and the AGU-Vallen software tool (see plots in Table 6-14, page 123).

Wavelet transforms (WT) results (Table 6-14) using the AGU-Vallen software showed a good resolution of both frequency and time. Therefore, the exact time at which the highest frequencies (energetic frequency component) of bubble burst occurred can be extracted from the joint time-frequency plot. The colour scale of the WT contour map shown in Table 6-14 has red representing the highest-magnitude region of the WT and pink the smallest (zero) magnitude region. The wavelet coefficient (WT peak magnitude) is a magnitude of scale

representing the energy or strength of the event. The wavelet analysis, as shown in Table 6-14, shows that the energy of bubble burst increases as the bubble size increases. The frequency range of burst event from bubble size 1.4 mm is up to 200 kHz. For bubble size 2.8 mm, it is increased slightly up to 230 kHz. While for the larger sizes of 5.6 mm and 8.4 mm, the frequency range is up to around 450 kHz and 600 kHz respectively. The frequency of the burst event from bubble generated using nozzle sizes 1.4 mm and 2.8 mm shows a slight difference, probably because the bubble size generated through these two nozzle sizes are not very difference.

There is a relationship between potential energy (bubble energy) of a bubble and bubble burst; bubble energy is proportional to bubble size (R_{max}^{3}), see Equation 5-1 (page 81). Physically, as can be seen in Figure 2-8 (page 25), the bigger the bubble size, the higher the ‘spike shape’ of the jet generated during the burst process at the free surface. The collapse of this spike will cause a greater wave surface compared to the collapse of the smaller bubble size.

Table 6-14: Burst waveform (top) and time-frequency plot (bottom) associated with bubble burst as a function of nozzle size: The same data used in this WT transform are used in Figure 6-25 (page 119)

Nozzle	Wavelet analysis (time-frequency plot) using AGU-Vallen
1.4 mm	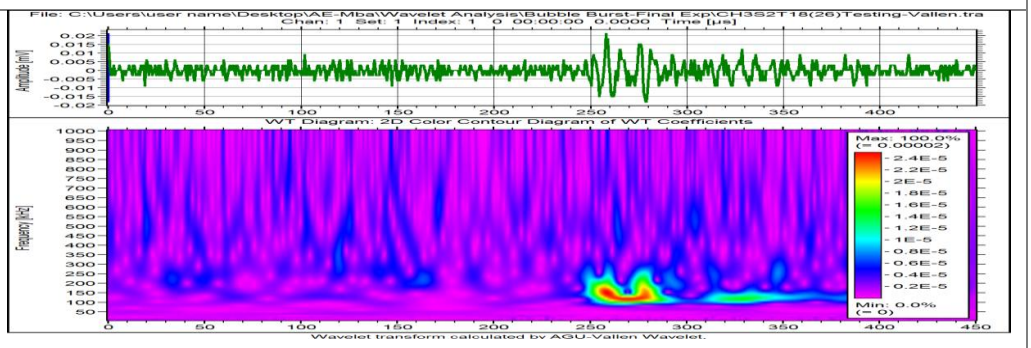
2.8 mm	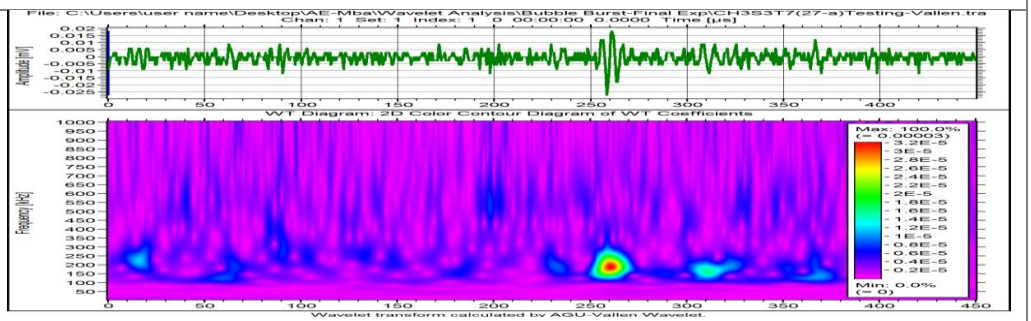
5.6 mm	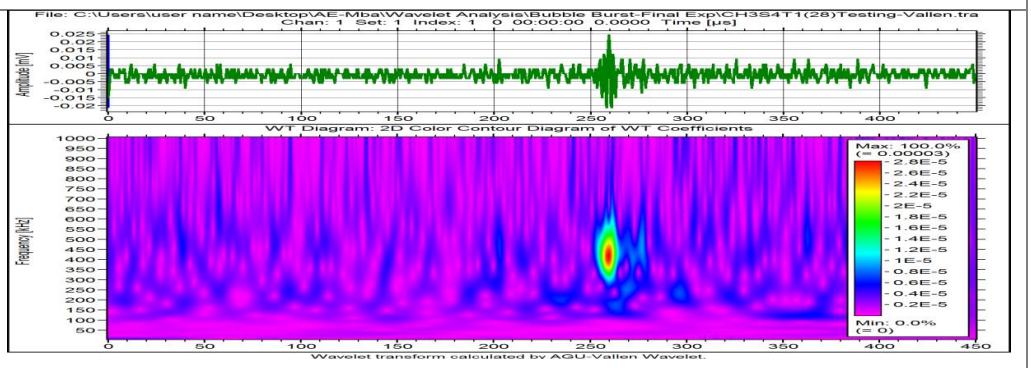
8.4 mm	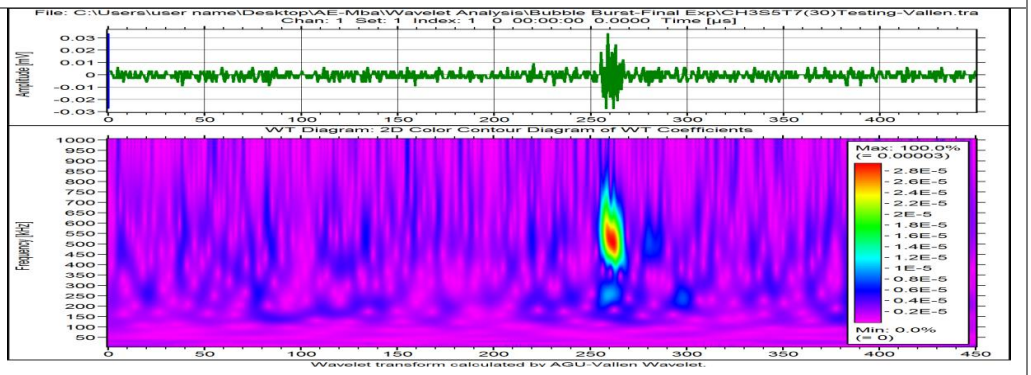

6.2.5 FFT of AE from bubble burst

A Fourier analysis revealed the frequency characteristics for the bubble burst AE signal for all sizes of nozzle, see Table 6-15 (page 125) which presents the average of the FFT. This averaged frequency spectrum (taken from the same 10 test samples used in the previous section 6.2.3) showed an increase in amplitude across the broad frequency range. The FFT plot, Figure 6-15, shows that the first peak of frequency components is at ~120 KHz for all nozzle sizes. Peak amplitude at the main (primary) frequency component 120 kHz from the frequency spectra was chosen to distinguish the effect of bubble size. A higher peak amplitude was observed with the larger nozzle/bubble size. Table 6-16 (page 126) presents a summary of peak amplitude at a frequency of 120 kHz for all bubble/nozzle sizes; for nozzle sizes 1.4 mm, 2.8 mm, 5.6 mm and 8.4 mm these were 5×10^{-6} Volts, 6×10^{-6} Volts, 7×10^{-6} Volts and 14×10^{-6} Volts respectively. The results show that the bubble size has correlation with the amplitudes of the peaks in the frequency spectrum and this implies that bubble/nozzle size can be found from an FFT analysis of AE waveform data obtained from AE sensors. The bigger the bubble size, the higher the bubble energy which is associated with the strength of the bubble at burst occurrence. This strength of burst event is interpreted in terms of amplitude (dB, Volt etc.) at the output of the AE system. The AE data from burst event can be presented in a time domain (Amplitude-Time plot/waveform) and frequency domain (Amplitude-Frequency plot/FFT).

Note: as can be seen in Table 6-15, the sharp peaks in the spectra are the characteristics of the sensor used.

Table 6-15: Frequency spectra of signal acquired by Sensor-3 as a function of nozzle size

	Frequency Spectra of bubble burst
1.4 mm	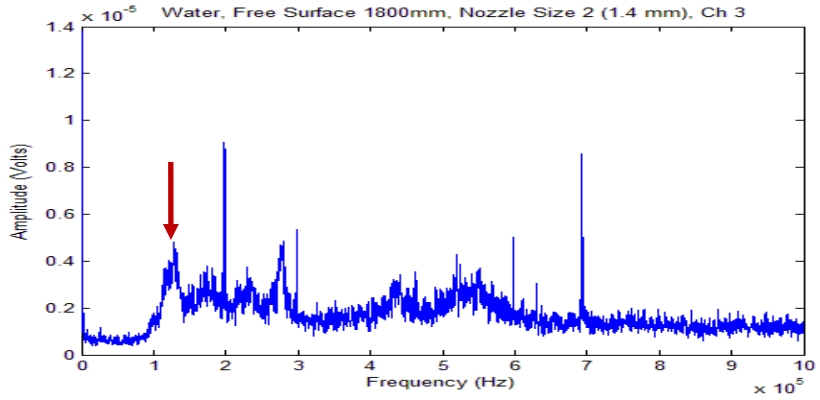
2.8 mm	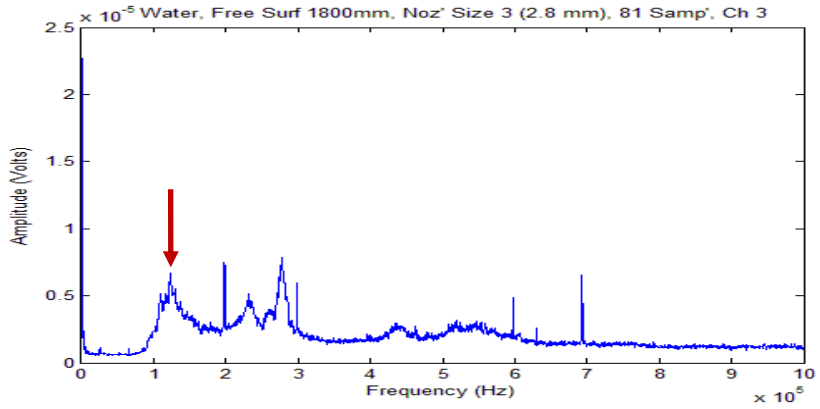
5.6 mm	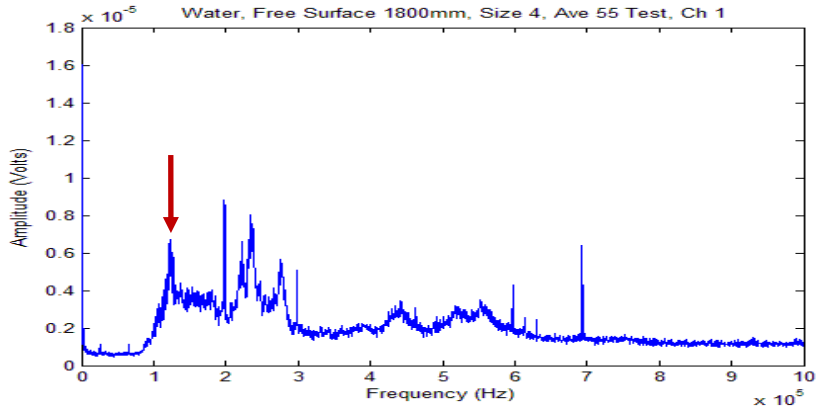

8.4 mm	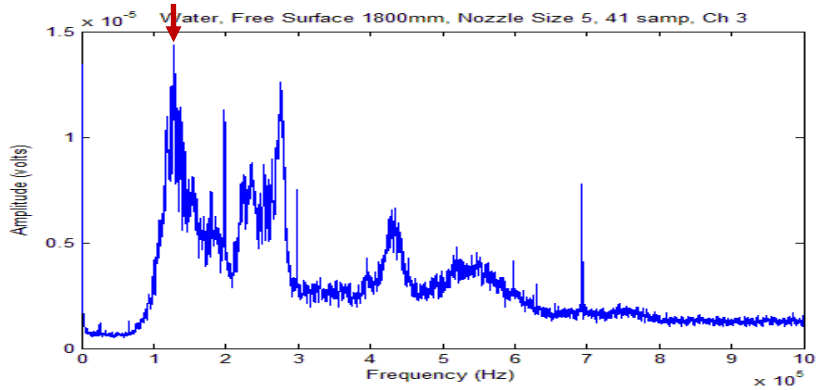

Table 6-16: Comparison of peak amplitude at frequency of 120 KHz for all nozzle sizes

	Size 1.4 mm	Size 2.8 mm	Size 5.6 mm	Size 8.4 mm
Peak amplitude at 120 kHz (10^{-6} V)	5	6	7	15

A plot of the data in Table 6-16 is shown in Figure 6-28 (page 127). It shows how the fundamental peak frequency at 120 kHz increases with the increase of nozzle/bubble size. The results show agreement with those previously presented: that the first two nozzle sizes, 1.4 mm and 2.8 mm, give only slightly different results because the differences in bubble size generated by these two nozzles are similar.

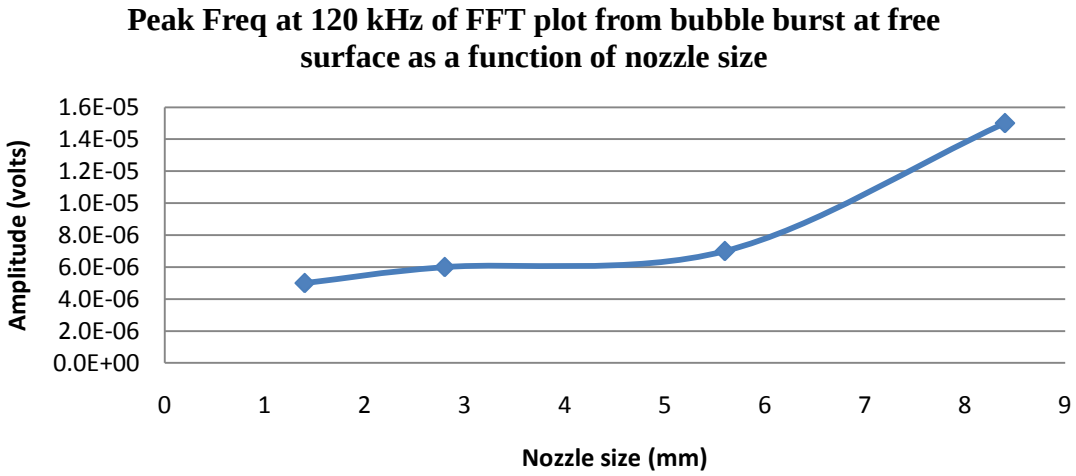

Figure 6-28: Fundamental peak frequency at main 120 kHz to differentiate the effect of bubble size.

6.3 Third test; Glycerine (10 cP)

The bubble test rig used in the previous test (Section 6.2 Second test; water 1cP) was modified to overcome the background noise problems described earlier. The 50 mm aluminium sheet was replaced by 10 mm thick stainless steel. Stainless steel was chosen due to its property of corrosion-resistance. Stainless steel contains sufficient chromium (~11 %) to form a passive film of chromium oxide, which prevents further surface corrosion. In addition, a new nozzle design was introduced for better control of continuous single bubble formation with an air leak pressure technique. In this modified bubble rig, the same procedure and sensor layout was used as in the previous experiment but with a glycerine solution (10 cP) replacing the water to investigate the effect of higher viscosity on AE activity from bubble inception to burst.

6.3.1 AE detection: Bubble burst

AE amplitude from a single bubble burst in a glycerine solution of viscosity 10 cP was used for comparison with the results obtained from the first and second experiments (with tap and saltwater). It was found that the larger the nozzle size and viscosity of solution, the higher the AE signal amplitude obtained from bubble burst at a free surface.

However, the AE HITs (defined as detecting and measuring an AE signal, see page 48) from the bubble burst still experienced interference from AEs generated which were due to hydrogen bubble formation as a result of the chemical reaction between the stainless steel wall and glycerine solution (10 cP), see Figure 6-29. AE signatures associated with the bubble burst, and recorded by Sensor-3, are shown in figure 6-30 and were visually verified during testing.

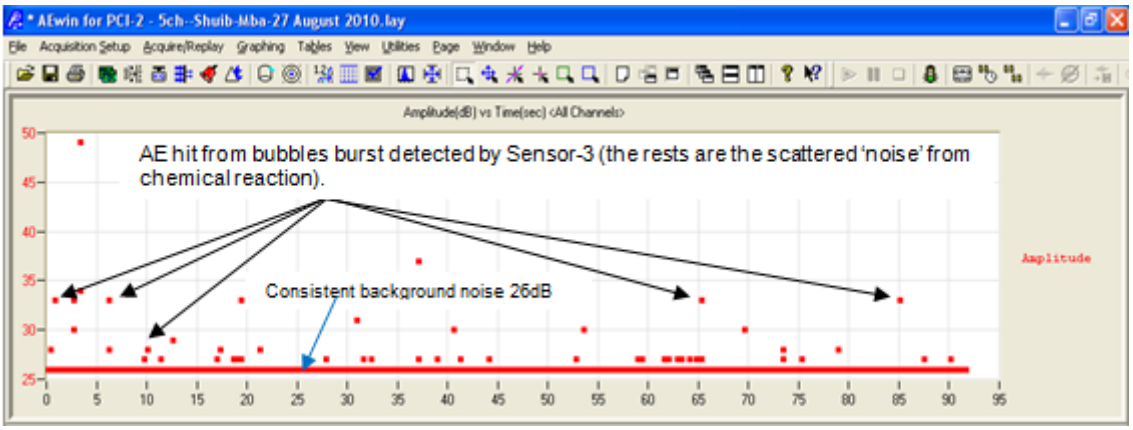

Figure 6-29: Example of bubble generated from chemical reaction

A comparison of AE amplitude (dB) from free surface bubble burst for all four nozzle sizes acquired by Sensor-3 is shown in Figure 6-30 (page 129). The results were analysed statistically from 8 samples for each nozzle. This limited number of test samples was due to the interference of AE HITs from micro bubbles generated from corrosion/oxide formation process of metal (Aluminium

and Stainless steel), see Appendix D, Paper 3, page 180. The average value and standard deviation for the data is presented in Table 6-17; the average AE amplitude of free surface bubble burst in the glycerine solution (10 cP) with nozzle sizes 1.4 mm, 2.8 mm, 5.6 mm and 8.4 mm are 29 dB, 29 dB, 31 dB and 33 dB respectively. Generally, this shows that the bigger the nozzle, the higher the amplitude of the bubble burst. Again, nozzles 1.4 mm and 2.8 mm diameter show the same average value (29 dB). From observations and the video recordings, it was found that these two nozzles did produce bubbles of a similar size. The plot of average AE amplitude as a function of nozzle size for free surface bubble burst in a glycerine solution (10 cP) is shown in Figure 6-31 (page 130). It can be seen that bubbles from the two nozzle sizes, 1.4 mm and 2.8 mm, produce much the same amplitude AE signal but there is then an abrupt increase in levels for the two nozzle sizes 5.6 mm and 8.4 mm.

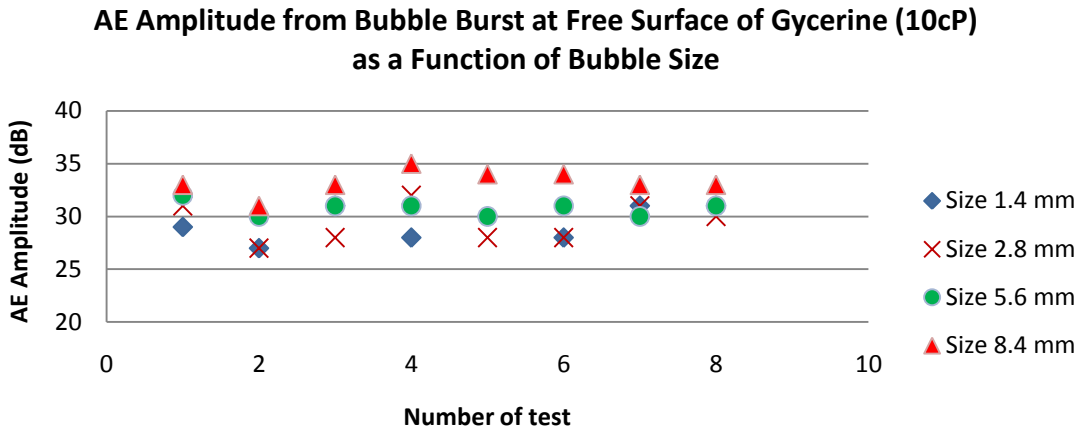

Figure 6-30: AE Amplitude of bubble burst at the free surface of glycerine (10 cP) as a function of nozzle size as detected by Sensor-3

Table 6-17: Comparison of average and standard deviation of AE amplitude of free surface bubble bursts (glycerine 10 cP) with nozzle size, as detected by Sensor-3

Nozzle size	1.4 mm	2.8 mm	5.6 mm	8.4 mm
Ave Amp (dB)	29	29	31	33
Stdev (dB)	2	2	1	1

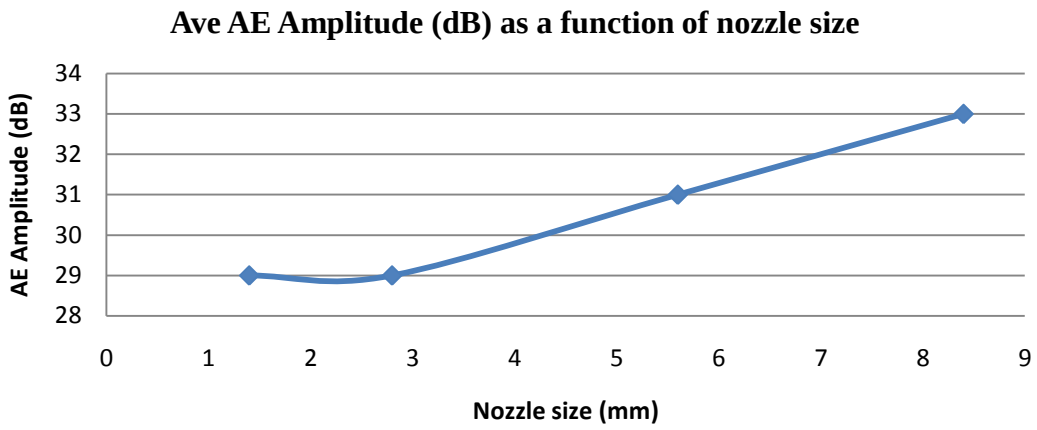

Figure 6-31: Average AE amplitude of bubble burst (glycerine 10 cP) as a function of nozzle size as detected by Sensor-3

6.3.2 Waveform analysis: Bubble burst

The average AE duration of free surface bubble burst for glycerine solution (10 cP) as a function of bubble/nozzle size is shown in Figure 6-32 (page 131). The AE duration was determined by taking the time interval between the start and end of the waveform crossing the threshold value (0.61 mV). Generally, the plot shows that AE duration for free surface bubble burst increases with an increase of nozzle size. However, once again, there is little difference between the first two nozzle sizes due to the slight difference in bubble size generated by these two nozzles. The average and standard deviation of AE duration were calculated from 8 test samples and are presented in Table 6-18 (page 131). The results of the average AE duration of bubble burst at the free surface in the glycerine solution (10 cP) for nozzle sizes 1.4 mm, 2.8 mm, 5.6 mm and 8.4 mm are 31.3 μs, 33.0 μs, 36.1 μs and 48.6 μs respectively.

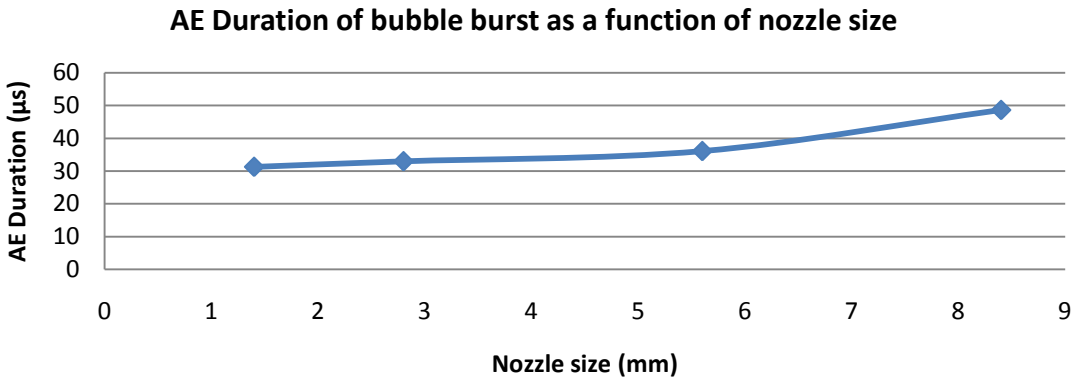

Figure 6-32: Comparison of average AE bubble burst duration at free surface of glycerine solution (10 cP) as a function of nozzle size; Sensor-3

Table 6-18: Comparison of Average and standard deviation of AE duration (s) of bubble burst (glycerine 10 cP) as a function of nozzle size detected by Sensor-3

Nozzle size	1.4 mm	2.8 mm	5.6 mm	8.4 mm
Ave AE Duration (µs)	31.3	33.0	36.1	48.6
Stdev (µs)	10	20.7	24.3	8.81

The same trend is shown for AE energy, see Figure 6-33 (page 132). The average was calculated from the same 8 test samples used for AE duration (Figure 6-32). The average AE energy plot of free surface bubble burst energy for the glycerine solution (10 cP) as a function of nozzle size is shown in Figure 6-33. The average and standard deviation of the samples used in Figure 6-33 are presented in Table 6-19 (page 132). The results of the average AE energy of free surface bubble burst for the glycerine solution for nozzle sizes 1.4 mm, 2.8 mm, 5.6 mm and 8.4 mm are 3.69×10^{-15}J, 4.25×10^{-15}J, 6.28×10^{-15}J and 19.9×10^{-15}J respectively. Again the same trend was obtained as in previous plots of average AE amplitude and duration, where there was a slight increase going from the 1.4 mm nozzle to the 2.8 mm nozzle, see Figure 6-33, and, again, this was attributed to the small difference in size of bubble generated by

these two nozzles. As in previous plots there is an obvious increase in going from the 5.6 mm diameter nozzle to the 8.4 mm nozzle.

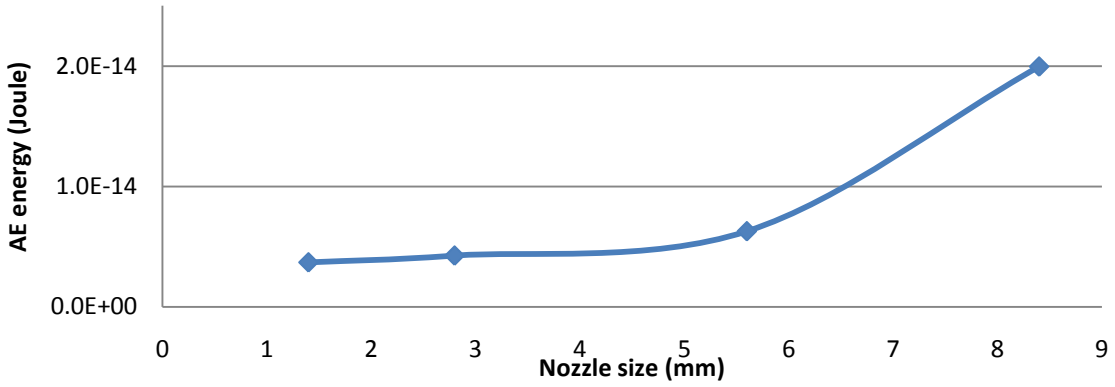

Figure 6-33: Plot of the comparison of the average energy of bubble burst at the free surface as a function of nozzle size

Table 6-19: Comparison of Average and standard deviation of AE Energy (J) of bubble burst (glycerine 10 cP) as a function of nozzle size detected by Sensor-3

Nozzle size	1.4 mm	2.8 mm	5.6 mm	8.4 mm
Ave AE Energy (J x 10^{-15})	3.69	4.25	6.28	19.9
Stdev (J x 10^{-15})	2.86	1.99	1.86	8.98

6.3.3 Frequency domain analysis: Bubble burst

Figure 6-34 (page 133) presents the plots of the average FFT of AE signal waveform samples of bubble burst at the free surface of the glycerine solution 10 cP. The FFT results show that the main/primary frequency for all bubble/nozzle sizes is 120 kHz. This main frequency component is the same as obtained in the previous experiments. However, in this higher viscosity (10 cP) experiment the amplitude at peak frequency (120 kHz) did not show a trend as noted in the previous experiments with water and saltwater. This is depicted by the plot in Figure 6-34.

	Frequency Spectra of bubble burst (glycerine 10 cP)
Nozzle Size: **1.4 mm**	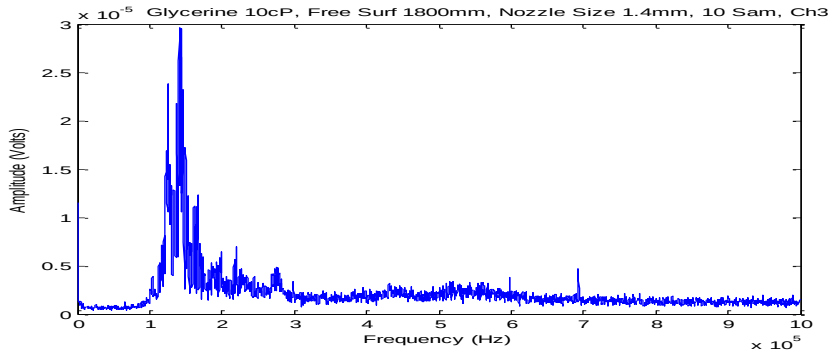
Nozzle Size: **2.8 mm**	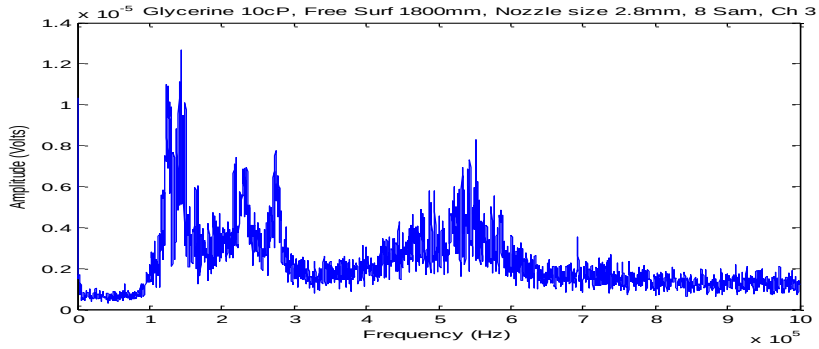
Nozzle Size: **5.6 mm**	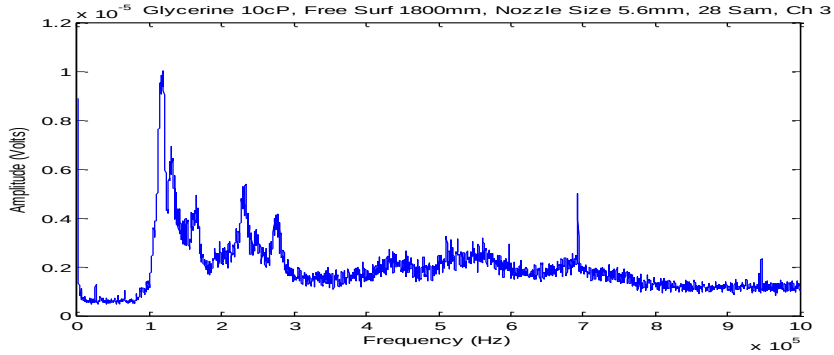
Nozzle Size: **8.4 mm**	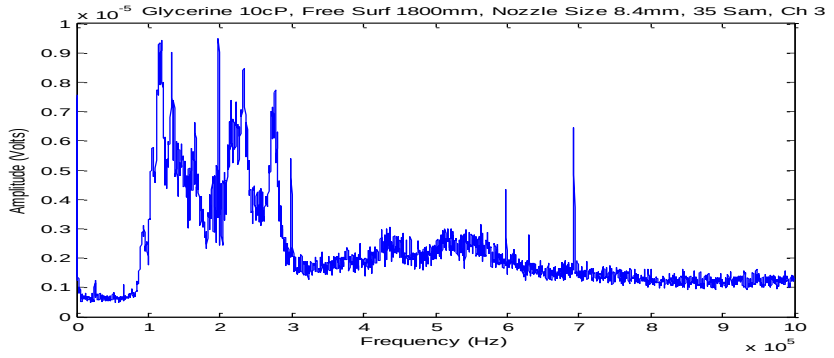

Figure 6-34: Average FFT analysis bubble burst at free surface of glycerine (10 cP)

Table 6-20: Comparison of peak frequency at 120 kHz for all sizes in glycerine solution (10 cP)

	Size 1.4mm	Size 2.8mm	Size 4.4mm	Size 8.4 mm
Peak frequency at 120 kHz	2.9 x 10^{-5} V	1.3 x 10^{-5} V	1.0 x 10^{-5} V	0.95 x 10^{-5} V

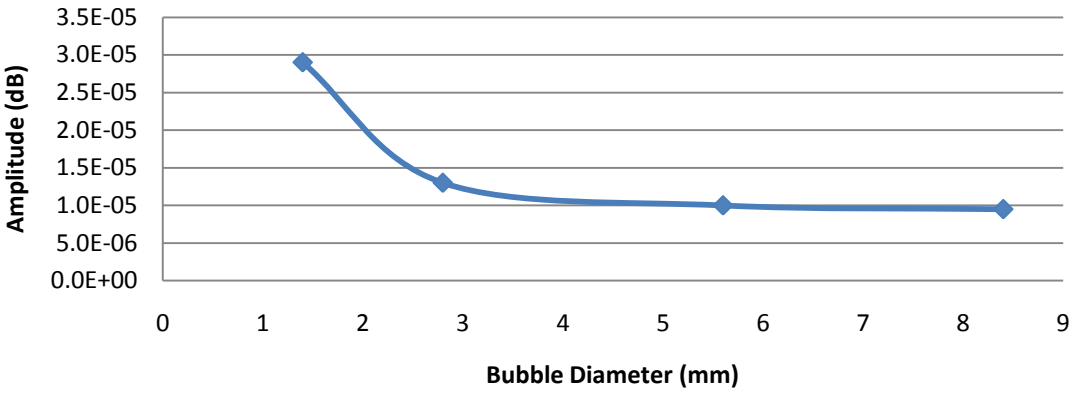

Figure 6-35: Peak frequency at 120 kHz

The result of peak frequency at 120 kHz as a function of bubble size, as shown in Figure 6-35, shows a decreasing trend with the increase of bubble size. This contradicts the previous results from the first and second experiment, therefore implying that this method is not reliable for bubble sizing.

6.4 Conclusion

The results from the experiments show that AE technology is sensitive and successful in the detection of AE from a single bubble activity, particularly bubble formation and burst at the free surface. However, observations have indicated no AE detected by AE sensors during bubble rise up to the free surface. It is worth correlating AE with bubble burst since this event is independent from external forces, except bubble properties such as bubble size, bubble shape and liquid properties such as liquid viscosity, liquid density. The results indicate the usefulness of AE technology for monitoring bubble phenomena in two phase gas-liquid flow systems.

7 DISCUSSION

The discussion will emphasise the effect of bubble size and liquid viscosity on the AE signal generated at bubble formation and free surface bubble burst. The bubble dynamics of these events are briefly presented to support the results obtained and the comparisons made. AE from bubble activity is dependent on bubble and liquid properties. Moreover, liquid properties, particularly viscosity, have been demonstrated as influencing AE bubble inception and burst. Table 7-1 (page 136 and137) is a useful reference that provides an overall picture of the experimental work with the different conditions.

Table 7-1: Summary of Test Experiments, Conditions and Result Characteristics

Condition	First Test	Second Test	Third Test	Observation 1st Test (Water & Saltwater)	Observation 2nd Test (Water), Al thickness 50 mm	Observation 3rd Test (Glycerine), Mild Steel, Th
Free surface x column height	Φ150 mm x 575 mm	(100 x 300) x 1800 mm	(100 x 300) x 1800 mm	A. **Detected** AE from intrusive method: 1) Bubble inception 2) Bubble burst. B. **Not detected** AE from: 1) Bubble oscillation during rise-up. 2) Bubble hitting the free surface. C. **AE hit amplitude**: 1) Increase with increasing bubble size (in both tap water 1 cP & saltwater 2 cP). 2) Increase with increased liquid viscosity (saltwater, 2 cP). D. **Peak at primary (main) frequency**	A. **Detected** AE from: 1) Intrusive and non-intrusive methods of bubble inception. 2) Intrusive method for bubble burst. B. **Not detected** AE from: 1) **Non-intrusive method** of bubble **burst**. 2) Bubble oscillation during rise up. 3) Bubble hitting the free surface. C. **AE Amplitude from intrusive sensor** was greater than non-intrusive sensor. D. **AE Amplitude inception** (brass nozzle) was higher than bubble burst.	A. **Detected** AE from: 1) Only detected AE from intrusive method from bubble inception and bubble burst. B. **Not detected** AE from: 1) **Non-intrusive method** for bubble **inception** and **burst**. C. It was found that **higher viscosity** (e.g. Glycerine, 10 cP) **suppresses and dampened AE from bubble inception**.
Liquid used	Water (1 cP) Saltwater (2 cP)	Water (1 cP)	Glycerine sol. (10 cP)			
Free surface height	575 mm	1800 mm	1800 mm			
Nozzle material	Plastic tube	Brass	Brass			
Nozzle end shape	Flat	Cone	Cone			
Nozzle diameters	1.4 mm 4.4 mm 8.4 mm	1.4 mm 2.8 mm 5.6 mm 8.4 mm	1.4 mm 2.8 mm 5.6 mm 8.4 mm			
Rig Wall Material	Perspex pipe	Aluminium (50 mm)	Stainless Steel (10mm)			
Sensor Mounting	Intrusive	Intrusive Non-intrusive	Intrusive Non-intrusive			
Sensor No	Sensor-1 (Intrusive) Sensor-2 (Intrusive) Sensor-3 (Intrusive)	Sensor-1 (Intrusive) Sensor-2 (Intrusive) Sensor-3 (Intrusive) Sensor-4 (Non-intrusive) Sensor-5 (Non-	Sensor-1 (Intrusive) Sensor-2 (Intrusive) Sensor-3 (Intrusive) Sensor-4 (Non-intrusive) Sensor-5 (Non-			

		intrusive)	intrusive)	component 120 kHz: 1) Increase with increasing bubble size (in both tap water 1 cP & saltwater 2 cP). 2) Increase with increased viscosity (saltwater, 2 cP). E. **AE Amplitude burst event** higher than bubble inception (plastic nozzle). F. **AE Amplitude** (classical AE parameter) obtained directly from the system is **the best indicator** for bubble. G. **AE duration** & **AE energy** (waveform post-processing) are proportional with bubble size.	E. **Peak at primary frequency**, 120 kHz: 1) Increase with increasing bubble size (in both intrusive and non-intrusive method). 2) Higher at intrusive method compared with non-intrusive. F. Clearly showed **primary frequency** 120 kHz for both methods intrusive and non-intrusive. G**. AE duration** & **AE energy** (post-processing) were proportional to bubble size. However, **size 1.4 and 2.8 mm were not producing a significant difference at bubble inception**.	D. **Primary (main) frequency** component was **120 kHz** for bubble burst. E**. AE duration, AE energy** (post-processing) were **proportional** to **bubble size**. However, **size 1.4 and 2.8 mm were not producing a significant difference at bubble inception**.
Sensor Location	Sensor-1 (Bottom) Sensor-2 (Mid) Sensor-3 (Top)	Sensor-1 (Bottom) Sensor-2 (Mid) Sensor-3 (Top) Sensor-4 (Bottom) Sensor-5 (Top)	Sensor-1 (Bottom) Sensor-2 (Mid) Sensor-3 (Top) Sensor-4 (Bottom) Sensor-5 (Top)			
Threshold	24 dB	26 dB	26 dB			
Gain	60 dB	40 dB	40 dB			
Background noise	None	Interference	Interference			
Test parameters	AE Amplitude AE Duration AE Energy FFT	AE Amplitude AE Duration AE Energy FFT Wavelet	AE Amplitude AE Duration AE Energy FFT Wavelet			
CONCLUSION Demonstrated that AE technology can be employed to detect a single bubble activity particularly bubble inception and burst. Correlation between AE and bubble size has been established. Bubble size and liquid viscosity contributed to the level of energy AE generated.						

The first experiment produced inconsistent results for bubble inception due to the nozzle shape (the flat tip surface area of the hoses were different for every nozzle diameter) which affected AE emission during pinch-off. This experiment demonstrated that bubble characteristics are influenced by the design of the nozzle's end (Werther, 1978). A sharpened (cone-shaped) tip for the nozzle as used in the second and third experiments has been shown to prevent irregular bubble formation (Leighton, 1994a).

In the second and third experiments, the AE sensors were arranged in such a way as to be either intrusive or non-intrusive to compare the signal acquired. The test rig in the second experiment highlighted the capability of the AE sensor to be used non-intrusively in the detection of single bubble pinch-off at both a nozzle underwater and free surface bubble burst event. Furthermore, a comparison between AE parameters was made for amplitude, duration and absolute energy for signals acquired intrusively and non-intrusively. Initially it was assumed that the size of the bubble was proportional to nozzle diameter, but the results obtained showed this assumption to be incorrect. It was observed that the first two nozzles of diameters 1.4 mm and 2.8 mm did not produce different bubble diameters.

In the second and third experiments performed, Sensor-5 (positioned at the top) which was mounted non-intrusively did not detect an AE signal from free surface bubble burst. This might be attributed to bubble dynamics when bursting at a free surface and it is postulated that in the event of bubble burst at a free surface, a fraction of the bubble's energy is lost to the air above the free surface and only a fraction of the energy released is transferred to a shockwave which could only be detected by the intrusive and nearest sensor which was Sensor-3 (positioned at the top, intrusively) (De-Bosset et al., 2007). The energy released to the water was not above the threshold after it had passed through the 50mm thick aluminium sheet and this is why a signal of the burst event was not detected by Sensor-5. On the other hand, the energy radiated from the bubble inception event was sufficient to pass through the aluminium wall and be picked up by Sensor-4 (positioned at the bottom, non-intrusively).

The second test with the aluminium wall in the test rig presented an opportunity to assess the sensitivity of AE technology in detecting AE events from a chemical reaction. The source of AE during chemical reactions included micro-bubble generation. Once corrosion has started, it is expected that a large number of AE events will be recorded in a short space of time (Birkin et al., 2007). This is evidently shown by the results of the AE HIT plot; see Figure 7-6 (page 149).

AE technology has been used for corrosion monitoring, particularly for steel and its alloys (Oltra et al., 1993; Mazille et al., 1995; Spasova et al., 2006; Spasova and Ojovan, 2008). Prateepasen et al., (2006) employed AE technology to detect corrosion on austenitic stainless steel. Their results showed that the AE count number was associated with the corrosion rate. They confirmed that the AE sources came from corrosion activity where hydrogen bubbles were generated from chemical reactions in the corrosion process. In an earlier study, Ing et al. (2003 and 2005) used AE technology to detect corrosion in reinforced concrete by observing AE hits. They performed experiments on the samples before and after corrosion. By comparing the AE hit data they demonstrated the ability and practicality of AE to detect corrosion in concrete at the early stages and before any external evidence was visible. These two examples show the large scope of AE in corrosion monitoring.

The effect of higher viscosity on AE from bubble inception and free surface burst was investigated in the third experiment using a glycerine solution (10 cP) in the modified bubble-test rig. Only Sensors-1 and -3 picked up the AE from bubble inception and burst respectively. The average AE amplitude from bubble inception detected by intrusive Sensor-1 was the same for all nozzle sizes, 27 dB. It was found that from 162 single bubbles injected by the nozzle of diameter 8.4 mm only 11 of these pinch-off events were detected by Sensor-1. This clearly shows that the liquid viscosity has contributed to the damping of the shockwave from air bubble pinch-off. Figure 7-1 (page 142) is presented to support this conclusion; the plot demonstrates that the AE amplitude (dB) from bubble inception in glycerine (10 cP) is lower than inception in water (1 cP). In

addition, the amplitude obtained from bubble inception for all nozzle diameters was the same (27 dB). It shows agreement with the statements made by Chapman and Plesset (1971) and Addali (2010) that increased liquid viscosity would suppress AE levels.

Table 7-2 (page 142) shows the comparison of AE HITs detected by Sensor-1 compared with the number of gas bubbles injected through each nozzle in the glycerine solution. It was confirmed visually that the size of a bubble at inception in the glycerine solution (10 cP) was different for the 1.4 mm and 8.4 mm diameter nozzles; the AE amplitude detected was 27 dB for both sizes of bubble. The detection rate for Sensor-1, which is positioned close to the nozzle, had an overall average of 9.8%, for all nozzle sizes. On the other hand, the average AE amplitude from the burst event from bubbles generated through these nozzle sizes (1.4 mm and 8.4 mm) showed differences in AE amplitude (26.2 dB and 32.5 dB) for the respective nozzle sizes, see Table 6-8 (page 109). Table 7-3 (page 142) shows the comparison of AE HITs detected by Sensor-1 compared with the number of gas bubbles injected in water (1 cP). The overall AE detection from bubble inception in water (1 cP) was 48.2 % which is five times higher than in glycerine (10 cP).

Table 7-4 (page 143) shows the comparison of AE HITs of burst events detected by Sensor-3 in Glycerine (10 cP) compared with the number of gas bubbles injected (Sensor-1). The detection rate for Sensor-3 which is positioned close to the free surface has an overall average of 20.5 %, for all nozzle sizes. This result shows that the percentage of AE HITs detected by Sensor-3 for free surface bubble burst events was less affected by liquid viscosity compared with the bubble inception event at the nozzle in the higher viscosity liquid (glycerine solution 10 cP - Figure 7-2, page 143).

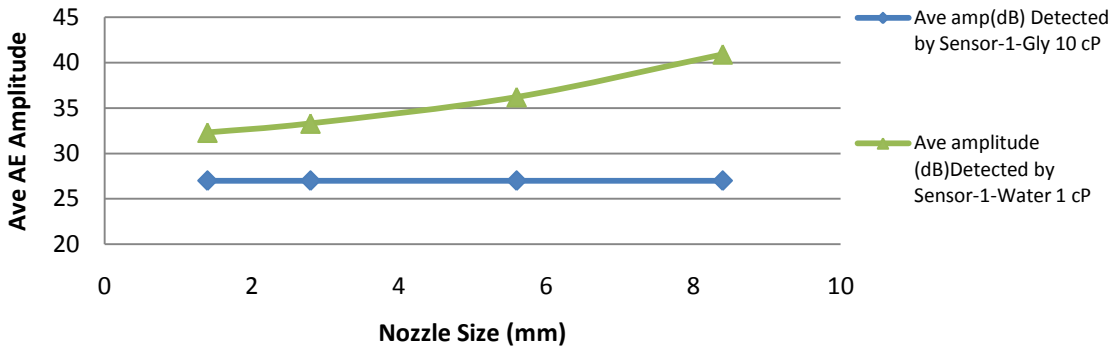

Figure 7-1: Comparison of AE amplitude (dB) of bubble inception detected by Sensor-1 in glycerine (10 cP) and water (1 cP)

Table 7-2: AE from bubble inception detected by intrusive Sensor-1 in glycerine (10 cP)

Nozzle size	**1.4 mm**	**2.8 mm**	**5.6 mm**	**8.4 mm**
Ave Amp (dB)	27	27	27	27
Number of gas bubbles injected through the nozzle	49	113	105	162
Number of bubble inception events detected by Sensor-1	3	4	24	11
% of detection	6.1%	3.5%	22.9%	6.8%
Ave % detection of bubble inception events by Sensor-1 in glycerine (10 cP)	9.8 %			

Table 7-3: AE from bubble inception detected by Sensor-1 in water (1 cP)

Nozzle size	**1.4 mm**	**2.8 mm**	**5.6 mm**	**8.4 mm**
Ave Amp (dB)	32.3	33.3	36.2	40.9
Number of gas bubbles injected through the nozzle	78	106	381	216
Number of bubble inception events detected by Sensor-1	34	63	125	123
% of detection	43.5	59.4	32.8	56.9
Ave % detection of bubble inception events by Sensor-1 in water (1 cP)	48.2 %			

Table 7-4: AE from bubble burst detected by Sensor-3 in Glycerine (10 cP)

Nozzle size	1.4 mm	2.8 mm	5.6 mm	8.4 mm
Ave Amp (dB)	29	29	31	33
Number of gas bubbles injected through the nozzle	49	113	105	162
Number of bubble burst events detected by Sensor-3	11	15	28	35
% detection	22%	13%	26%	21%
Ave % detection of bubble burst events by Sensor-3 in Glycerine (10 cP)	20.5%			

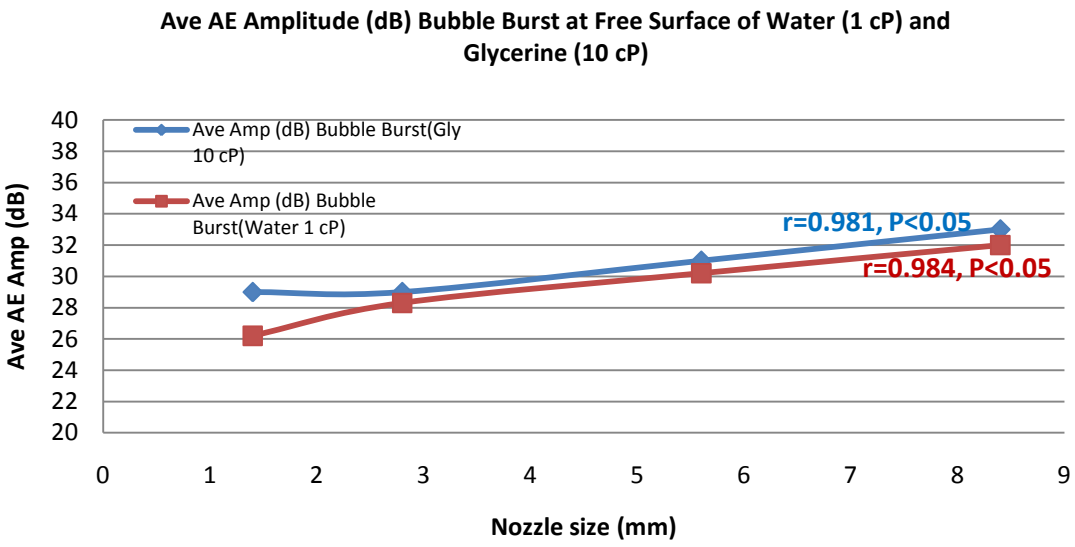

Figure 7-2: Comparison average of AE amplitude from free surface bubble burst; tap water (1 cP) and glycerine (10 cP)

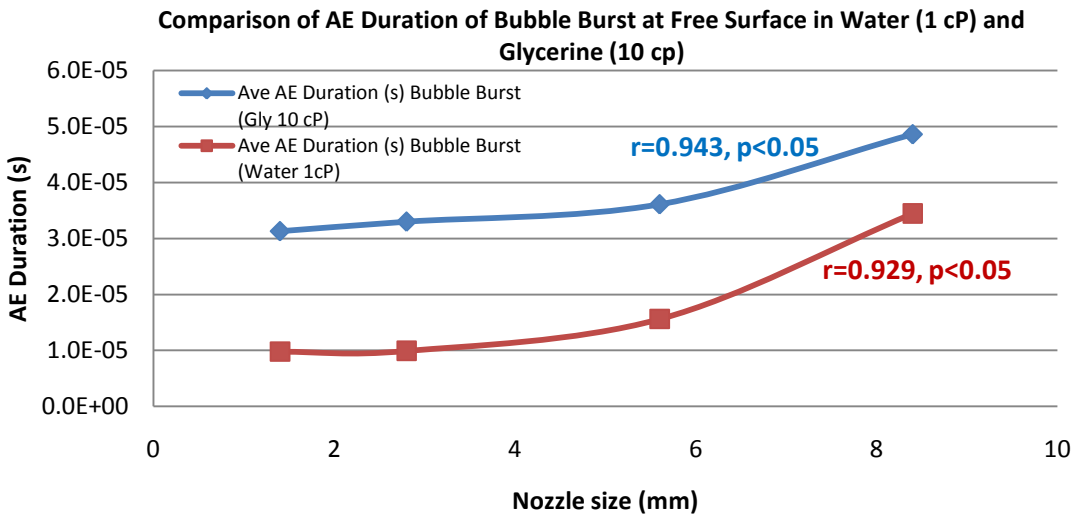

Figure 7-3: Comparison average of AE duration for free surface bubble burst; tap water (1 cP) and glycerine (10 cP)

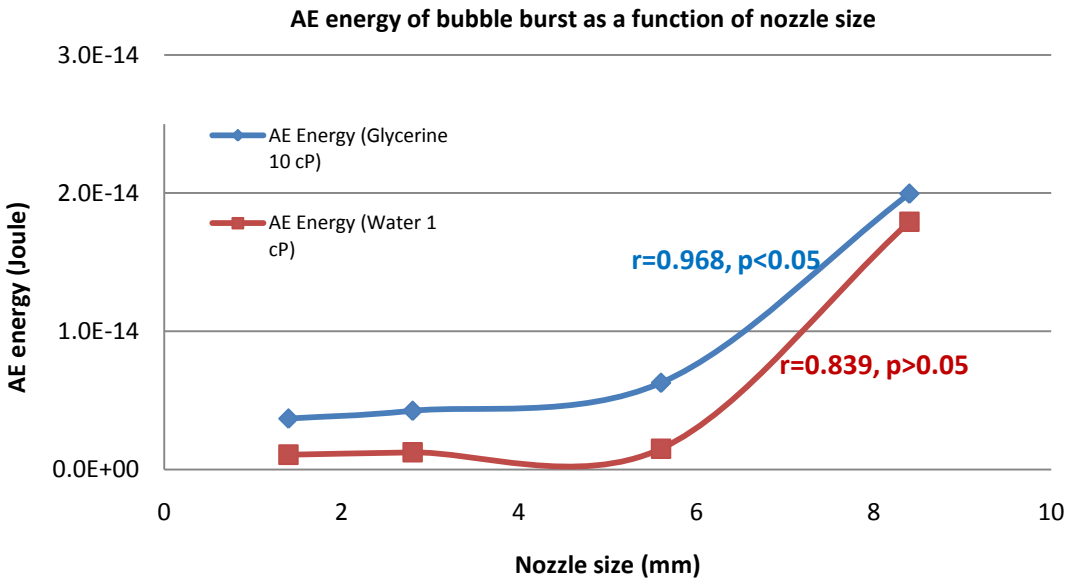

Figure 7-4: Comparison of average AE energy from free surface bubble burst; tap water (1 cP) and glycerine (10 cP)

The AE from bubble inception is attributed to the re-entrant jet that causes a pressure pulse during detachment of the bubble. The AE parameters obtained directly from the system (AE amplitude, duration and absolute energy) and by advanced processing (FFT and WT) of raw waveform data all show similar results for the two nozzles of 1.4 mm and 2.8 mm diameter because these two nozzles generated much the same size of bubble.

A glycerine solution (10 cP) was used to demonstrate the effect of higher viscosity on the AE signal from bubble inception at the nozzle and free surface bubble burst. Comparison of the results from the second and third experiments shows the damping of the acoustic wave or viscosity effect, see Figures 7-2 to 7-4 (page 143-144).

Even though the AE amplitude parameter was said to be the best indicator of bubble sizing from burst events, the results obtained showed very close results (dB) for the different liquid viscosities tested. Figure 7-2 (page 143) justifies this observation where the plot shows that the amplitude difference between bubble bursts in water (1 cP) and the glycerine solution (10 cP) is only 1 dB. Therefore, it is concluded that the AE amplitude parameter cannot be used for liquid viscosity classification. The results from post signal processing, such as AE duration (see Figure 7-3, page 144), and AE energy (see Figure 7-4, page 144), are more appropriate where they have a more distinctive range of the results for liquid viscosity classification/characterisation, rather than the AE amplitude parameter in the case that the different result between the water and glycerine solutions is 1 dB.

A Pearson correlation shows the relationship between two variables in a linear trend. Pearson product-moment correlation coefficient was calculated using the SPSS statistics software package. The bivariate correlation tool in SPSS was applied; this refers to the correlation between two continuous variables and is the most common measure of a linear relationship. This coefficient has a range of values from -1 to +1. The number indicates the strength of the relationship,

while the sign (+ or -) indicates the direction – either a positive or negative relationship.

For the glycerine solution (10 cP), the output confirms the results of the scatter plot (Figure 7-2, page 143) in that there is a significant positive relationship between AE amplitude and bubble/nozzle size ($r=.981$, $p<.05$). Therefore, higher sizes are associated with higher AE energy. For lower viscosity, water (1 cP), the results of the correlation show the same trend as in the glycerine solution (10 cP), a positive correlation with higher strength of relationship, ($r=.984$, $p<.05$).

The plot in Figure 7-3 (page 144) of the higher viscosity condition (glycerine solution 10 cP) shows a significant positive relationship between AE duration and bubble/nozzle size ($r=.943$, $p<.05$). Similar to AE amplitude, the higher sizes are associated with higher AE duration. For lower viscosity, water (1 cP), the results of the correlation shows the same trend as in the glycerine solution (10 cP), a positive correlation with relative lower strength of relationship, ($r=.929$, $p<.05$).

For higher viscosity (glycerine 10 cP) AE energy shows a significant positive relationship between AE energy and bubble/nozzle size ($r=.968$, $p<.05$), see Figure 7-4 (page 144); higher viscosity (glycerine 10 cP) results in a higher strength of relationship. However, for lower viscosity, water (1 cP), the output confirms the results of the scatter plot in Figure 7-4 that there is no significant positive relationship between AE energy and bubble/nozzle size ($r=.839$, $p>.05$). This might be attributed to errors in generating the bubble via the nozzle.

The Pearson correlation results calculated from the data obtained from difference viscosity conditions (water and glycerine) have confirmed the contribution of viscosity to the AE from bubble activity. The strength of relationship for all AE parameters (AE amplitude, AE duration, AE energy and WT coefficient) is apparently increased with the increase of bubble/nozzle size.

Divoux et al. (2008) stated that acoustic energy depends not only on the energy initially contained inside a cavity but also on the characteristic time associated with the film bursting. Therefore the bubble properties (particularly shape and size) contribute to the AE energy of bubble burst. Bubble burst is associated with bubble parameters such as bubble diameter, bubble cusp length (shape) and bubble film thickness which depends on the liquid viscosity (Divoux et al., 2008). These researchers used a microphone, which was located 3 cm above the free surface to acquire the signal from a bubble burst and investigated the acoustic energy associated with the shape of the bubble just before it burst at a free surface, and the effect of liquid viscosity (% of concentration, C) on such energy. Figure 7-5 shows the results of Divoux et al. (2008) which demonstrate that the acoustic signal was associated with bubble shape just before the free surface burst as a function of gel concentration, C (liquid viscosity).

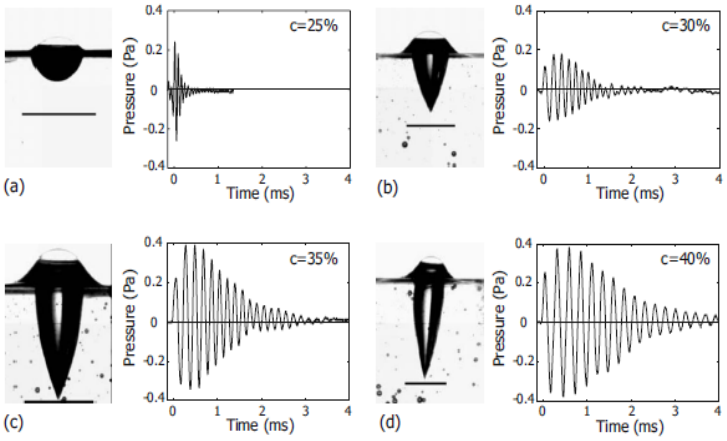

Figure 7-5: Images of the bubble immediately before bursting and associated acoustic signals, and liquid/gel concentration (Divoux et al., 2008)

It is therefore not surprising that these characteristics also affect Acoustic Emission (100 kHz - 1 MHz) characteristics. This also goes some way to explain the variation in results noted as it is very difficult to guarantee identical bubble shapes at the point of bursting. Bubble shape, just before bursting, was not aimed at in this study programme; AE detection from bubble inception and bubble burst has been set as the main aim for this first known attempt on the application of AE in detecting a single bubble dynamics.

In the first experiment there was a slight increase of viscosity: tap water (1 cP) to saltwater (2 cP). FFT analysis of the bubble inception waveform in both tap and saltwater showed that the amplitude at the peak frequency increased with the increase of bubble size (assumed to be proportional to the nozzle diameter). By contrast, in the third experiment with the glycerine solution (10 cP) the results obtained showed that amplitude at peak frequency decreases with increase of bubble size at the free surface burst. This demonstrates that viscosity can boost or suppress AE from bubble activity. Results from the third test also showed that increase in viscosity can suppress the AE signal from bubble inception. This reiterates the findings of others (Chapman and Plesset, 1971; Addali, 2010) who came to the same conclusion.

The average value of AE amplitude (dB) from non-intrusive Sensor-4 was less than the average value from intrusive Sensor-1. This is because the AE signals originating from the bubble inception attenuated through both water and the metal sheet before being detected by Sensor-4. This attenuation will be a function of the properties of the transmission path media, such as bonding structure, thickness and viscosity.

Comparisons of the waveforms obtained from Sensor-1 (intrusively) and Sensor-4 (non-intrusively) showed the transient duration at the raw waveform from Sensor-4 was longer compared with the waveform from Sensor-1. This result was due to signal propagation in the solid media (aluminium wall) and the increased distance of Sensor-4 from the AE source.

The results obtained in this experimental programme, especially in the second and third experiments, showed that for the injection of air through the small nozzles of 1.4 mm and 2.8 mm diameter there was no difference in bubble size.

Beside the main aims in this programme, the experiments have demonstrated the sensitivity of AE technology to detect bubble activity due to chemical reaction or corrosion processes. AE technology was capable of detecting the hydrogen bubbles associated with surface degradation of aluminium. Figure 7-6

shows the HIT signal amplitude level (dB) of hydrogen bubbles activities detected in the corrosion experiment.

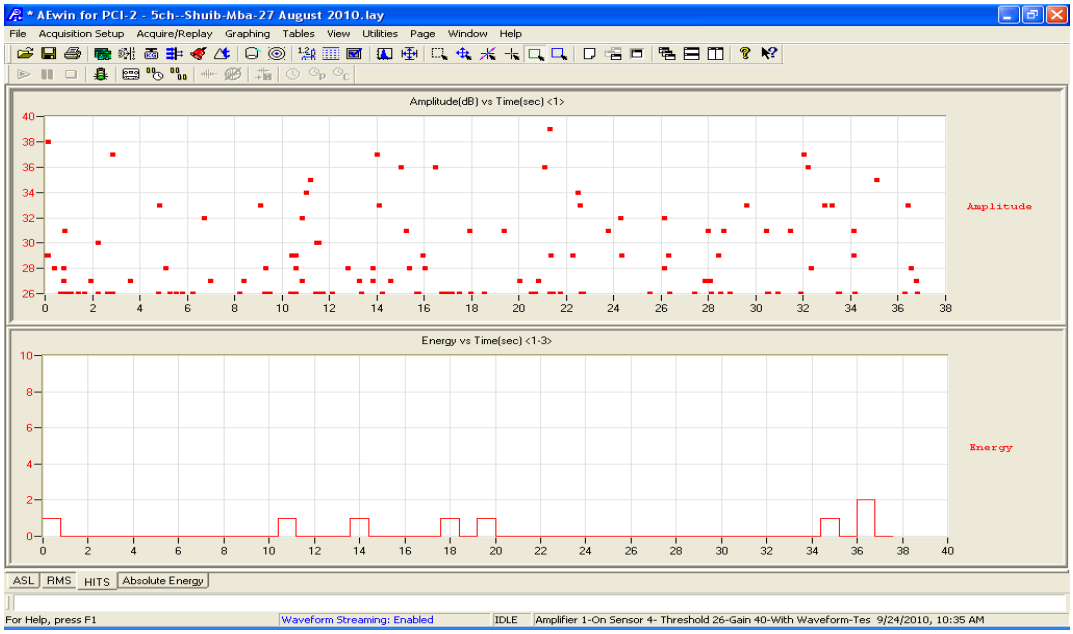

Figure 7-6: A thousand hits of '*background noise*' from chemical reaction; without gas injection. The higher amplitude of background noise hit is 39 dB.

7.1 Conclusion

Referring to Figures 7-2, 7-3 and 7-4 for AE amplitude (obtained directly from the AE system), AE duration and AE energy respectively (both AE duration and AE energy obtained from waveform analysis with threshold procedure), it has been demonstrated that AE duration and AE energy are the critical AE features in this study when considering the results between two different viscosities. AE amplitude, obtained directly from the system, only gives 1 dB difference between Water (1 cP) and Glycerine (10 cP), which indicates that AE amplitude cannot be used as the critical AE feature for monitoring the effect of different liquid viscosities on bubble dynamics, bubble formation and burst at the free surface. In addition, it is felt that 1 dB resolution in AE amplitude output is a limitation for this case.

8 CONCLUSION & RECOMMENDATION FOR FUTURE WORK

8.1 Conclusion

This work presents preliminary investigations into the application of AE technology to bubble sizing in a vertical column. The Acoustic Emissions measured in the investigation cover the frequency range 100 kHz to 1,000 kHz. Pressure pulses associated with bubble inception at the nozzle and free surface burst are broadband in nature and can be detected by an AE piezoelectric sensor.

It has also been established that the AE signal amplitude from bubble inception and burst at the free surface in water increases with bubble size. A similar trend was obtained from bubble burst for a higher viscosity, glycerine solution (10 cP). However, for bubble inception in the glycerine solution (10 cP), the results showed that the amplitude of the wave pulse generated from bubble inception was suppressed or dampened. Therefore, the bubble burst at the free surface was the best event to be correlated with bubble size for possibly all viscosity conditions.

Through this experiment, evidence has been established of the applicability of the AE technology for non-intrusive detection and process monitoring of bubble activity for a two-phase system. It is evident that AE technology provides an effective detection and measurement method for bubble size in two-phase flow systems.

These findings are novel and make a contribution to the development of Acoustic Emission technology.

In summary the following are concluded:

1. AE technology is capable of detecting single bubble inception and burst at a free surface.

2. It was established that the AE amplitude, duration, energy and rise time of bubble burst at the free surface increases as the bubble size increases for a defined viscosity.
3. Higher frequency content (range up to 700 kHz) was noted in the first 10 μs of the event for both bubble inception and burst.
4. Observations indicated no AE waves were detected from bubble oscillation during its motion from inception to free surface..
5. AE technology is capable of detecting single bubble inception through a 50 mm aluminium sheet and stainless steel.
6. Observation showed the frequency of 120 kHz to be the most sensitive (main frequency/primary frequency) to bubble inception and burst for all the sizes tested.

The successful detection of single bubble activity in this experiment has provided a basis for the application of AE technology to measuring flow parameters and monitoring slug flow in two-phase systems such as in horizontal pipelines. In addition, AE technology offers a simple procedure of non-invasive techniques which can be applied to metal pipes and opaque liquids. In the fullness of time such applications could be instrumental in monitoring the flow of various multi-phase conditions as experienced in numerous industries.

8.2 Recommendations for future work

The dependence of the amplitude of the AE signal emitted by a single bubble at inception at the bottom of a liquid column, on the viscosity of the liquid was problematic. The effect of increasing viscosity needs to be investigated to determine whether there is a viscosity transition point effect on the AE signal from bubble inception. This is because the damping of the wave occurs as it travels through the medium and possibly there are viscous forces enhancing or suppressing the AE signal energy.

The correlation developed between the size and AE generated from bubble inception and free surface burst need to be generalised by considering other bubble, liquid and nozzle properties including;

- Bubble shape parameters such as bubble cusp length as a function of viscosity.
- Height and velocity of counter jet during the burst dynamic at a free surface.
- Liquid density effect: according to theory, wave transmission in liquid is dependent on density, viscosity and surface tension, so liquid density will contribute to shockwave propagation.
- Liquid surface tension effect: experiments should be performed using a fluid with lower viscosity and surface tension than water. Paraffin could be used.
- Nozzle material effect: different types of nozzle material with the same design would investigate the effect of material. Jet re-entrance just after bubble pinch-off at the nozzle tip is a justification to investigate the effect of material on the AE generated from a jet re-entrance event.
- Nozzle tip's shape effect: different shapes including end-flat nozzle tips could be used to investigate the effect of nozzle shape design.

Lastly, it would be interesting to continue this investigation with additional measuring devices added to the current bubble test rig. These could include a pressure gauge and pressure probe gauge in order to measure internal bubble pressure before collapse/burst for accurate calculation of gas bubble energy. This theoretical gas bubble energy can then be compared with the measured acoustic energy of bubble burst. The use of high speed cameras in determining bubble size before free surface burst would give a better picture correlation between the size, shape and AE signal from free surface bubble burst. The application of High Speed Holography also strongly suggested for acquisition of accurate shape and size of bubble since High Speed Holography can overcome the problems of out-of-focus caused by bubble moving in 3-dimensional motion.

REFERENCES

- Addali, A. (2010). *Monitoring gas void fraction in two-phase flow with acoustic emission*, PhD Thesis, Cranfield University, UK.

- Aitken, F., McCluskey, F.M.J. and Denat, A. (1996). An energy model for artificially generated bubbles in liquids, J. Fluid Mech, 327, pp. 373-392.

- Al-Dossary, S., Raja Hamzah, R.I and Mba, D. (2008). Acoustic Emission Waveform Changes For Varying Seeded Defect Sizes, *Advanced Materials Research*, 13-14, pp. 427-432. ISBN 1022-6680.

- Al-Dossary, S., Raja Hamzah, R.I. and Mba, D. (2009) Observations of changes in acoustic emission waveform for varying seeded defect sizes in a rolling element bearing, *Journal of Applied Acoustics*, 70(1), pp. 58-81, ISSN 0003- 682X.

- Al-Fayez, L. (2004). *Detection of incipient cavitation and the best efficiency point for centrifugal pumps using acoustic emission*, PhD Thesis, School of Engineering, Cranfield University, UK.

- Al-Fayez, L. and Mba, D. (2005). Detection of incipient cavitation and the best efficiency point of a 2.2MW centrifugal pump using Acoustic Emission. *Journal of Acoustic Emission*, 22, pp. 77-82.

- Al-Ghamdi, A.M. and Mba, D. (2006). A comparative experimental study on the use of Acoustic Emission and vibration analysis for bearing defect identification and estimation of defect size. *Mechanical Systems and Signal Processing*, 20(7), pp. 1537-1571.

- Al-Ghamdi, A.M., Cole, P., Such, R. and Mba, D. (2004). Estimation of bearing defect size with Acoustic Emission, *INSIGHT*, 46(12), pp. 758-761.

- Al-Lababidi, S., Addali, A., Yeung, H., Mba, D. and Khan, K. (2009). Gas void fraction measurement in two-phase gas/liquid slug flow using acoustic emission technology, *Journal of Vibration and Acoustics*, ASME, 131(6), 064501, pp. 693-702.

- Al-Lababidi, S. and Sanderson, M.L. (2004). Transit Time Ultrasonic Modelling in Gas/Liquid Intermittent Flow Using Slug Existence Conditions and Void Fraction Analysis. In: *Proceedings of the 12th International Conference on Flow Measurement, FLOMEKO'04*, Guilin, China, Sept 12-17 2004**.**

- Alm, J.F. and Walker, J.S. (2002). Time-Frequency Analysis of Musical Instruments. *Society for Industrial and Applied Mathematics*, 44(3), pp. 457-476.

- Al-Maskari, A.S.A. (1985). *Detection of cavitation in a centrifugal pump using acoustic emission.* Msc thesis. School of Engineering, Cranfield University, UK.

- American Society for Testing and Materials (1982). Standard definitions of terms relating to acoustic emission, ASTM E610-82.

- Ayorinde, E.O. (2009). Application of Acoustic Emission Technology to the Characterization and Damage Monitoring of Advanced Composites; In I.M. Daniel et al. (eds.), *Major Accomplishments in Composite Materials and Sandwich Structures: An Anthology of ONR Sponsored Research*, @ Springer Science+Business Media B.V. pp. 441-461.

- Baker, K.G., Robertson, V.J. and Duck, F.A. (2001). A review of therapeutic ultrasound: Biophysical effects, *Physical Therapy*. 81(7), pp. 1351-1358.

- Boulahbal, D., Farid Golnaraghi, M. and Ismail, F. (1999). Amplitude and phase wavelet maps for the detection of cracks in geared systems. *Mechanical and Signal Processing*, 13(3), May, pp. 423-436.

- Bayray, M. and Rauscher, F. (2006). Wavelet transform analysis of experimental AE wave forms on steel pressure vessel. *Journal of Acoustic Emission,* 24, pp. 22-43.

- Benjamin, T.B. and Ellis, A.T. (1966). The collapse of cavitation bubbles and the pressure thereby produced against solid boundaries, Phil. Trans. Royal Society, London, 260, no. 1110, pp. 221-240.

- Birkin, P., Offin, D. and Leighton, T. (2007). Cavitation, shockwave and electrochemistry - An experimental and theoretical approach to a complex environment. *19th International Congress on Acoustics*, Madrid, 2-7 Sept.

- Blake, J.R. and Gibson, D.C. (1981). Growth and collapse of a vapour cavity near a free surface, *Journal of Fluid Mechanics*, 111, pp. 123-140.

- Boyd, J.W.R. and Varley, J. (2004). Acoustic Emission Measurement of Low Velocity Plunging Jets to Monitor Bubble Size, *Chemical Engineering Journal*, 7, pp. 11-25.

- Brennen, C.E. (1995). Cavitation and Bubble Dynamics. Oxford University Press, USA.

- Brennen, C.E. (2005). *Fundamentals of Multiphase flow*. Cambridge University Press, p. 93.

- Brennen, C.E. (2011). An introduction to cavitation fundamental. *3rd International Cavitation Forum*, 4th-6th July 2011, The University of Warwick, UK.

- Bruzelius, K. and Mba, D. (2004). An initial investigation on the potential applicability of Acoustic Emission to rail track fault detection. *NDT & E International*, 37(7), pp. 507-516.

- BS EN 1330-9:2000. Non-destructive testing –Terminology, Part 9: Term used in acoustic emission testing.

- BS EN 13554:2002. Non-destructive testing –Acoustic Emission – General principle. 2002.

- Buogo S. and Canneli, G.B. (2002). Implosion of an underwater spark-generated bubble and acoustic energy evaluation using the Rayleigh model, *Acoustical Society of America*, 111(6), pp. 2594-2600.

- Chapman, R.B. and Plesset, M.S. (1971). Thermal effects in the free oscillation of gas bubbles. *ASME Journal Basic Engineering*., 93, pp. 373-376.

- Davidson, J.F. and Harrison, D. (1971). *Fluidization*, Academic Press.

- Deane G.B. and Czerski H.A. (2008). Mechanism stimulating sound production from air bubbles released from a nozzle. *Journal of the Acoustical Society of America*, 123, pp. 126-132.

- De-Bosset, A., Obreschkow, D., Kobel, P., Dorsaz, M. and Farhat, N. (2007). Direct effects of gravity on cavitation bubble collapse, *58th International Astronautical Congress*, 1-5, 1AC-07-A2.4.04.

- Devin, C. Jr (1959). Survey of thermal, radiation, and viscous damping of pulsating air bubble in water, *Acoustical Society of America*, 31(12), pp. 1654-1667.

- Divoux, T., Vidal, V., Melo, F. and Géminard, J.C. (2008). Acoustic emission associated with the bursting of a gas bubble at the free surface of a non-Newtonian fluid, Physic Review, E 77.

- Eastop, T.D. and McConkey, A. (1993). Applied Thermodynamics for Engineering Technologist, Fifth Edition, Pearson-Prentice Hall.

- Elforjani, M. and Mba, D. (2009). Detecting of natural crack initiation and growth in slow speed shafts with the Acoustic Emission Technology, *Journal of Engineering Failure Analysis*, 16(7), pp. 2121-2129, Oct 2009.

- Evans, G.M., Machniewski, P.M. and Bin, A.K. (2004). Bubble size distribution and void fraction in the wake region below a ventilated gas cavity in downward pipe flow. Trans IChemR, Part A, *Chemical Engineering Research and Design*, 82(A9), pp. 1095-1104.

- Farhat, M., Obreschkow, D., Kobel, P., Dorsaz, N. and De Bosset, A. (2006). Interaction of a cavitation bubble with a spherical free surface, *Sixth International Symposium on Cavitation, CAV2006*, Wageningen, The Netherlands, Sept, 1-6.

- Ferlez, R.J. and Lang, D.C. (1998). Gear-Tooth Fault Detection and Tracking Using the Wavelet Transform, Prognosis of Residual Life

Machinery and Structures, *Proceedings of the 52nd Meeting of the Society for Machinery Failure Prevention Technology*, pp. 451-460.

- Gaitan, D.F. (1990). *An experimental investigation of acoustic cavitation in gaseous liquids*, PhD Thesis, University of Southwestern Louisiana. USA.

- Gannam, B.M.H. (2009). *Mathematical Theory of Wavelets*. Degree of Master of Science in Mathematics, Faculty of Graduate Studies, at An-Najah National University, Nablus, Palestine.

- Grosse, C.U. and Reinhardt, H.W. (2002). Signal conditioning in acoustic emission analysis using wavelets. *NDT.net* - September 2002, 7(9).

- Hammitt, F.G. (1966). Damage to solids caused by cavitation, *The Royal Society*, vol. 260, pp. 245-255.

- Hamstad, M.A. (2007a). Acoustic emission signals generated by monopole (pencil-lead break) versus dipole sources: Finite element modelling and experiment. Journal of Acoustic Emission, 25, pp. 92-106.

- Hamstad, M.A. (2007b). Acoustic emission source location in a thick steel plate by Lamb modes. *Journal of Acoustic Emission*, 25, pp.194-214.

- Hamstad, M.A., O'Gallagher, A. and Gary, J.A. (2002). Wavelet transform applied to Acoustic Emission signal: Part 1: Source identification. *Journal of Acoustic Emission*, 20, pp.39-61.

- Hardy, H.R. (2003). *Acoustic Emission, Microseismic Activity: Principles, techniques, and Geo technical applications*. p. 105. Netherlands, A.A. Balkema Publishers.

- Hess-Nielsen, N. and Wickerhauser, M.V. (1996). Wavelet Time-frequency Analysis. *Proceedings of the IEEE*, Vol. 84, No. 4, April, pp. 523-540.

- Heterodyne (2011). http://en.wikipedia.org/wiki/Heterodyne (accessed Sept 2011)

- Holler, V., Ruzicka, M., Drahos, J., Kiwi-Minsker, L. and Renken, A. (2003). Acoustic and Visual Study of Bubble Formation Processes in Bubble Column Staged with Fibrous Catalytic Layers. *Catalysis Today*, 79-80, pp, 151-157.

- Holroyd, T. (2000). *Acoustic Emission & Ultrasonics*. First Edition. Coxmoor Publishing Company, Oxford.

- Husin, S., Addali, A. and Mba, D. (2010). Acoustic Emission for monitoring two-phase flow. *29th European Conference on Acoustic Emission Testing*, Vienna, Austria, September 8th to 10th. ISBN 978-3-200-01956-0. *www.ndt.net/article/ewgae2010/papers/95_Mba.pdf.* (accessed Jan 2, 2011).

- Husin, S. and Mba, D. (2010). Acoustic Emission of Single Bubble Activities. *International MultiConference of Engineers and Computer Scientists 2010*, London, 30th Jun-2nd July, International Association of Engineers, ISBN: 978-988-18210-7-2, ISSN: 2078-0958, pp. 1466-471.

- Husin, S., Folashade, A., Addali, A. and Mba, D. (2011) Observation of slug flow using acoustic emission. *24th International Congress on*

Condition Monitoring and Diagnostics Engineering Management (COMADEM 2011), Stavanger, Norway, 30th May- 1st June 2011.

- Ing, M., Austin, S. and Lyons, R. (2005). Cover zone properties influencing acoustic emission due to corrosion. *Cement and Concrete Research*, 35(2), Feb 2005, pp. 284-295.

- Ing, M., Austin, S.A. and Lyons, R. 2003. Condition monitoring of reinforced concrete structures at risk from reinforcement corrosion. In: Anumba, C.J. (ed.). *Innovative Developments in Architecture, Engineering and Construction : Proceedings of the 2nd International Conference on Innovation in Architecture, Engineering and Construction*. Loughborough, UK, June 25-27, 2003. Rotterdam : Millpress Science Publishers, pp. 215-226.

- Isseline, J.C., Alloncle, A.P. and Autric, M. (1998). On laser induced single bubble near a solid boundary: Contribution to the understanding of erosion phenomena. Journal of Applied Physics, 84(10), pp. 5766-5771.

- Jin, G.T. and Kim S.D. (1990). Bubble properties and pressure fluctuations of a single bubble in water. *Journal of Chemical Engineering of Japan*, 23(5), pp. 523-530.

- Kaplan, I. (2002). Frequency Analysis Using the Wavelet Packet Transform.
  Http://www.bearcave.com/misl/misl_tech/wavelets/packfreq/index.html, (accessed April 22, 2011).

- Kihm, K.D. (1996). Investigation of the effect of coal particle sizes on the interfacial and rheological properties of Coal-water slurry fuels. *Texas A&M University Report no DE-FG22-94PC94120*.

- Kim, S.J. and Lee, S.K. (2008). Identification of impact force in thick plates based on the elastodynamics and time-frequency method (II) - Experimental approach for identification of the impact force based on time frequency methods. *Journal of Mechanical Science and Technology* 22, pp. 1359-1373.

- Kline, R.A. (1983). Acoustic Emission signal characterization; In Matthews, J.R (1983). *Acoustic Emission*, Gordon and Breach, New York. pp. 105-138.

- Kloeppel, J.E. (2002). Scientists measure energy dissipation in a single cavitating bubble. *Physical Sciences* (217) pp. 244-1073.

- Kolaini, A.R. (1999). Effects of salt on bubble acoustic in water, Journal of the Acoustical Society of America. 105(4), pp. 2161-2186.

- Kuwahara, T. and Yamaguchi, H. (2007). Void fraction measurement of gas-liquid two-phase flow using magnetic fluid, *Journal of Thermophysics and Heat Transfer*, 21(1), pp. 173-180.

- Laschimke, R., Burger, M. and Vallen, H. (2004). Acoustic emission from transpiring plants-New results and conclusions. Journal of Acoustic Emission, 22, pp. 102-109.

- Lauterborn, W. (1976). Numerical investigation of nonlinear oscillations of gas bubbles in liquids. *Journal of the Acoustical Society of America*, 59(2), pp. 283-293.

- Lauterborn, W. and Ohl, C-D. (1997). Cavitation Bubble Dynamics. *Ultrasonics Sonochemistry*, 4, pp. 65-75.

- Leighton, T.G and Walton, A.J. (1987). An experimental study of the sound emitted from gas bubbles in a liquid. European Journal of Physics. 8, pp. 98-104.

- Leighton, T.G. (1994a) *The Acoustic Bubble*, Academic Press, London.

- Leighton, T.G. (1994b) Acoustic Bubble Detection-1: The Detection of Stable Gas Body. *Environmental Engineering,* Sept 1994, pp. 9-16.

- Leighton, T.G. (1996). *The Acoustic Bubble (paperback edition),* London, San Diego, Academic Press.

- Leighton, T.G., Fagan, K.J. and Field, J.E. (1991a). Acoustic and Photographic Studies of Injected Bubbles, European Journal of Physics. 12, pp. 77-85.

- Leighton, T.G., Lingard, R.J., Walton, A.J. and Field, J.E. (1993). Bubble Sizing by the Nonlinear Scattering of Two Acoustic Frequencies in *Natural Physical Sources of Underwater Sound*, pp. 453-466.

- Leighton, T.G., Lingard, R.J., Walton, A.J. and Field, J.E. (1991b). Acoustic Bubble sizing by combining of subharmonic emissions with imaging frequency. *Ultrasonics*, 29, pp. 319-323.

- Leighton, T.G., Phelps, A.D., Ramble, D.G. and Sharpe, D.A. (1996). Comparison of the Abilities of Eight Acoustic Techniques to Detect and Size a Single Bubble. *Ultrasonics*, 34, pp. 661-667.

- Longuet-Higgins, M.S., Kerman, B. and Lunde, K. (1991). The Release of Air Bubble from an Underwater Nozzle. Journal of Fluid Mechanics, 230, pp. 365-390.

- Loutas, T.H., Sotiriades, G. and Kostopoulos, V. (2004). On the application of wavelet transform of AE signals from composite materials. *DGZfP-Proceedings BB 90-CD*, Lecture 42, EWGAE.

- Manasseh, R. and Chanson, H. (2001). Void-fraction and acoustic characteristics of gas bubbles entrained by a circular plunging jet. *Proceedings, 4th International Conference on Multiphase Flow*, New Orleans, USA, May 27 - June 1, 2001, paper 347, pp. 1-12.

- Manasseh, R., Bui, A., Sandercock, J. and Oi, A. (2001). Sound emission processes on bubble detachment. *Proceedings 14th Australian Fluid Mechanics Conference*, Adelaide, South Australia, 9-14th Dec, 1: pp.857-860.

- Manasseh, R., Riboux, G., Bui, A. and Risso, F. (2007). Sound emission on bubble coalescence: imaging, acoustic and numerical experiments, *16th Australian Fluid Mechanics Conference*, Gold Coast, Australia, 2-7 Dec 2007, pp. 167-173.

- Manasseh, R., Riboux, G. and Risso, F. (2008). Sound generation on bubble coalescence following detachment, *International Journal of Multiphase Flow*, 34, pp. 938-949.

- Maradei, C., Piotrkowski, R., Serrano, E. and Ruzzante, J.E. (2003). Acoustic emission signal analysis in machining process using wavelet packets. Lat. Am. Res [online], ISSN: 1851-8796. 33(4), pp. 443-448.

- Matsuo, T., Cho, H. and Takemoto, M. (2006). Utilization of cascade optical fiber AE system for source location of Lamb waves through a cross-ply CFRP plate. *Journal of Acoustic Emission*, 24, pp. 84-96.

- Matthews, J.R. and Hay, D.R. (1983). Acoustic Emission evaluation; In Matthews, J.R (1983). *Acoustic Emission*, Gordon and Breach, New York. *Acoustic Emission*, Gordon and Breach, New York. pp.1-14

- Mazille, H., Rothea, R. and Tronel, C. (1995). An acoustic emission technique for monitoring pitting corrosion of austenitic stainless steels**.** *Corrosion Science*, 37(9), September 1995, pp. 1365-1375.

- Mba, D. and Hall, L. (2002). The transmission of acoustic emission across large-scale turbine rotors. *NDT and E International*, 35(8), pp. 529-539.

- Mba, D., Cooke, A., Roby, D. and Hewitt, G. (2004). Detection of shaft-seal rubbing in large scale power generation turbines with Acoustic Emissions; Case study. *Journal of power and energy - part A, I Mech E*, 218(2), Part A, ISSN 0957-6509. pp. 71-82.

- McAllister E.W. (2009). *Pipeline rules of thumb handbook - quick and accurate solutions to your everyday pipeline engineering problems* (7th edition), Gulf Professional Publishing, ISBN: 1856175006.

- Miller, R.K. and McIntire, P. (1987). *Non-destructive Testing handbook*, second edition, Volume 5; Acoustic Emission Testing, American Society for Non-destructive Testing.

- Minnaert, M. (1933). On Musical Air-Bubbles and the Sounds of Running Water. Philosophical Magazine, 16, pp. 235-248.

- Neill, G.D., Reuben, R.L. and Sandford, P.M. (1997). Detection of Incipient Cavitation in Pumps using Acoustic Emission. *Journal of Process Mechanical Engineering, IMechE*, 211(4), pp. 267-277.

- Neppiras, E.A. (1980). Acoustic emission. *Physics reports (review section of Physics Letters)*, North-Holland Publishing Company, 61(3), pp. 159-251.

- Obreschkow, D., Kobel, P., Dordaz, N., De Bosset, A., Nicollier, C. and Farhat, M. (2006). Cavitation dynamics inside liquid drops in microgravity. *Physical Review Letters*, 97, 094502, pp. 1-4.

- Oltra, R., Chapey, B. and Renaud, L. (1993). Abrasion-corrosion studies of passive stainless steels in acidic media using acoustic emission techniques. *Corrosion Science*, 35(1-4), pp. 641-645.

- Pandit, A.B., Varley, J., Thrope, R.B. and Davidson, J.F. (1992) Measurement of bubble size distribution: An Acoustic Technique. *Chemical Engineering Science*, 47(5), pp. 1079-1089.

- Phelps, A.D. and Leighton, T.G. (1996). High-resolution bubble sizing through detection of the subharmonic response with a two frequency excitation technique. *Journal of the Acoustical Society of America,* 99, pp.1985-1992.

- Physical Acoustic Corporation (2003). *PCI-2 Based AE System User's Manual*, Rev 1a.

- Physical Acoustic Corporation (2011). http://www.pacndt.com/index, 2011 (accessed April 22, 2011).

- Piotrkowski, R., Gallego, A., Castro, E., Garcı´a-Hernandez, M. and Ruzzante, J. (2005). Ti and Cr nitride coating/steel adherence assessed by acoustic emission wavelet analysis. *NDT&E International,* 38, pp. 260-267.

- Plesset, M.S. (1966). Shockwaves from cavity collapse. *The Royal Society*, vol. 260, pp. 241-244.

- Prateepasen, A., Jirarungsatean, C. and Tuengsook, P. (2006). Identification of AE source in corrosion process. *Key Engineering Materials*, vol. 321-323, pp. 545-548.

- Pryor, A.H., Mosher, M. and Lewicki, D.G. (2001). The Application of Time-Frequency Methods to HUMS. Presented at the *American Helicopter Society's 57th Annual Forum*, Washington D.C., May 9-11.

- Raja Hamzah, R.I. and Mba, D. (2009). The influence of operating condition on acoustic emission (AE) generation during meshing of helical and spur gear. *Tribology International*, 42(1), pp. 3-14.

- Raja Hamzah, R.I. and Mba, D. (2007). Acoustic Emission and Specific Film Thickness for Operating Spur Gears. *ASME*, 129(4), pp.860-868.

- Rayleigh, Lord (1917). On the pressure developed during the collapse of a spherical cavity, *Philosophical Magazine*, 34(199), pp. 94-98.

- Representation of transient and continuous AE signals. http://www.vallen.de/zdownload/pdf/sea204E.pdf (accessed April 22, 2011).

- Robert, E., Lettry, J., Farhat, M., Monkewitz, P.A. and Avellan, F. (2007). Cavitation bubble behaviour inside a liquid jet. *Physics of Fluid*, 19, 067106, pp. 1-12.

- Rodney, C.F.W (1990). *Underwater Acoustic Systems*. Macmillan.

- Ross, D. (1976). *Mechanics of underwater noise*. Chapter 7: Cavitation. Pp. 202-242. Pergamon Press.

- Rydberg, K.E. (2001). Energy efficient water hydraulic systems, *The Fifth International Conference on Fluid Power transmission and Control*, HangZhou, China, 2-7 April, pp. 440-46.

- Sathyam, U.S., Shearing, A. and Prahl, S.A. (1995). The effects of spot size, pulse energy, and repetition rate on the microsecond ablation of gelatine under water. *Laser-Tissue Interaction VI, Proc SPIE*, 2391, pp. 336-344.

- Serrano, E.P., and Fabio, M.A. (1996). Application of the Wavelet Transform to Acoustic Emission Signals Processing. *IEEE Transaction on Signal Processing*, 44(5), pp.1270-1275

- Shangguan, H., Casperson, L.W. and Prahl, S.A. (1997). Pressure impulse during microsecond laser ablation, *Applied Optics*, 36(34), pp. 9034-9041.

- Sinha, N.N. (2003). Bubble-based resonance-Doppler sensor for liquid characterization. http://archives.sensorsmag.com/articles/0702/sinha.pdf. (accessed April 22, 2011)

- Sinha, N.N. (2006). *Characterization of Liquids Using Gas Bubbles*. United States Patent No: US 7,010,962 B2. Mar. 14.

- Spasova, L.M. and Ojovan, M.I. (2008). Characterisation of Al corrosion and its impact on the mechanical performance of composite cement wasteforms by the acoustic emission technique. *Journal of Nuclear Materials*, 375(3), pp. 347-358.

- Spasova, L.M., Ojovan, M.I. and Scales, C.R. (2006). Acoustic Emission monitoring of aluminium corrosion in cemented-based wasteforms. *Advanced Materials Research*, 13-14 (2006) pp. 223-229.

- Strasberg M. (1956). Gas bubbles as source of sound in liquids. *J. Acoustical Soc. America*, 28, pp. 20-26.

- Suzuki, H., Kinjo, T., Hayashi, Y., Takemoto, M. and Ono, K. (1996). Wavelet transform of Acoustic Emission signals. *Journal of Acoustic Emission,* 14(2), pp. 69-84.

- Szkodo, M. (2006). Cavitation erosion behaviour of laser processed Fe-Cf-Mn and Fe-cr-Co alloys, *Journal of Achievement in Materials and Manufacturing Engineering*, Issue 1-2, pp. 239-242.

- Tan, C.K. and Mba, D. (2005). Identification of the Acoustic Emission source during a comparative study on diagnosis of a spur gearbox. *Tribology International*, 38(5), pp. 469-480.

- Tan, C.K., Irving, P. and Mba, D. (2005). Diagnostics and prognostics with Acoustic Emission, Vibration and Spectrometric Oil Analysis for spur gears; a comparative study. *INSIGHT*, 47(8), pp. 478-480.

- Tho, P., Manasseh, R. and Oi, A. (2007). Cavitation microstreaming patterns in single and multiple bubble systems. Journal of Fluid Mechanics, 576, pp. 191-233.

- Tien, T.M., Lee, C.H. and Huang, C.J. (2007). Study of bubble size distribution for breaking wave propagates over a submerged dike, 3(4), pp. 448-451.

- Toutountzakis, T. (2003). *Acoustic Emission for gear defect diagnosis*. MSc Thesis, Cranfield University, UK.

- Toutountzakis, T., Tan, C.K. and Mba, D. (2005). Application of Acoustic Emission to seeded gear fault detection. *NDT & E International*, 38(1), pp 27-36.

- Trefethen, L. (1969). *Surface tension in fluid mechanics*. Tufts University. National Committee for Fluid Mechanics film notes. No 21610.

- Tse, K., Martin, T., McFarlane, C.M. and Nienow, A.W. (1998). Visualisation of bubble coalescence in a coalescence cell, a stirred tank and a bubble column. *Chemical Engineering Science*, 53(23), Publisher: Elsevier, pp. 4031-4036.

- Urick, R.J. (1983). *Principles of underwater sound*, 3rd edition, Peninsula Publishing, California, USA.

- Vorkurka, K. (1990). Amplitudes of free bubble oscillations in liquids. *Journal of Sound and Vibration*, 141(2), pp. 259-275.
- Wang, W.J. and McFadden, P.D. (1996). Application of wavelets to gearbox vibration signals for fault detection. *Journal of Sound and Vibration*, 192(5), pp. 927-939.

- Weninger, K.R., Camara, C.G. and Putterman, S.J. (1999) Energy focusing in a converging fluid flow: implications for sonoluminescence, *Physical Review Letter*, 83(10), pp. 2081-2084.

- Wentzell, P.D., Vanslyke, S.J. and Bateman, K.P. (1991). Evaluation of acoustic emission as a mean of quantitative chemical analysis. *Analytica Chimica Acta*, Elsevier Science Publisher, Amsterdam. 246, pp. 43-53.

- Werther, J. (1978). Influence of the distribution design on bubble characteristics in large diameter gas fluidized beds. *Fluidization: Proc. 2nd engineering foundation conference*, Trinity College, Cambridge, England, 1-6 April 1978.

- Wissler, A. and Del Grosso, V.A. (1951). The velocity of Sound in sea Water. *The Journal of Acoustical Society of America*, 23(2), 1951, pp. 219-223.

- Xu, R.Q., Chen, X., Shen, Z.H., Lu, J. and Ni, X.W. (2004). Optical deflection technique for investigation of laser-induced oscillating bubble on metal surface. *Japanese Journal of Applied Physics*, 43(8A), pp. 5595-5599.

- Yasuda, T., Takahashi, N., Baba, M., Tei, K. and Yamaguchi, S. (2008). An experimental study on micro-bubble generation by laser-induced breakdown in water. *The Review of Laser Engineering*, Supplemental Volume, pp. 1273-1275.

- Yen, G. and Lu, H. (2002). Acoustic Emission Data Assisted Process Monitoring. *ISA Transactions* 41, pp. 273-282.

- Yoon, D.J., Weiss, W.J. and Shah, S.P. (2000). Assessing damage in corroded reinforced concrete using Acoustic Emission. *Journal of Engineering Mechanics*, 273, March, pp. 273-283.

- Zhao, G., Jiang, D., Diao, J. and Qian, L. (2004). Application of wavelet time-frequency analysis on fault diagnosis for steam turbine. *SURVEILLANCE 5 CETIM* 11-13 Oct, http://perso.univ-lemans.fr/~jhthomas/28_zhao.pdf, (accessed Feb 13, 2011).

APPENDICES

Appendix A : Waterfall plots; AE bubble burst energy, bubble size and liquid viscosity

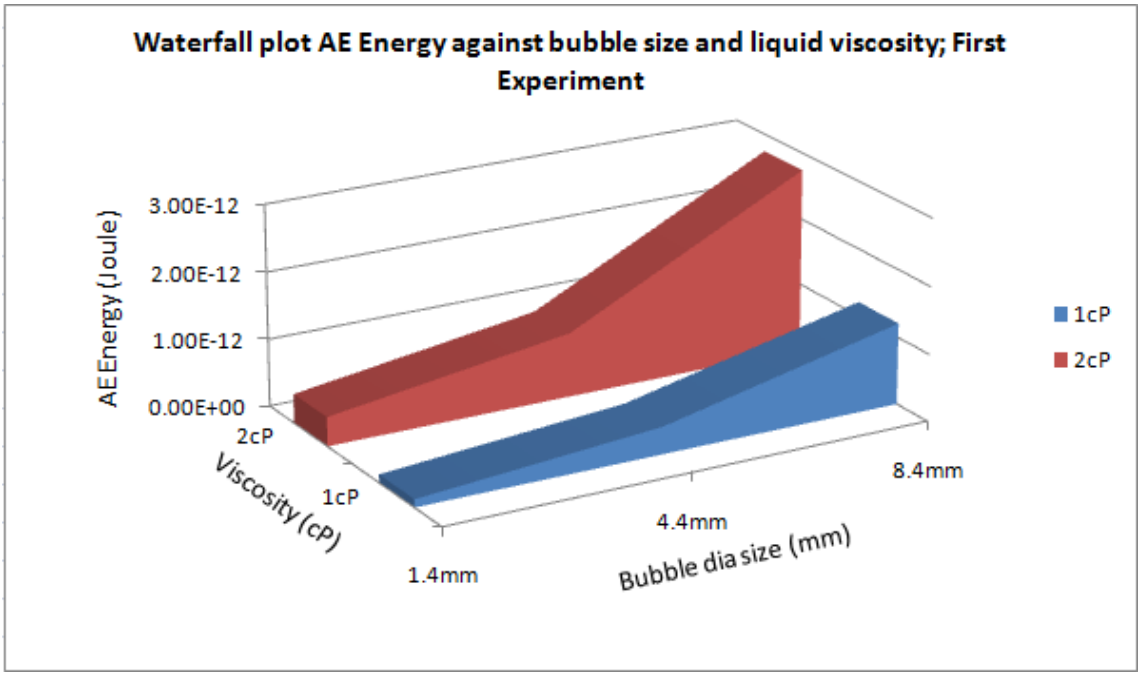

Figure A-1: Data from the first experiment; water (1 cP) and saltwater (2 cP)

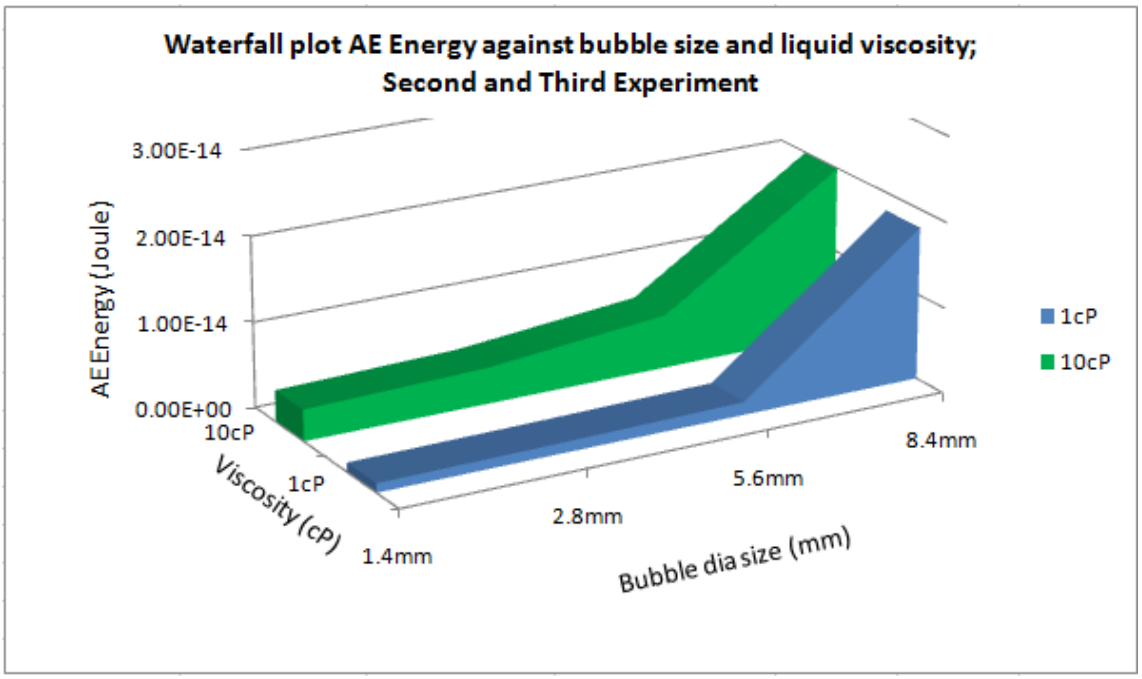

Figure A-2: Data from the second and third experiment; water (1 cP) and glycerine solution (10 cP)

Appendix B : Comparison of Theoretical Bubble Energy and AE measured Energy of Bubble Burst

Theoretically, the energy of a spherical vaporous cavitation/bubble and gases cavitation/bubble can be calculated using Rayleigh's formulae, Eq 6-1 (Rayleigh, 1917; Sathyam et al., 1995; Shangguan et al., 1997; Xu et al., 2004; Blake and Gibson, 1981, Yasuda et al., 2008; Robert et al., 2007; Obreschkow et al., 2006; Buogo and Canneli 2002; De-Bosset at al., 2007). The energy from bubble collapse/burst, E_B is equal to the work done by the liquid on the bubble during its collapse, which is obtained by multiplying the pressure difference by the maximum bubble's volume, see Eq 5-1. For the case of a bubble with conditions of a non-condensable gas content and adiabatic behaviour, the energy equation is given by Eq B-1 (Neppiras, 1980). The equation considers that a bubble is a spherical shape and maintains the shape until its collapse at a free surface.

$$E_B = \frac{4}{3}\pi R_{Max}^3 \left(P_o + \frac{P_g}{\gamma - 1}\right) \quad \textbf{(B-1)}$$

where p_o is the static pressure of the surrounding liquid (hydrostatic pressure), p_v is the vapour pressure inside the bubble and R_{max} is the bubble's maximum radius, P_g is the pressure gas inside the bubble due to permanent gas content and γ is the polytrophic gas component.

The bubble energy is proportional to its maximum volume. The potential energy of a bubble is maximum when the bubble reaches it maximum radius at the end of growth/expansion (De-Bosset at al., 2007). In this study, it is assumed that a bubble maintains its spherical shape until it collapses, and as such Eq B-1 was employed for estimating the bubble energy. Theoretical bubble energy calculated considers the value P_o= 1 bar, P_V=0.0233 bar and polytrophic component, $\gamma = 1.33$ (Lauterborn, 1976).The values taken for the surface

tension in water, saltwater and glycerine solution are 0.0725 N/m, 0.0750 N/m and 0.0690 N/m respectively (Trefethen, 1966; Kihm, 1995). A plot of comparison of theoretical bubble energy as a function of bubble size in water (1 cP, σ=0.0725 N/m), saltwater (2 cP, σ=0.0750 N/m) and glycerine (10 cP, σ=0.0690 N/m) is shown in Figure B-1.

Figure B-1 shows that the theoretical gas bubble energy (from Eq B-1) in saltwater is the highest compared with the water and glycerine solutions, whilst the lowest theoretical bubble energy is in the glycerine solution. This theoretical bubble energy is dependent on bubble size and surface tension of the liquid.

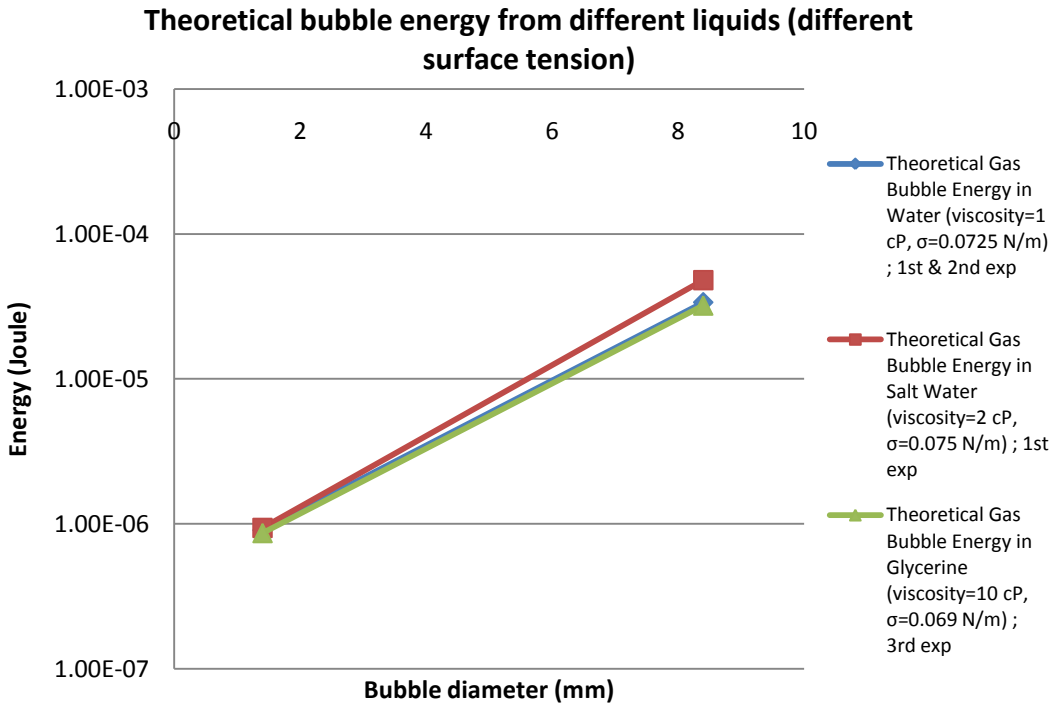

Figure B-1: Theoretical bubble energy as a function of relative difference bubble size (1.4 mm and 8.4 mm) and liquid (different viscosity and surface tension)

Figure B-2 (page 176) shows the comparison between the theoretical bubble energy and measured AE energy from bubble burst at a free surface in different liquids (water and saltwater) in the 1st experiment. It was found that measured

AE energy from bubble burst in a higher viscosity (saltwater; 2 cP, σ=0.075 N/m) is higher than in water (1 cP, σ=0.0725 N/m). In addition, the curve of measured AE energy from bubble burst is linear where it increases with the increase in bubble size. This demonstrates that bubble size generated via the nozzles in the first experiment was proportional to nozzle size.

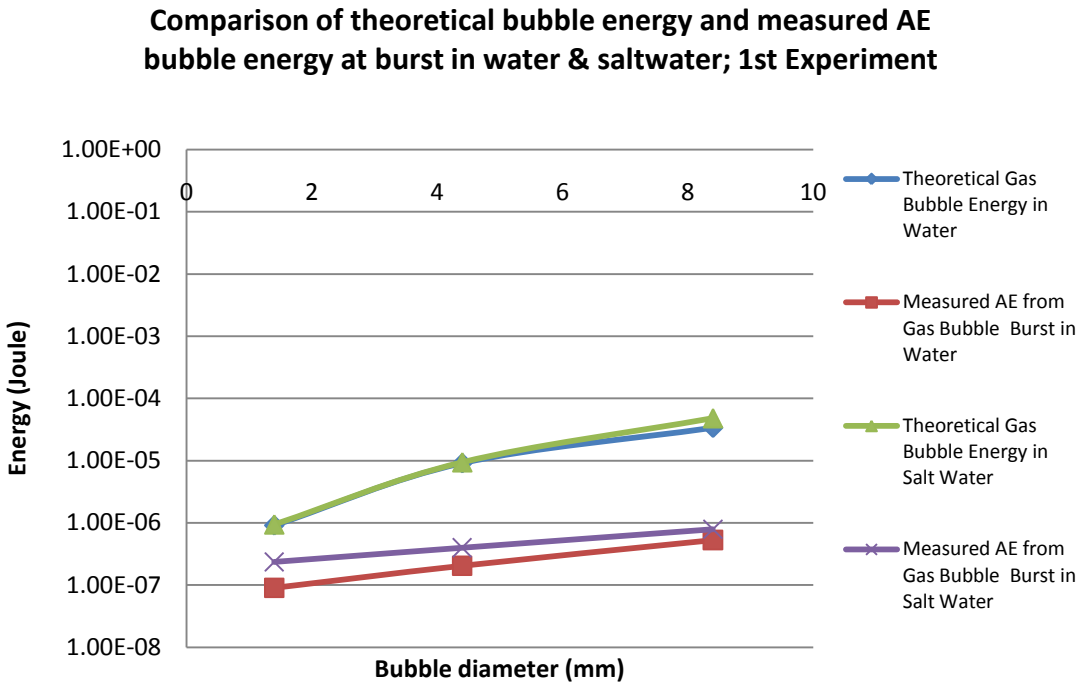

Figure B-2: Comparison of theoretical bubble energy and measured AE energy from bubble burst in water and saltwater

The measured AE energy bubble at burst in water and glycerine from the second and third experiments can be compared since both of them used the same test rig with the same sensor locations. Figure B-3 (page 177) shows a comparison between theoretical bubble energy and measured AE bubble at burst in water (from 2nd experiment) and glycerine solution (from 3rd experiment). The plot show that the measured AE energy from bubble burst in the glycerine solution is higher than in water. The curve for the plot of measured AE energy should be linear as obtained in the first experiment. The curve of

measured AE energy, as can be seen in Figure B-3, is contributed by the size of bubble produced from the first two nozzles (1.4 mm and 2.8 mm) in the second and third experiments but was not proportional/equivalent with the nozzle size.

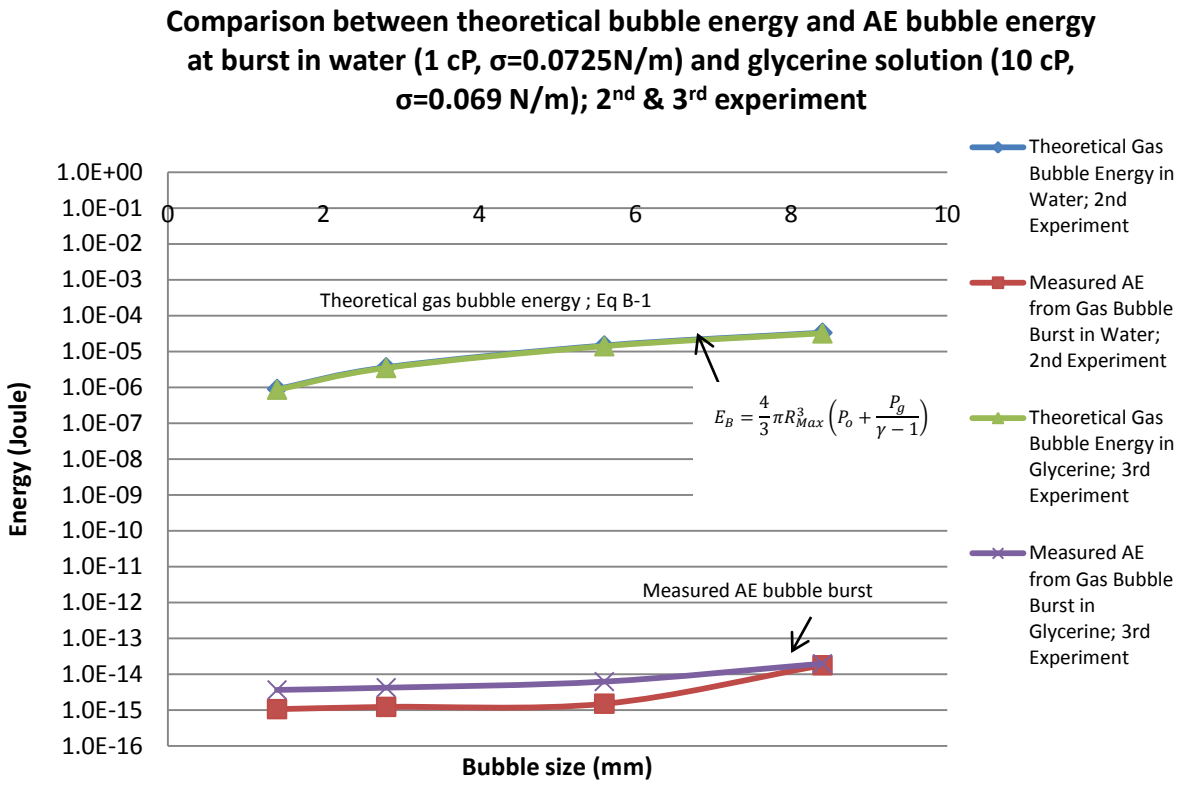

Figure B-3: Comparison of theoretical bubble energy and measured AE energy from bubble burst in water (1 cP, σ=0.0725 N/m) and glycerine solution (10 cP, σ=0.069 N/m)

A comparison of the results of measured AE energy bubble burst from the three experiments is shown in Figure B-4 (page 178). It was found that the results of the measured AE energy bubble burst in the same liquid (water) obtained from the second experiment was lower than the results obtained from the first experiment. The distance of the sensor from the source in the test rig that was used in the second experiment attributed to a lower measured AE energy bubble burst. Figure B-4 provides a comparison on the liquids used in the same test rig, not between test rig.

It can be concluded that the results from this experiment demonstrated that the measured AE energy from bubble burst was dependent on the liquid viscosity and bubble size.

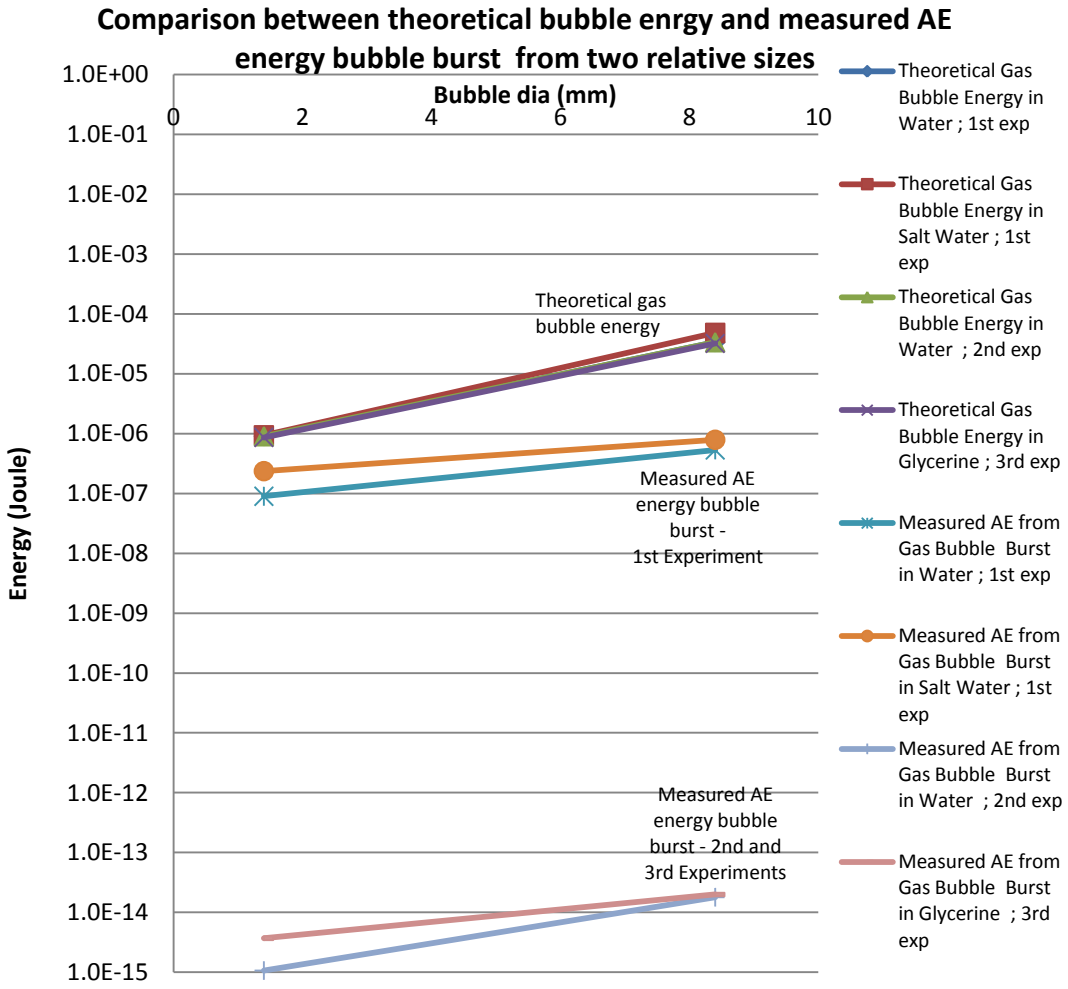

Figure B-4: Comparison of theoretical bubble energy and measured AE energy from bubble burst in water (1 cP, σ=0.0725 N/m) and glycerine solution (10 cP, σ=0.069 N/m)

Appendix C : Calibration Certificate for WD Type Sensor

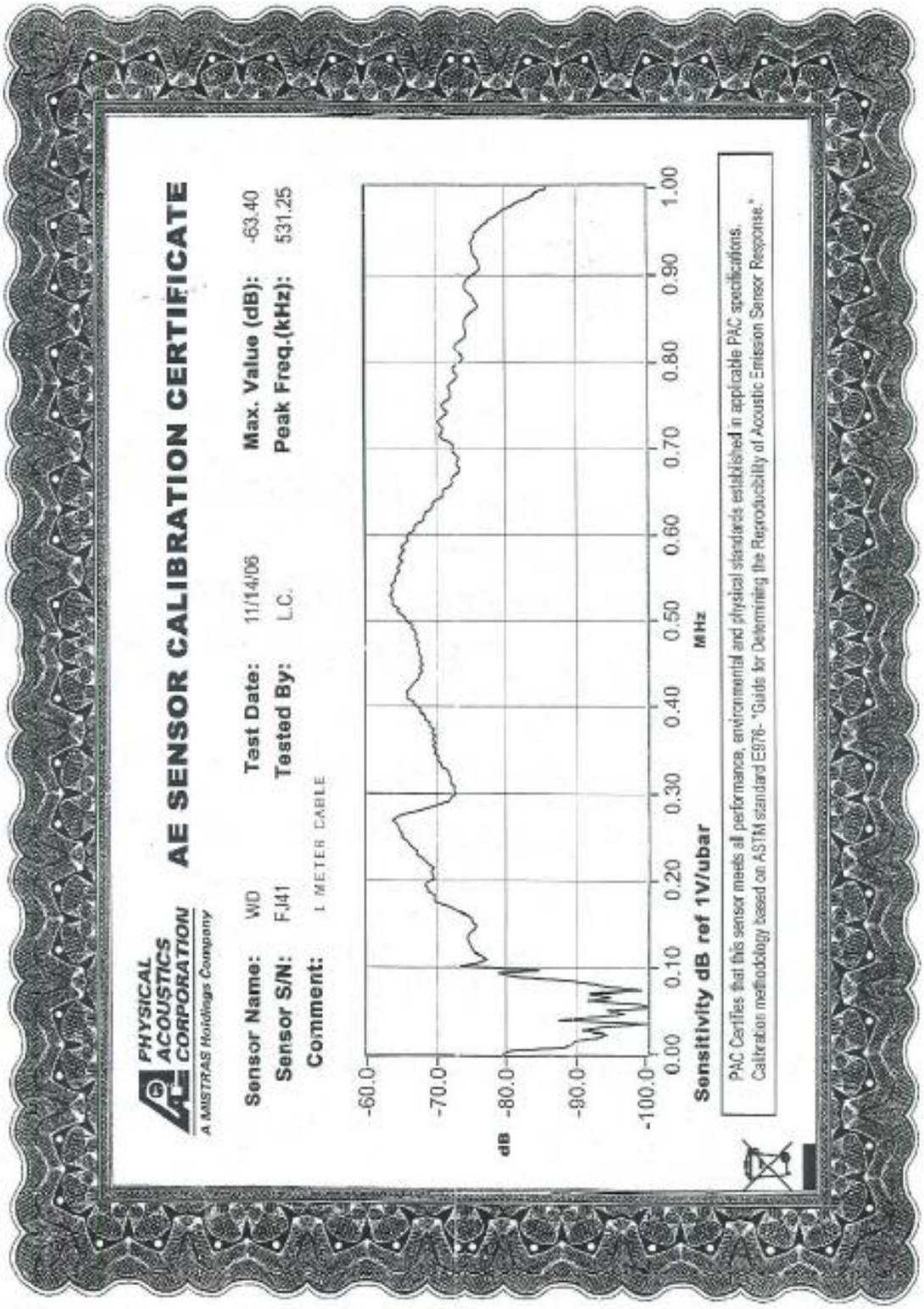

Appendix D : Publication Paper 3

Husin, S., Addali, A. and Mba, D. "Sensitivity of Acoustic Emission (AE) Technology in Monitoring Oxide Formation on an Aluminium Surface". INSIGHT-BINDT. (Accepted for publication on 17th Sept 2011).

Sensitivity of Acoustic Emission (AE) Technology in Monitoring Oxide Formation on an Aluminium Surface

Shuib Husin[1], AbdulMajid Addali[2] and David Mba[2]

[1]*Dept of Mech Eng, Universiti Kula Lumpur, Malaysia*

[2]*School of Engineering, Cranfield University, UK*

Abstract

A series of experiments has been performed to assess sensitivity of Acoustic Emission (AE) technology in monitoring oxide formation on an Aluminium surface (6082/HE 30). The tests were conducted at room temperature and results show a direct correlation with increasing oxide formation and an accompanying increase in AE activity.

Keywords:

Acoustic Emission (AE), bubble dynamics

1 Introduction

Acoustic Emissions (AE) are transient elastic waves generated by a sudden change in the local stress field within a material [(1)]. For ferrous materials (e.g. irons and alloy steels) one form of surface degradation is commonly known as corrosion or rusting. It can be defined as the disintegration of a material into its constituent atoms due to chemical reactions with its surrounding [(2)]. For non-ferrous metals such as aluminium, aqua-degradation is a common phenomenon. In the presence of water the surface will degrade and an oxide layer can built to great thickness.

AE technology has been used for corrosion monitoring, particularly for steels and its alloys [(3,4,5,6)]. Prateepasen et al [(7)] employed AE technology to detect the corrosion on austenitic stainless steel. Their results showed that the AE count number can be associated with the corrosion rate. They confirmed that the AE sources came from corrosion activity where hydrogen bubbles were generated from chemical reactions of the corrosion process. In an earlier study, Ing et al., [(8,9)] used AE technology to detect corrosion in reinforced concrete by observing AE hits. They performed experiments on the samples before and after corrosion. By comparing the AE hit data they demonstrated the ability and practicality of AE to detect corrosion in concrete at early stages before any external evidence was visible. These two examples show the large scope of AE in corrosion monitoring. The purpose of this investigation is to assess capability of AE technology for monitoring oxide formation on an aluminium surface.

2 EXPERIMENTAL APPARATUS AND PROCEDURES

Two sets of apparatus were employed for this investigation. The first employed a 50 mm thick aluminium plate with an AE sensor (type WD) mounted onto its surface and the opposite face of the aluminium plate was submerged in tap water (half of its thickness), see figure 1. The second apparatus was a water column built of 50 mm thick aluminium wall, see figure 2. This was used to investigate the effect of wetted surface area on corrosion and associated AE activity generated. The column was filled with water for several weeks to allow an oxide layer to build on the aluminium surface. Two broadband piezoelectric transducers (Physical Acoustic Corporation type WD) were mounted onto the aluminium wall (see figure 2) with a pre-amplification of 40 dB. The sampling rate for acquisition of AE waveform was 2 MHz.

A trigger threshold level of 24 dB was set for acquisition of AE data. Background noise measurements were performed on an oxide free aluminium plate to obtain AE reference values. The plate was then submerged to half its thickness in tap water for seven weeks to develop an oxide film, see figure 3. Similarly, figure 4 shows the surface degradation observed on the Aluminium column after a couple of weeks in contact with water.

Figure 1: Aluminium plate submerged half its thickness in water

Given this is a passive test where no external forces are applied; all Acoustic Emissions generated can be attributed to oxidation only.

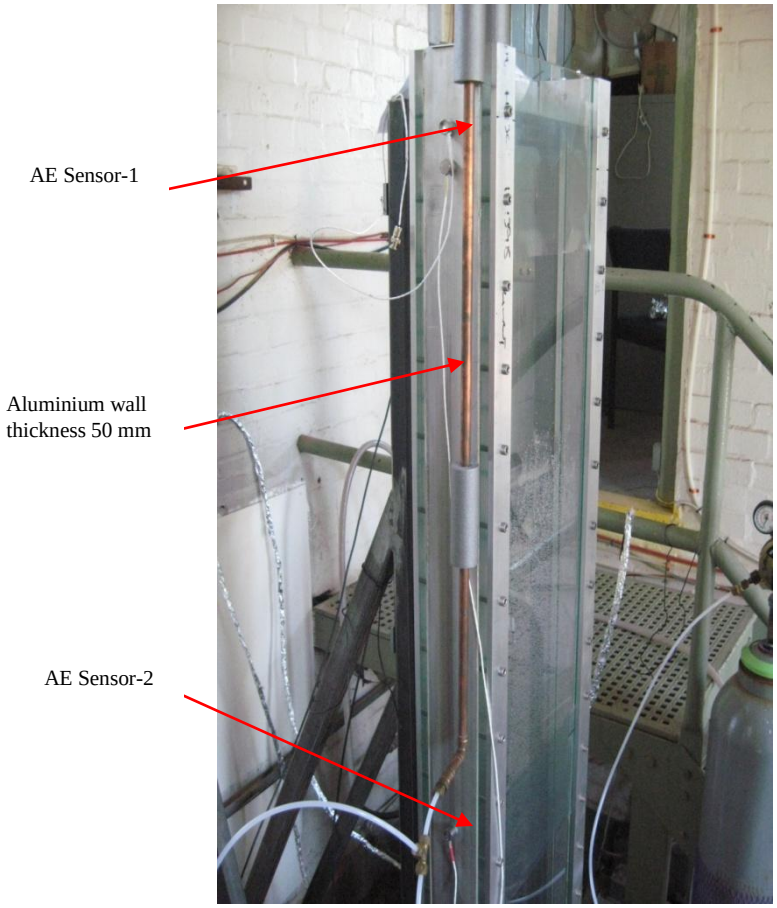

Figure 2: Water column test rig

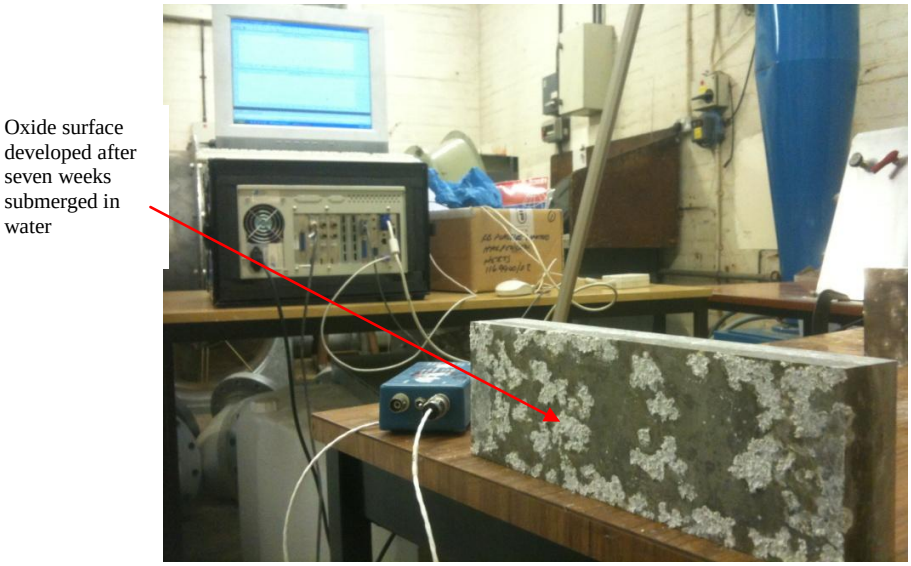

Figure 3: Surface degradation (oxide) developed after seven weeks submerged in water

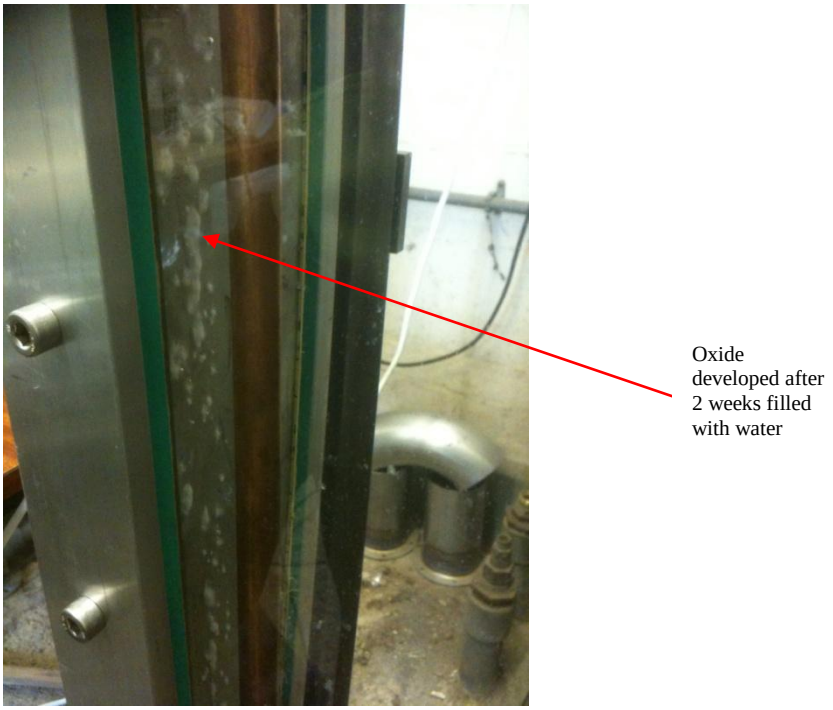

Figure 4: Water column aluminium wall condition with developed oxide when filled with water for a couple of weeks

Measurements of AE HIT's were taken throughout the duration of these tests. A HIT is used to describe the AE event that is detected by a particular sensor and can be described by several parameters such as threshold, duration, counts and rise time. In this investigation the HIT amplitude was used for correlation. A HIT is described by three timing parameters; the HIT definition time (HDT), HIT lockout time (HLT) and peak definition time (PDT). These were set at 200 µsec, 800 µsec and 1 milisec respectively. Correct setting of the PDT will result in an accurate measurement of peak amplitude while the appropriate definition of HDT will ensure that each signal generated from the structure is reported as one HIT, as it defines the period over which a HIT can be acquired. With an accurate setting of HLT spurious measurement during the signal decay will be avoided; essentially it defines the period between successive HITs; its second function is to inhabit the measurement of reflections.

3 RESULTS AND OBSERVATIONS

Visual observations of stages of oxide formation on the aluminium plate are presented in figure 5. It shows increasing concentrations of oxide content on the plate. Correspondingly the increase in AE energy and amplitude during this period can be seen in figure 6. All AE HITs recorded were attributed to chemical reaction/activities of the oxidation process. It was also noticed that gas bubbles were generated as a results of the reaction. After two weeks submerged in water, the result was as in figure 5(b) and there is an increase in the amplitude of the hits up to 32 dB with relatively few hits.

Degradation surface as a function of time submerged in water

(a) Surface at first day of the experiment

(b) Surface after two weeks submerged in water

(c) Surface after four weeks submerged in water

(d) Surface after seven weeks half submerged in water

Figure 5: Surface degradation of Aluminium sample as a function of time

After four weeks half submerged in water, the result shows the maximum amplitude of the AE HITs reached 35 dB and the number of HITs had increased by 30%. By week-5 the amplitude had reached 38 dB. There are possibly several contributions to the generation of AE, including chemical reaction and the generation of bubbles as noted by Prateepasen et al [7].

The number of AE HITs and AE amplitude associated with the HITs increased with increased with the increase in expose time with water. It was noted that AE HITs measured on the aluminium plate (figure 6) were lower than observed on the aluminium column (figure 7). This was due to the increase of surface area in contact with the water. Interestingly it was noted, for both cases, that the amplitude of AE events at the start of the test increased significantly (0 dB to 30 dB) for the 10 days after which an increase of only 8 dB was noted for the next 25 days. Conversely, the number of HITs have increased significantly after 10-days of exposure. This would suggest an increase in corrosion reaction rates which generated several AE events at similar amplitude as the exposure increases.

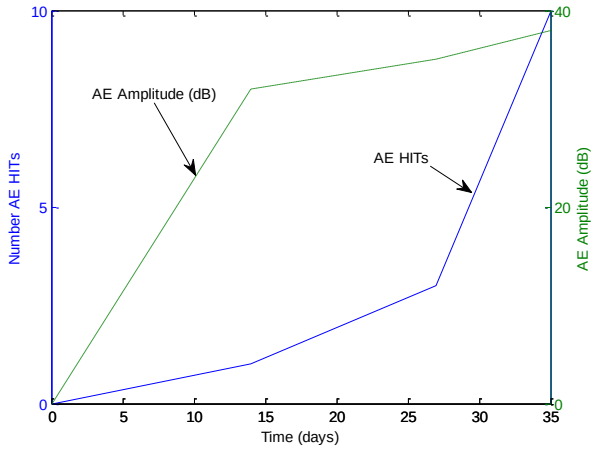

Figure 6: HITs recorded from aluminium sample plate as a function of time (days)

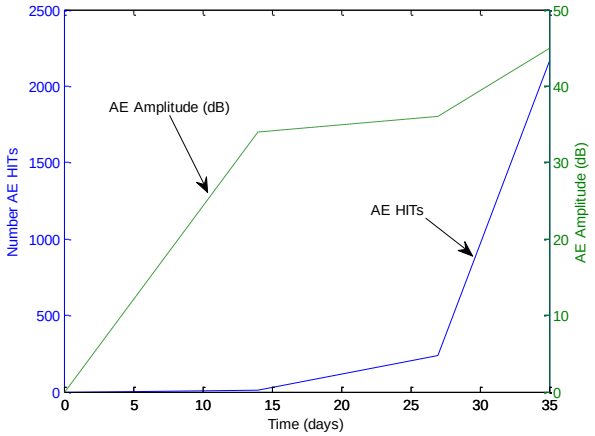

Figure 7: HITs recorded from aluminium column filled with water as a function of time (days)

Sample time waveform plots associated with different exposure times (1-day, 14-days and 28-days) is presented in figure 8. In addition, a time-frequency plots at 28-days. For the aluminium plate and water column are presented in figure 9 and 10. The time waveforms show, as expected, increasing amplitudes over the test duration. The time-frequency plots show the frequency range of 100 kHz to 400 kHz for events associated with oxide formation with a concentration of energy at 250 kHz.

The sources of AE are attributed to the chemical reaction and the creation of bubbles at the reaction surface. Both of these are known to generate AE [7,10].

Aluminium plate

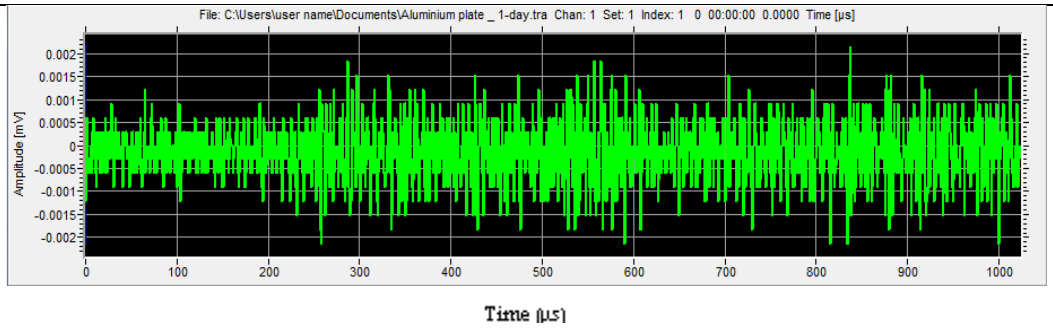

(a) Waveform at the first day of experiment

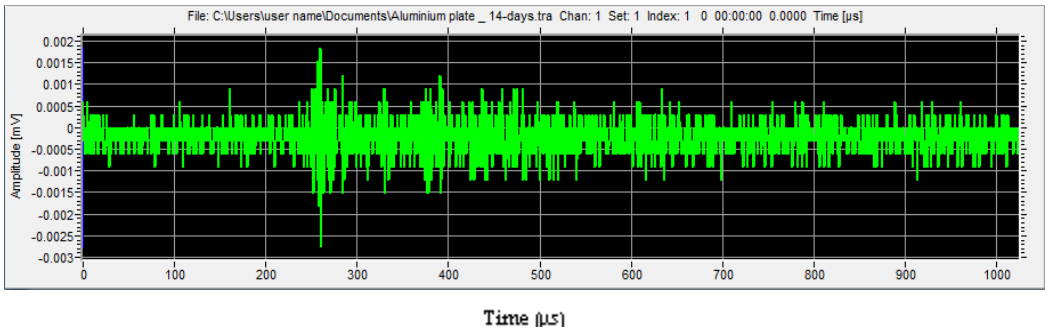

(b) Waveform at two-weeks

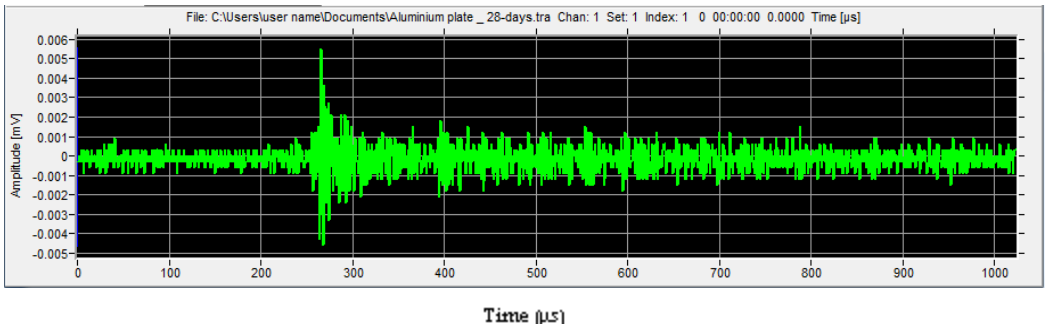

(c) Waveform at four-weeks

Figure 8: Time waveform plot Aluminium plate associated with difference exposure time

Aluminium plate

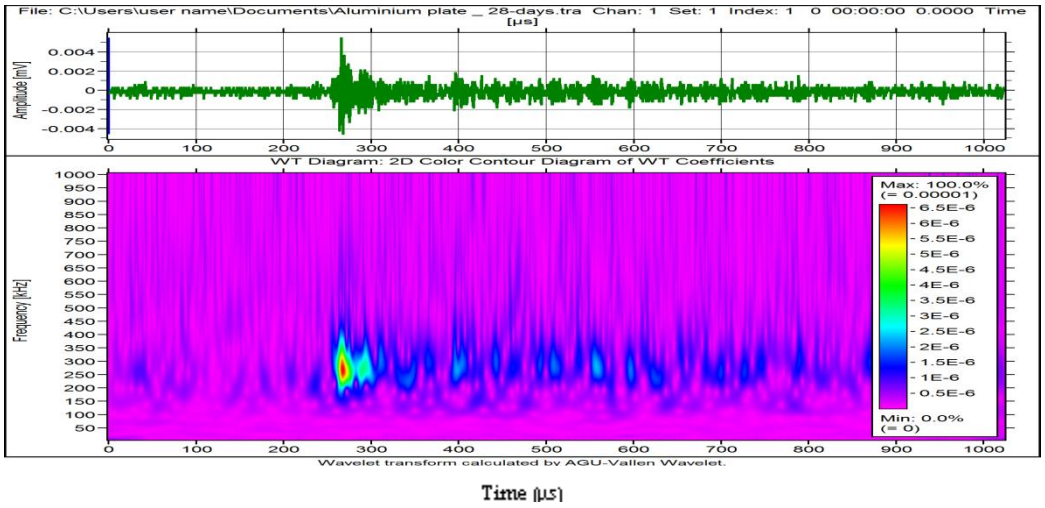

Figure 9: Time-frequency plot at 28-days from Aluminium plate

Aluminium column

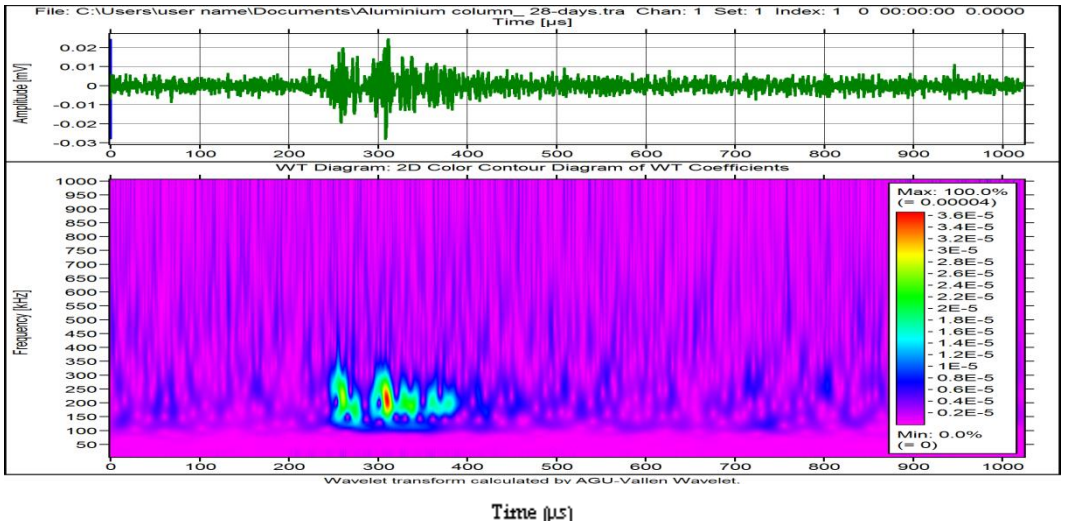

Figure 10: Time-frequency plot at 28-days from Aluminium column

4 CONCLUSION

These observations highlight the potential of AE technology for monitoring the rate of oxide formation on aluminium surface. It was established that the AE HITs amplitude and numbers of AE HITs increases with an increase of oxide rate on the aluminium surface.

References

[1] Miller, R.K, and McIntire, P. (1987). Non-destructive Testing Handbook, second edition, Volume 5; Acoustic Emission Testing. American Soceity for Non-destructive Testing.

[2] Rathi, V.R., Nirmal, S.D., and Kokate, S.J. (2010). Corrosion study of mild steel, or steel and CRS steel by weight loss method. J. Chem. Pharm. Res, 2(2), p.97-100.

[3] Oltra, R., Chapey, B., and Renaud, L. (1993). Abrasion-corrosion studies of passive stainless steels in acidic media using acoustic emission techniques. Corrosion science, vol 35, nos 1-4, p.641-645, UK

[4] Mazille, H., Rothea, R., and Tronel, C. (1995). An acoustic emission technique for monitoring pitting of austenitic stainless steels. Corrosion Science, volume 37, Issue 9, Sept 1995, p.1365-1375. UK.

[5] Spasova, L.M., Ojovan, M.I., and Scales, C.R. (2006). Acoustic Emission monitoring of aluminium corrosion in cemented-based wasteforms, Adv. Mater. Res., 13-14 (2006), p.223-229.

[6] Spasova, L.M. and Ojovan, M.I. (2008). Characterisation of Al corrosion and its impact on the mechanical performance of composite cement wasteforms by the acaoustic emission technique, Journal of Nuclear Materials, Volume 375 (3), p.347-358

[7] Prateepasen, A., Jirarungsatean, C., and Tuengsook, P. (2006). Identification of AE source in corrosion process. Key Engineering materials, vol 321-323, p. 545-548

[8] Ing, M., Austin, S.A., and Lyons, R. (2005). Cover zone properties influencing acoustic emission due to corrosion. Cement and Concrete Research, vol 35, Issue 2, Feb 2005, p. 284-295.

[9] Ing, M., Austin, SA., and Lyons R. (2003). Condition monitoring of reinforced concrete structures at risk from reinforcement corrosion. IN: Anumba, C.J. (ed). Innovative Developments in Architecture, Engineering and Construction: Proceedings of the 2nd International Conference on Innovation in Achitecture, Engineering and Construction. Loughborough, UK, June 25-27, 2003. Rotterfam: Millppress Science Publishers, p. 215-226.

[10] Husin, S and Mba, D. (2010). Acoustic Emission of single bubble activities. Int. Multi Conference of Engineers and Computer Scientists, London, 30th Jun-2nd July 2010, International Association of Engineers, ISBN: 978-988-18210-7-2, ISSN: 2078-0958, p. 1466-471